A STUDY OF CONTACT BETWEEN A PROFILE METER STYLUS AND POLYMER FILMS ON ROUGHENED SUBSTRATES

by

David R. Gilliam

Thesis submitted to the Faculty of the
Virginia Polytechnic Institute and State University
in partial fulfillment of the requirements for the degree of
Master of Science
in
Mechanical Engineering

APPROVED:

N. S. Eiss, Jr., Chairman

C. E. Knight

H. H. Mabie

December, 1985

Blacksburg, Virginia

A STUDY OF CONTACT BETWEEN A PROFILE METER STYLUS AND POLYMER FILMS ON ROUGHENED SUBSTRATES

by

David R. Gilliam

N. S. Eiss, Jr., Chairman

Mechanical Engineering

(ABSTRACT)

When a polymer film is deposited onto a roughened substrate, the film masks over the underlying substrate roughness. Then when attempting to measure the roughness of the polymer film surface using a stylus-type profile meter, the pressure between the tip of the stylus and the film is sufficient to plastically deform the polymer surface. The result is a possible erroneous measurement of the surface roughness of the polymer film. This thesis reports on attempts to quantify the actual roughness of the polymer film from the measurement obtained by the profile meter. Extensive surface profile data were collected and analyzed to determine the characteristics of the surface of the substrate and of the coating on the substrate. The tracks made by the stylus in the film were then observed in a scanning electron microscope, from which the depth of the stylus tracks were measured. The effects of the film thickness, stylus traversing speed, and substrate roughness on the stylus penetration depth, the variation in the depth, and the measured film roughness are assessed and discussed. It was found that using the fastest stylus traversing speed minimizes the variation of the stylus penetration depth and thus results in the most accurate measurement of the film surface.

To predict this stylus indentation depth, a plane strain plastic deformation model is developed using slip-line field theory. It is found that the slip-line model gives good estimates of the stylus indentation depth when the film thickness is large.

ACKNOWLEDGEMENTS

The author expresses sincere thanks to his advisory committee, Professors H. H. Mabie, C. K. Knight, and N. S. Eiss, Jr., Chairman. He is grateful to Professors Mabie and Knight for their help in the preparation of this thesis and for being part of the quality education he has received at Virginia Tech. Dr. Eiss is thanked for his guidance and the hours of enlightening conversation.

Thanks are extended to the Mechanical Engineering Department and N.A.S.A. Langley Research Center for their financial support during the author's graduate study.

Finally, the author is very indebted to his parents, , for their constant encouragement and support throughout his college education.

TABLE OF CONTENTS

LIST OF FIGURES

1.0 INTRODUCTION

The use of polymers in research has increased drastically in the past decade. Particularly, tribologists have found that, due to their unique friction and wear characteristics, polymers may be the solution to many of the friction and wear problems inherent in machinery. One property of some polymers which is especially important to tribologists is low surface energy. Low surface energy assures that there will be less adhesion between the polymer surface and the surface with which it is in contact.

The project from which this thesis topic was generated is entitled "A Fundamental Investigation of the Sticking of Insect Residue to Aircraft Wings." One purpose of the project is to study the effects of surface energy and surface roughness on insect adhesion. Four polymers with different surface energies were coated upon substrates of four different surface roughnesses. A stylus-type profile meter was used to measure the surface roughness of the films on the substrates. It was found that the stylus penetrated the polymer film, as shown in Figure 1, thus giving an inaccurate measurement of the film surface profile.

The purpose of the research reported in this thesis is to study the deformation of the film by the stylus and to attempt to devise a method for estimating the surface roughness of a polymer film over a roughened substrate. This entails extensive data collection and analysis, along with the development of a theoretical model to predict the indentation of the stylus into the film. The film thickness is measured and the ef-

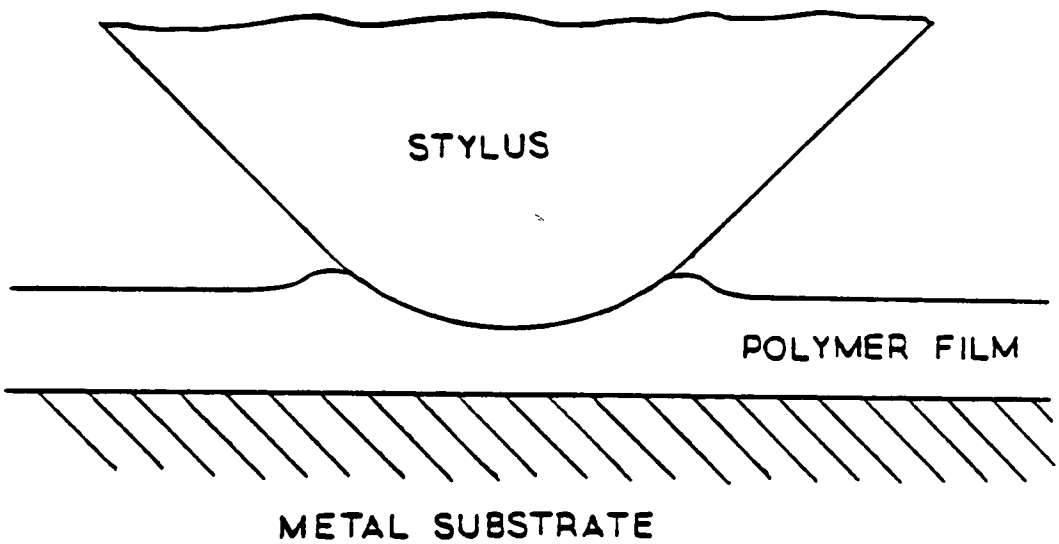

Figure 1. A stylus indenting a polymer film on a metal substrate.

fect of the thickness on the stylus penetration depth and on the surface roughness measurement is assessed. The results are then compared and discussed, and recommendations are made as to how the results may be made better through more preliminary work and better selection and preparation of polymers.

2.0 LITERATURE REVIEW

This literature review will be divided into three parts. First, models of plastic deformation caused by indenters are reviewed and their potential for modeling the interaction between a diamond stylus in moving contact with a polymeric film on a steel substrate is assessed. Second, the area of mechanical and viscoelastic properties of polymers is reviewed for information relevant to the solution of the present problem. Third, numerical analysis techniques used to analyze the data obtained in the course of this work are discussed.

2.1 PLASTIC DEFORMATION MODELS

Plastic deformation is most frequently analyzed by a method of slip-lines. A slip-line field is a mapping of the contours of maximum shear stress as a body is plastically deformed, where the directions of the slip-lines correspond to the directions of maximum shear stress. Knowing these maximum shear stress directions, and certain boundary conditions, such as the coefficient of friction on a surface, one can estimate the forces necessary to cause the deformation. Slip-line fields have found greatest application in the area of metal deformation, and most literature is directed toward solving problems of that type [1-8].[1]

---

[1] Numbers enclosed in [ ] represent references listed at the end of the thesis.

While slip-line fields have been applied to a variety of contact and indentation problems [6,9,10,11,12], none have been formulated for a stylus making a permanent groove in a polymeric film. Since the stylus tip is approximately spherical in shape, an analogous problem is the Brinell hardness test. This problem has not been analytically solved either. An attempt was made in 1944 by Ishlinsky [13] in which he proposed a partial field for ball indentation. He could estimate the configuration of the field near the indenter/metal interface, but he was unable to predict the shape of the material which is pushed above the original surface. Ishlinsky was mainly limited by computational difficulties and was unable to find a satisfactory solution. A complete solution would require following the motion of material from first contact of the indenter with the workpiece. Today, even with the computational facilities available, no one has attempted to find an analytical solution for the Brinell hardness test. Brinell hardness numbers have been generated through correlation of experimental data. Thus, there has been no urgent need for an analytical solution, and the initiative has not yet been taken to solve this complex unsteady plastic flow problem.

Pyramid indentation, or the Vickers Hardness Test, has been experimentally and analytically studied in depth [11]. The actual pyramid indention problem has not been solved analytically yet. Instead, a slip-line field has been found by Hill et. al. [9] for plane strain wedge indentation of an ideal rigid plastic material to approximate pyramid indentation. Since the stylus is pyramidal in shape, stylus penetration could be approximated as a wedge for large indentation depths. But, since the author has observed that the stylus does not penetrate past its

spherical tip, this model fails to give an adequate representation of the problem.

Another model which has been investigated is of a cone indentation [9], which corresponds to hardness tests Rockwell C, A, and N and Shore A and D. This model seems to have promise at first observation because it is an axisymmetric model instead of a plane strain model. However, the same problem becomes apparent as with the wedge indentation model. The stylus is a 90-degree four-sided pyramid with spherical tip. The stylus could be approximated as a cone for large indentations, but, again, it does not penetrate past its spherical tip. Also, the model does not give a solution for the indentation of a cone with a half-angle greater than 32 degrees.

A model which is the inspiration for the stylus indentation model developed in this thesis is the expansion of a semi-circular cavity in an ideal rigid-plastic material [1,2]. The slip-line field was proposed to describe the swaging or expansion operation. The model is of interest in this thesis because it predicts the configuration of a slip-line field around a curved, or, more specifically, circular surface. The expansion of a cavity is an unsteady problem. In this model, it is assumed that the cavity is expanded from a point with equal rate of radius increase in all directions, spanning 180 degrees. This assumption makes the slip-line field unchanging. Even though the size of the field increases as the size of the cavity increases, the proportions of the slip-line field are constant. This property of the model is called "geometric similarity" and a method for solving these types of unsteady problems was proposed by Hill [1]. Therefore, this problem can be easily solved to

give the stresses necessary to cause the plastic flow. The stylus indentation model would span a maximum of 90 degrees, with the span increasing as the depth of indentation increases. This restriction means that the property of geometric similarity is lost and some simplifying assumptions must be made to obtain an estimate of the stylus forces on the polymer film. The model developed in this thesis to describe the stylus indentation will be discussed in detail in Chapter 5.

2.2 POLYMER PROPERTIES

One purpose of this research was to study the plastic deformation of a polymer film subjected to the load of a stylus. To do so, it is required to develop an understanding of the properties of polymers under conditions of plastic flow. Argon and Bessonov [14] discuss in detail the theory and mechanics of polymer plastic deformation. They also have collected experimental results to compare to the relations which they have derived. Evidence is presented to show that, unlike metals, inelastic strain in lightly cross linked polymers is fully recoverable at and above the glass transition temperature (T_g). Below T_g, the amount of recovery is inversely proportional to the degree of plastic straining. However, in polymers with low molecular weight and no cross linking, as are studied in this thesis, no true rubbery behavior is demonstrated above T_g, and the plastic flow is less recoverable, as is observed with metals.

Argon and Bessonov state that the resistance to plastic deformation below T_g consists of two parts: a) an entropy term which accounts for the resistance to molecular alignment during straining, and b) a term

which accounts for the energy loss as bonds are broken in aligning molecular chains. Taking these ideas as a base and applying the concept of overcoming free energy barriers as the molecules are realigned, they derive an expression for the plastic shear resistance as a function of the shear strain rate, in terms of several parameters, including the shear modulus, the mean molecular radius, and Poisson's ratio.

The hydrostatic pressure effect on the strength of polymers is an important factor to consider. When a polymer is subjected to pressure, the molecules are compacted, which serves to increase the strength of the material. It has been observed over the years that the yield behavior of metals can be approximated by yield criteria such as the distortion energy theory (von Mises-Hencky) and the maximum shear stress theory (Tresca) [15]. These theories do not account for the effects of pressure and have been used successfully to study the yield behavior of metals. The strength of polymers, on the other hand, is affected by pressure, so these theories will not give an accurate representation of polymer yield behavior. Argon and Bessonov present experimental results assembled by another researcher which shows that polymers obey a modified von Mises criterion. Under biaxial stress, the criterion is an ellipse the center of which is translated into the third quadrant, along the line of pure pressure. Ward [16] presents similar results for polystyrene which show that the yield behavior can be fit to a Mohr-Coulomb criterion, similar to a Tresca criterion, where the polygon is shifted into the third quadrant.

Several investigators [17,18,19] have performed experiments to quantify the effect of pressure on the mechanical properties of polystyrene

and other polymers. All the researchers found that an increase in pressure resulted in increases in the elastic modulus, the yield stress and the strain at yield. Curves were presented which were very helpful in this study.

In any study involving polymers, the viscoelastic properties, and their effect upon the phenomenon being studied, must be considered. The purpose of the search for literature in this area was not to go into great depth in the theory of viscoelastic behavior, but more so to understand how viscoelasticity will effect the stylus penetration model and to find information on the properties of the specific polymers used in the study, polysulfone and polystyrene.

Perhaps the foremost reference text on the properties of polymers is written by Ward [16]. Here can be found the information needed to gain the required insight into viscoelastic behavior and, perhaps more importantly, references to more specific works.

Two references [21,22] were found on the viscoelastic properties of polysulfone. These references included the study of relaxations in the polymer, such as the glass transition temperature, and curves of the moduli and the energy loss as a function of temperature. For polystyrene, one reference which was particularly helpful is a book by McCrum and Read [23] in which they cover both mechanical and dielectric properties of polymers. McCrum also presents curves of moduli and energy dissipation which were used later in the development of the stylus/film dynamic model.

2.3 NUMERICAL ANALYSIS TECHNIQUES

Analysis of experimental data for this thesis required finding the frequency content of the surface profiles. The calculation of the Fourier transform was performed by a Fortran computer program, "Fourier." The program calls an IMSL subroutine called "FFTRC." The algorithm used in the calculation is called the "fast Fourier transform" and was first proposed by Cooley and Tukey [24]. This algorithm greatly reduces computational time compared to the "ordinary" Fourier transform [25,26].

The numerical computation of slip-line fields required using the finite difference forms of the governing differential equations of plastic flow. The theory of plastic flow and the numerical methods necessary to solve plastic deformation problems has been presented by several authors [1-5]. Their work will be reviewed in detail in Chapter 5 as the theory of plastic flow is applied to the solution of the stylus indentation problem.

3.0 EXPERIMENTAL

The experimental work for this thesis consisted of several steps. First, substrates of known roughnesses were prepared and readings of the substrate surface profiles were obtained, several at each stylus tracing speed. Films of differing thickness were then deposited, or cast, upon these substrates. The surface of the polymer film was characterized by taking several profile meter readings on the film surface at each stylus traversing speed. Because the stylus deformed the soft films when the surface readings were taken, the stylus tracks were observed in a scanning electron microscope (SEM) and a sufficient number of photographs were taken to be able to measure the width of the stylus tracks, and to calculate the deviation of the width from the mean width and other statistical parameters. Measurements of film thickness were made using an optical instrument called an ellipsometer.

3.1 PREPARATION AND CHARACTERIZATION OF SUBSTRATES

The first step in this experimental study was to prepare substrates of differing roughnesses. The material chosen for the substrates was 410 stainless steel. This material was chosen primarily for two reasons. First, 410 stainless steel is a ferromagnetic material, which allows the use of a magnetic table to hold the specimens during grinding to the desired roughness. Second, the stainless steel is sufficiently hard so that the stylus will not damage the surface when surface readings are taken.

24 specimens, 25.4 mm (1 inch) square, were cut from 6.4 mm (0.25 inch) plate.

Surfaces were ground to four different surface roughnesses, nominally 0.1, 0.3, 0.6, and 0.8 μm R_a [27]. Typical surface profiles of the substrates are shown in Figure 2. Six specimens were ground at the same time by placing them longitudinally on the grinder table. The differing substrates were all ground under the same conditions of work speed and indexing speed, and the roughness was controlled by varying the grinding time. The smoothest surfaces required a grinding time of about five hours to achieve the almost "mirror" finish. Grinding the roughest surfaces took only a half of an hour.

The roughnesses of the substrates were then measured using the Talysurf 4 stylus profile meter shown in Figure 3. The profile meter has an electronic rectifying and integrating circuit which calculates the arithmetic average roughness R_a of the surface profile. Because it was necessary to calculate many other important characteristics of the profile, the data were stored so that it could be analyzed more fully at a later time using numerical analytical techniques. To do so, data were collected using the Zonic DMS 5003 FFT Processor. The analog signal of the Talysurf was input to channel 1 of the DMS (Data Memory System), where the signal was digitized into 1024 points in the time domain and stored. The data was then be sent to the IBM 370 mainframe computer through a program entitled "SEND" which was developed by Dr. Eiss's former student, John Herold.

When the "Send" command is issued, the computer prompts the user for other pertinent information, such as the stylus traversing speed, the

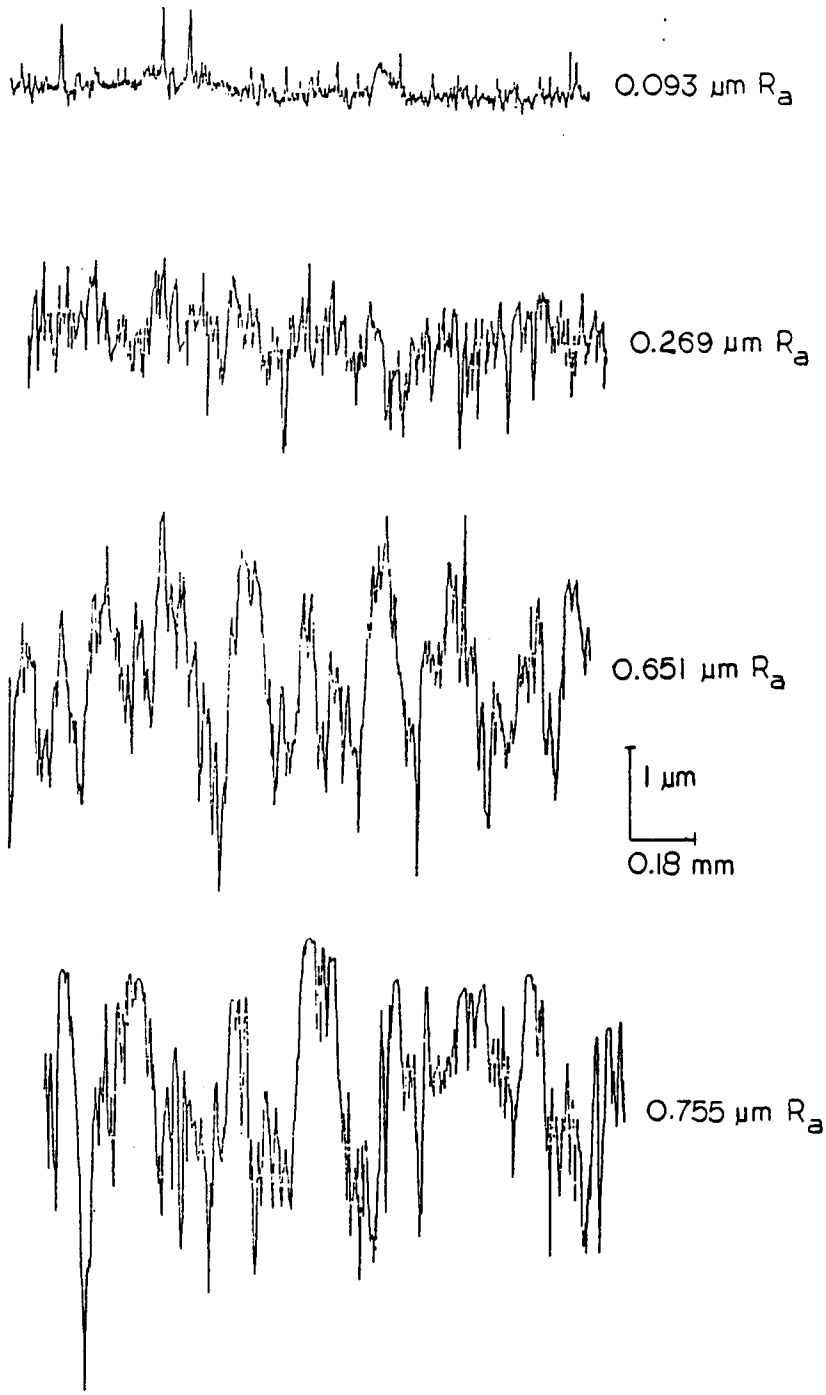

Figure 2. Typical surface profiles of the ground substrates.

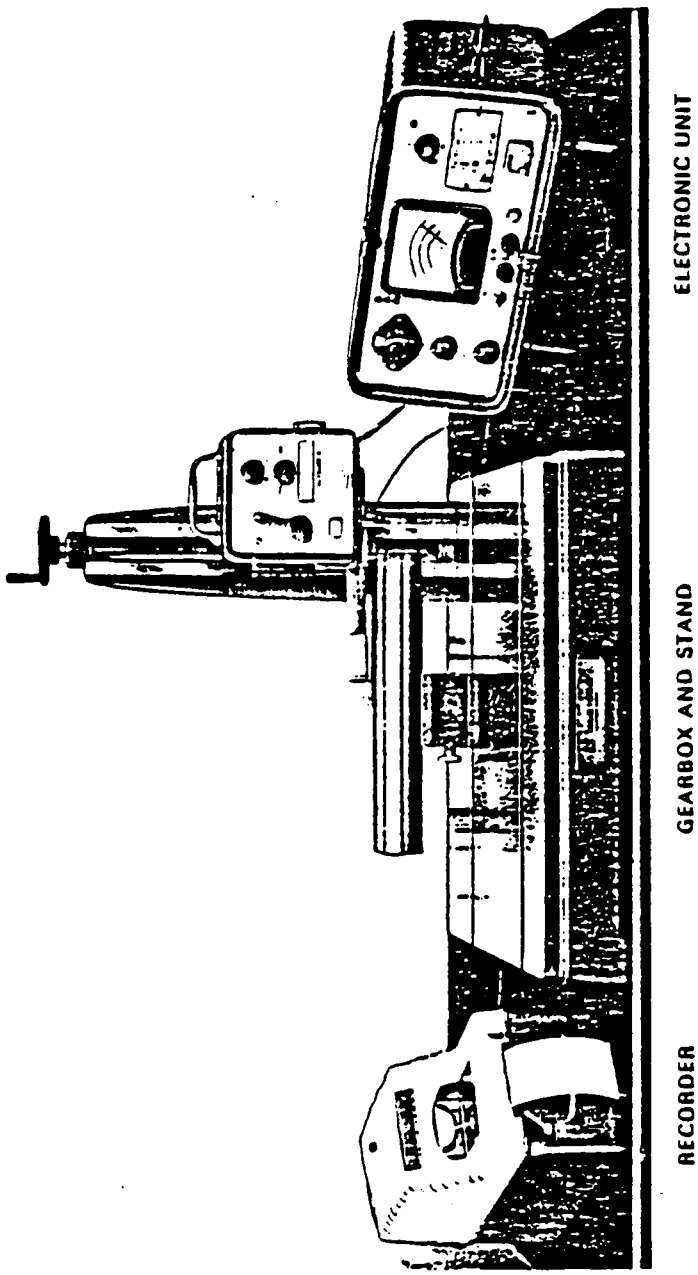

Figure 3. The Talysurf profile meter.

vertical magnification setting of the profile meter, the sampling rate of the FFT machine, and the full scale voltage setting for channel 1 of the DMS. The data is stored in the DMS in ASCII format. When the Send program is executed, the data is read by the IBM and is converted to an IBM language comparable to the ASCII code. The Send program calculates vertical and horizontal scaling factors corresponding to the parameters for which the user has been prompted. The Send program then calls another Fortran program entitled "DECODE" where the data is converted from the IBM code to numeric format so that the data may be operated upon by other Fortran computer programs.

Five surface profiles of the substrates were collected at each of the three gearbox speeds. When the profile meter is set for measuring the arithmetic average roughness of the surface, the stylus is traversed at a speed of 91.4 mm/min. For this traversing speed, the data were collected at a sample rate of 2 msec/sample, which converts to a sample interval of 3.046 μm. The two other traversing speeds, 18.3 and 3.6 mm/min, are primarily for making chart recordings. Data were collected at these speeds at sample rates of 5 and 20 msec/sample, respectively, which gave sample intervals of 1.525 and 1.2 μm, respectively.

3.2 COATING OF FILMS ON SUBSTRATES

Polymer films of four different thicknesses were deposited on the substrates of four different roughnesses. The chemical structure of the polymers used, polysulfone and polystyrene, are shown in Figure 4. The figure shows the monomer units of the molecules and the subscript "n"

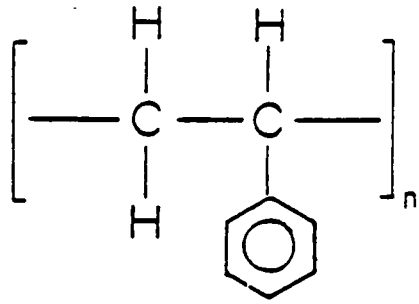

Polystyrene

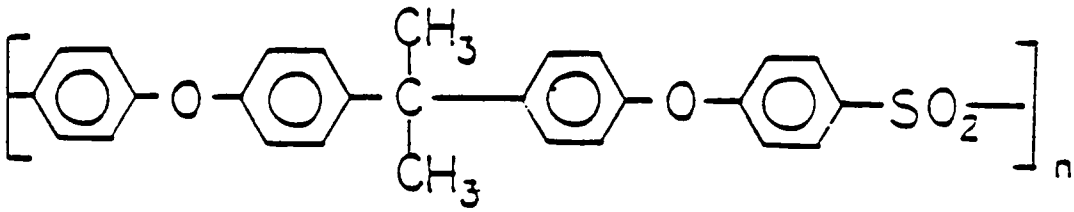

Polysulfone

Figure 4. Chemical structures of the polymers studied.

represents the degree of polymerization as the monomers join to form the polymer. The different film thicknesses were achieved by desolving 1.5, 3, 4.5, and 6 percent polymer in chloroform solvent on a weight basis. Because there were four substrate roughnesses, four film thicknesses, and two polymers to be tested, 32 substrates were required. Since only 24 substrates were initially prepared, films of the same material at two different thicknesses were cast on a single substrate.

The films were deposited on the substrates using an instrument called a "doctors's blade". A "doctors's blade" is a stainless steel hoop, 12.7 cm (5 inches) square, with each of the eight edges machined so that when the apparatus is placed on a surface, there is a gap between the edge and the surface. The eight gaps range in size from 0.127 mm to 1.27 mm (0.005 to 0.050 inches). The smallest, 0.127 mm, gap was found to give the smoothest and most uniform films, for the solution strengths used, and thus was used in this experiment. A sketch of the film depositing procedure is shown in Figure 5. Because the doctors's blade was larger than the specimens, two "side plates" were made with dimensions 5.0 by 15.2 cm (2 by 6 inches) such that the doctor's blade rode on the side plates as the film was deposited on the small specimens.

Films of two different thicknesses were deposited on each specimen by masking about half of the surface of the plate with transparent tape and casting a film on the exposed surface. After allowing about one minute of drying time, a razor was used to cut along the tape/film interface. The mask was then removed without destroying the just-deposited film. The half of the plate with the film was then masked over and a different film solution was cast on the now exposed surface. To

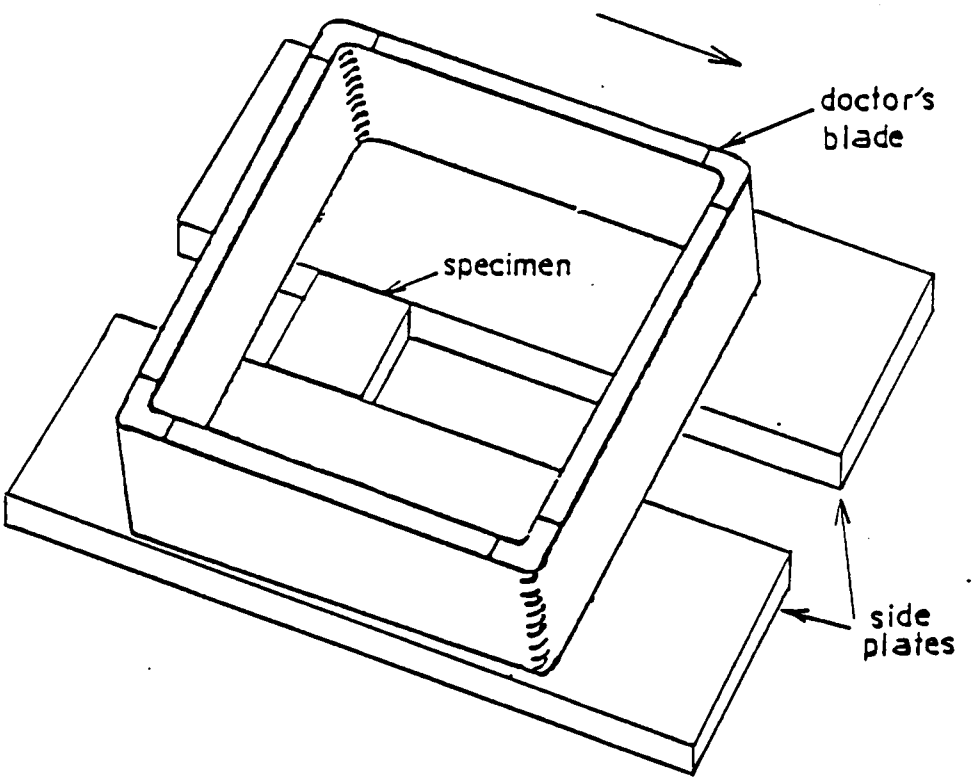

Figure 5. The film casting technique.

mask over the first film, great care was required. The adhesive sides of two pieces of tape were stuck together, leaving a 2 mm (0.05 inch) of adhesive surface width exposed. The first film was then masked over without touching the adhesive to the film, and consequently the mask could be removed without damaging the film.

Because the film solution casting process was certainly unorthodox and solution casting with a "doctors's blade" was known to produce films which were not as smooth and uniform as more refined casting methods, the film thickness variations on a single film and between separate "identical" films had to be measured. The method for performing these measurements will be discussed in detail later.

3.3 MEASUREMENT OF FILM THICKNESS

The thickness of the polymer films was measured using a Gaertner ellipsometer. The ellipsometer uses a helium laser which is polarized and shone onto a surface and the reflected light is picked up by an analyzer. From the change in polarization, determined by the analyzer, the thickness and the refractive index of the surface film can be found [28-32]. This method of determining the film thickness requires that the substrate upon which the film is deposited have a very high reflectance. For this reason, the roughened substrates could not be used when measuring the film thicknesses. Thus, an indirect approach had to be adopted.

This approach consisted of depositing the films on small "ferrotype" plates. "Ferrotype" plate is highly polished chromium plated steel sheet which is employed in the production of glossy photographs. This sheet

is used extensively in surface chemistry studies because of its surface smoothness and high reflectance. The sheet was cut into 25 mm (1 inch) square pieces. The polymer films were then cast on these sheets in a manner to closely simulate the deposition of films on the roughened substrates. This was done by masking half of the sheet with tape and depositing a film on the exposed surface. Two repetitions were made with each film solution for the two polymers studied. This gave a total of 16 specimens to be observed, which would hopefully give a measure of the variation of the film thickness on a single film and between identically prepared films. The thickness was measured at 25 locations over the film surface on one specimen and at 5 locations over the film surface of the "identical" specimen, to verify the repeatability of the casting process, and an average was calculated.

3.4 CHARACTERIZATION OF FILM SURFACES

The purpose of measuring the roughness of the polymer film surfaces was to determine the extent to which the film masked the substrate roughness. When the film was coated over the substrate roughness, the polymer filled in the valleys of the substrate, making the film thicker in the valleys than on the peaks, thus giving a lower roughness value than that of the substrate. This variation in film thickness occurs on a microscopic scale and cannot be controlled by the experimenter.

There is a nominal film thickness which would be expected as a result of using a specific polymer solution concentration to cast the film. The thickness of the films were not constant at this nominal value due to

imperfections in the casting process. Such imperfections caused gradients to be present in the film thickness in some areas and the film was not smooth in other areas. It was desired to take the profiles of the film surface in such a way to minimize any effects of these macroscopic film thickness variations. Before the surface readings were taken, the film surfaces were examined to choose an area where these imperfections were not present. Once found, five profiles at each of the three stylus traversing speeds were taken within this smooth area. The same sampling rates were employed to be consistent with the substrate surface readings and so that the film and substrate profiles could be directly compared. There was no way to position the stylus on the film so that it was exactly coincident with a stylus trace made on the substrate. Consequently, no phase relationship between the substrate and the film could be measured. However, the amplitudes of the substrate and film profiles could be compared. The method for calculating this amplitude relationship will be discussed later.

The stylus deformed the polymer when taking the surface profile, producing a "track" in the surface. The location of one track made at each stylus speed was marked with a tape arrow so that they could be observed in a microscope to measure the depth of penetration and to observe other important characteristics of the interaction between the stylus and the film.

3.5 OBSERVATION OF THE STYLUS TRACKS IN A SEM

After all the surface profiles of the polymer films were taken, the specimens were observed and photographed in a Scanning Electron Microscope (SEM). The operation was very time consuming and expensive, so only one track at each stylus speed was examined. The photomicrographs were used to measure the width of the sytlus track in the film. The depth of penetration of the stylus into the film was calculated using the width and the stylus geometry.

To determine the variation of this depth as the stylus was traversed across the surface, the width of the stylus tracks were sampled at discrete intervals along the track on the micrographs. Of course, the more samples of the depth taken, the more confidence there is in the results obtained. Ideally, one would like to take 1024 samples of the stylus trace depth, just as the Zonic DMS 5003 had taken 1024 samples of the surface profile. Unfortunately, this would require far more photographs than was economically and analytically justified.

For instance, for the traces made at a stylus speed of 91.4 mm/sec, the micrographs were taken successively along the length of the track at 2000X magnification. The width of the track was sampled at the same interval as the Zonic DMS 5003 had sampled the surface profile, every 3.05 μm, which converts to about every 6 mm on the micrographs. At this sample interval, 19 samples of the track width could be taken on each picture. Therefore, it would require 54 micrographs to sample the track width 1024 individual times! Handling that many photographs was simply not feasible, so other alternatives had to be considered.

As a solution, far fewer photographs were taken. For the traces made at a speed of 91.4 mm/min, only four photographs were made, from which 64 samples of the track width could be taken. For a stylus traversing speed of 18.3 mm/min, the sample interval of the DMS was 1.525 μm, or about 3 mm on the micrographs. Therefore, four micrographs were taken of the stylus scratch which allowed 128 samples of the track width. At a stylus speed of 3.6 mm/min, the DMS sample interval was 1.2 μm, which was 2.4 mm on the micrographs at 2000X magnification. Then, three micrographs were taken of the stylus track to give 128 samples of the track width. (See Table 1 for a summary.)

The width of the stylus tracks was measured using the Tektronix 4956 Graphics Tablet in conjuction with a program written by Dr. C. J. Hurst. Dr. Hurst's program was modified to suit my purposes. The Graphics Tablet is a 50 by 50 cm (20 by 20 inch) board through which two sets of tiny electrical wires are running. When the pen is placed at the point of interest, one wire grid determines the x-coordinate of the point while the other wire grid determines the y-coordinate. The tablet has a resolution of 0.127 mm (0.005 inch). The program, which reads these coordinates, was modified to measure the distance between two points, or the distance across the stylus track. Before starting the measurement, the tablet was set up with the scale. The scale used in the measurement was for a magnification of 2000X, divided by a factor cosine 20 degrees, because the photos were taken with the stage of the microscope tilted 20 degrees from horizontal for better optical resolution. Thus, a typical stylus track width of 5 mm on the photograph represented an actual width

of 2.66 μm on the polymer film. The corresponding resolution of graphics tablet at this scale is 0.068 μm.

For each stylus traversing speed, a horizontal scale was constructed with marks where the width of the stylus track would be sampled. For instance, the scale used for the stylus speed of 91.4 mm/min had the marks situated at intervals of 6 mm. The scale and the photograph on which to take the measurements were then placed horizontally on the tablet and the width of the track was sampled by taking two points at each interval, directly across the track from one another. The program read the data and subtracted the y-coordinates of two successive points to calculate the width of the stylus track. Then, the stylus tip geometry and track width were used to calculate the depth of the stylus track. A sample calculation is shown in Appendix E. The depth data were stored on tape and the program calculated statistics of the data, such as the mean penetration depth, the arithmetic average deviation from the mean, the mean square deviation, the RMS, the skewness, the kurtosis and the difference between the maximum and the minimum values of the depth.

3.6 ANALYSIS OF EXPERIMENTAL DATA

Different methods were devised to analyze the data collected in the previous section to determined what effects the parameters and materials have on the measurement of the film surface roughness.

A program written by John Herold entitled "STATS" was used for preliminary data analysis. The program calculates several statistical quantities of the surfaces including the arithmetic average roughness,

which is the only parameter the Talysurf profile meter has the capability of calculating. Another program written by John Herold calculates the Fourier transform of the surface profile of interest. This program was used to compare the frequency contents of the substrate and film surface profiles. The film thickness data was analyzed to determine the mean film thickness and the variation of the film thickness with position on specimen. All these analysis procedures will be discussed in the detail in the paragraphs to follow.

As mentioned in the previous section, surface profiles were collected in groups of five so that averaging could be performed to determine the experimental error. The "STATS" program has the capability of averaging the statistical parameters of up to ten surface profiles. In addition to the arithmetic average roughness, the "STATS" program also calculates the mean square deviation, the root mean square, the skewness, the kurtosis, and the maximum peak to valley height of the profile. A detailed description of these statistical parameters can be found in reference [27]. For each surface profile set, with the same film thickness, substrate surface roughness and polymeric material, the above statistical parameters were averaged to give the overall mean values for that data set. The results of this work are presented in Chapter 5.

4.0 PLANE-STRAIN MODEL OF STYLUS PENETRATION OF A POLYMER FILM

This chapter will discuss the development and implementation of a plane-strain slip-line field model of a profile meter stylus penetrating a polymer film. The plastic theory employed in the development of this model is discussed in Appendix A. A Fortran computer program was written to compute the slip-line field and the stresses in the deforming material. Another program was written to take the output of the above program and plot the resulting slip-line field. Copies of the programs are given in Appendix B.

There are basically two types of plastic flow problems. A steady motion problem is one in which the stress and velocity do not vary at any fixed point and the slip-line field does not change as the deformation progresses. The processes of drawing, extrusion, and orthogonal machining can be treated as steady motion problems. [1]

An unsteady problem generally is one in which the stress and velocity at a fixed point vary from moment to moment, rendering it much more difficult to solve. In some problems of this type the plastic region develops in such a way that the configuration of the slip-line field remains geometrically similar. That is, even though the size of the plastic region changes, the proportions of the field remain constant as the deformation continues. Examples of this type of situation are plane-strain wedge indentation and the expansion of a cylindrical or spherical cavity from zero radius in an infinite medium. [1,2]

A sketch of the proposed model is shown in Figure 6 for one specific indentation depth. The slip-line field is symmetric about the vertical centerline of the stylus, so only the right half of the field is shown in the figure. The model presented here is a type of unsteady model in which the proportions of the field change with the depth of the indentation, and thus does not exhibit geometric similarity. However, the latter example given in the previous paragraph was the inspiration for the stylus penetration model. The model for the expansion of a cylindrical cavity in a surface was proposed by R. Hill [1] and many of the characteristics of his model were employed in the development of the stylus penetration model.

4.1 ASSUMPTIONS AND BOUNDARY CONDITIONS

The slip-line field proposed for stylus indentation is for incipient deformation, meaning the cavity in the body is assumed to be preformed and then the stylus is applied to the cavity to bring the material to the yielded condition depicted by the slip-line field. This basic assumption greatly simplifies this otherwise very complex problem. A more realistic model would follow the motion of material from first contact of the stylus with the polymer to the stage of deformation the slip-line field represents.

It is also assumed that the deformation is of a semi-infinite material. Of course, in actuality, the polymer film is not semi-infinite and the substrate does have an effect on the depth of penetration of the stylus. Another simplifying assumption is that there is a normal pressure

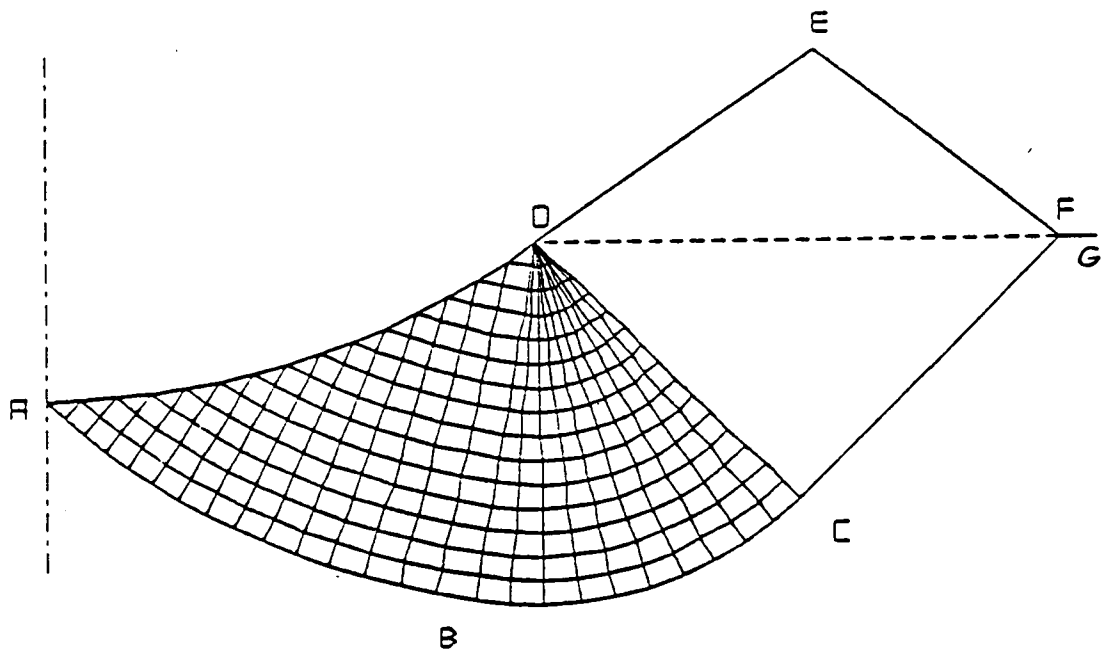

Figure 6. A slip-line field model for profile meter stylus indentation of a polymer film.

distributed over the stylus tip and that there is no friction between the stylus and the polymer. The frictionless assumption is a realistic one because of the low surface energy of the polymers being studied which insures low adhesion forces between the stylus and the film.

The program also takes into account the effect of hydrostatic pressure on the yield strength of the polymer. A simplified representation of the stress-strain behavior is shown in Figure 7. The material is assumed to be rigid ($E=\infty$) until stressed to the yield point where it becomes perfectly plastic. It is assumed that the yield strength varies linearly with hydrostatic pressure at a rate of 0.188 times the pressure [16]. The effect of strain rate on the yield strength is neglected in the model.

The following discussion will refer to Figure 6. By the frictionless assumption, there are no shear stresses over the cavity surface AD, which has a radius R. Thus, from Mohr's circle, the slip-lines, or the directions of maximum shear stress, must meet the surface AD at 45 degrees. Similarly, the slip-line CF must intersect the stress-free surface FG at 45 degrees. The stylus forces are applied only over the surface AD and not on DE. Since the surface of the coronet (a term coined by Hill [1]) CDEF is free from applied loads, the elements of the coronet must have unloaded from their former plastic state. The coronet moves outward as a rigid-body, carried on the plastically deformed material beneath. Thus, the slip-line CF is a straight line.

Since CF is a straight line, the normal pressure along this slip-line is constant by Hencky's theorem, Equation 38, and equal to p_o, for instance. The normal pressure along the slip-line CD is fixed in terms of p_o and the shape of CD is determined by the same theorem. The shear stress

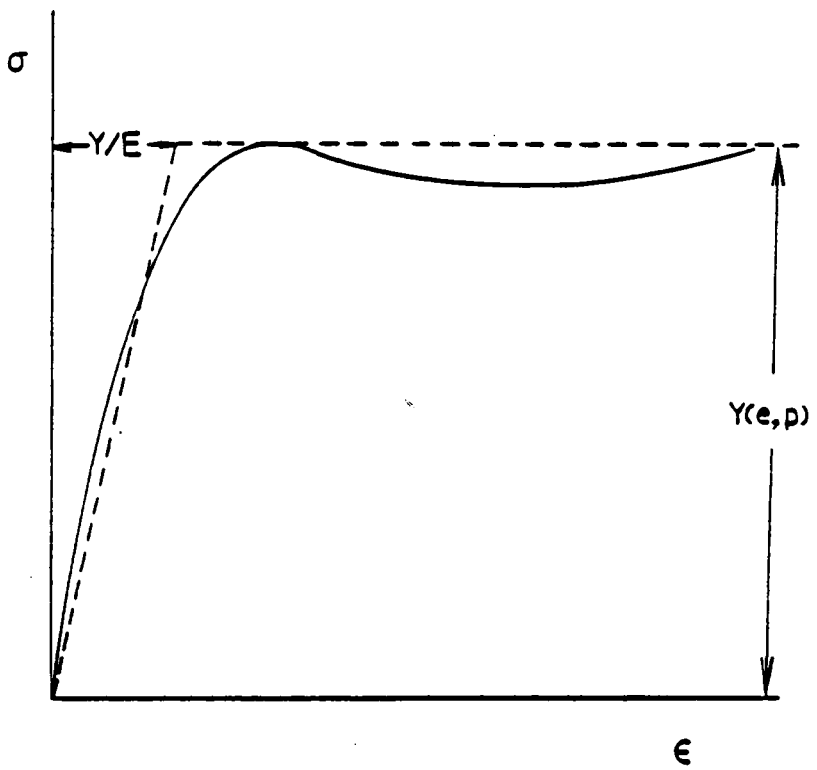

Figure 7. Stress-strain curve for a polymeric material.

at all points on CD and CF is the flow stress k; the sign of k is such that CF is an α-line. By constructing a free-body diagram of the coronet CDEF, one is convinced that the rigid-body can be in equilibrium only if CD is a straight line and $p_o = k$. It follows again from Hencky's theorem, Equation 36, that all β-lines in the field are straight, and the α-lines in the field ABD are involutes of a circle with radius $R/\sqrt{2}$. [1]

We still need to verify that CD is the base of the rigid coronet, which is true if the normal component of velocity on CD is uniform. By the second of Geringer's equations, Equation 33, the velocity component V is constant along each β-line, and is therefore zero throughout the field since it is zero on the plastic-rigid boundary ABC. Hence, by the other Geringer equation, the component U is constant along each α-line. Since the cavity is expanded radially at unit speed, by Equation 33, U is equal to $\sqrt{2}$ on ABC. Again, by Geringer's equations, the value of U is the same for all elements in the region ABCD, and the coronet slides outward along CF with speed $\sqrt{2}$.

4.2 THE COMPUTER PROGRAM

This section will discuss the elements of the computer program written to calculate the slip-line field for the stylus indentation problem. The progression of the calculations made by the program is as follows:

1. The surface of the cavity AD is computed as a cylindrical surface.

2. The slip-line ABC on the plastic-rigid boundary is calculated. The section AB is an involute of a circle and BC takes the form of a circular arc. (See Appendix C for a derivation.)

3. The coordinates, inclinations, and velocities are calculated at the remaining nodal points of the field starting from the boundary conditions on the cavity surface and the slip-line ABC.

4. The hydrostatic pressure at the nodal points is calculated in a reverse manner, starting with the known hydrostatic pressure on the coronet CDEF.

5. The normal stress on the cavity surface is computed from which is resolved the vertical forces exerted by the stylus to cause the deformation.

6. Now that a complete solution has been found for an ideal rigid-plastic material, a new yield stress distribution is calculated as a linear function of hydrostatic pressure [17] at the nodal points using a subroutine called "KCONVG".

7. A new slip-line field is calculated by solving the variable flow-stress equations, Equation 42 and Equation 37. These equations are nonlinear in x,y, and ϕ and are solved iteratively by writing a truncated Taylor series for each of the three equations. [33] These calculations are handled by a subroutine "VARIK".

8. Steps 4,5,6 and 7 are repeated until the flow stress distribution throughout the field reaches a steady state.

More details of these computational steps are discussed in Appendix C.

5.0 RESULTS

The results of this study are both experimental and theoretical. The experimental results include qualitative observations of the scanning electron micrographs of the stylus tracks in the polymer films. For any particular stylus track, an average penetration depth can be calculated. If the ensemble of penetrations is absolutely normalized to the average value, the arithmetic average value of the normalized penetrations can be calculated. This value will be termed the D_a. The experimental data, obtained from the micrographs and from surface profiles, were analyzed to assess the first- and second-order effects of the independent variables: film thickness, substrate roughness (R_a), stylus speed, and polymer, on the dependent variables: measured film surface roughness, stylus penetration depth, and D_a. The transfer function between the substrate and film surface profiles was also studied to determine the effects of the dependent variables. Results are presented to show the correlation between the percent of polymer solutions prepared and the resulting film thicknesses.

The theoretical results to be presented are related to the work performed in developing the plastic deformation model to describe the indentation of a polymer film over a hard substrate by a profile meter stylus. It was desired to find the force required to cause a specific indentation depth. Curves of force versus depth of indentation are presented for two different material types: 1) an ideally rigid-plastic material and 2) a material with mechanical properties sensitive to

hydrostatic pressure. Also, sketches of slip-line fields are presented which depict the approximate shape of the plastic region resulting from the stylus indenting the film at several indentation depths.

5.1 EXPERIMENTAL RESULTS

5.1.1 SEM PHOTOMICROGRAPHS

A Scanning Electron Microscope (SEM) was used to observe the deformation of the polymer films by the profile meter stylus. Micrographs representing all of the possible combinations of film thickness, substrate roughness, and stylus speed were taken, but only one stylus track for each situation was observed. This section will consist mainly of qualitative observations and discussion of the results obtained from the SEM work.

In taking and analyzing the micrographs, it was desired to observe and study certain characteristics of the stylus/film interaction. One such characteristic is the depth to which the stylus indents the polymer film as it is traverved across the surface. The depth of indentation was measured from the micrographs and the effects of the independent variables is presented in the section to follow.

Another concern is the variation of the depth. This variation is caused by the acceleration of the stylus as it traverses the surface and by the strength of the polymer and the stiffness of the underlying substrate. On the micrographs, the variation is observed relative to the surface of the polymer film. If the depth varies, this indicates that

the stylus instrument is not giving an accurate measurement of the roughness of the polymer film surface. For example, if the polymer film deposited on the substrate is thick and the substrate itself is very smooth, one can be confident that an accurate measurement of the film surface roughness has been obtained. An example of such a situation is shown in the micrograph of Figure 8. In this case, the effect of the substrate stiffness is small. Also, the acceleration effect is small because the thick film has masked over the smooth substrate resulting in a very smooth polymer film surface. Thus,there is very little variation in the depth of indentation.

For another example, if the roughness of the substrate is large and the film is very thin, as shown in the micrograph of Figure 9, there is a great deal of variation of the depth of indentation. Notice in the micrograph that the underlying substrate roughness can be seen through the film. One can easily differentiate the ridges and valleys in the ground surface. As the stylus is traversed across a peak, it is forced to accelerate upward, exerting a greater force on the surface and thus indents further. Also, notice that as it crosses through a valley, the stylus indents the film surface to a lesser degree. This variation of the depth of indentation results in an erroneous measurement of the film surface roughness.

As the stylus traversing speed was increased, it was observed that the depth of indentation decreased. This phenomenon can be explained by the viscoelastic behavior of the polymer and the geometry of the stylus. If the profile meter is set to give a faster stylus traversing speed, the

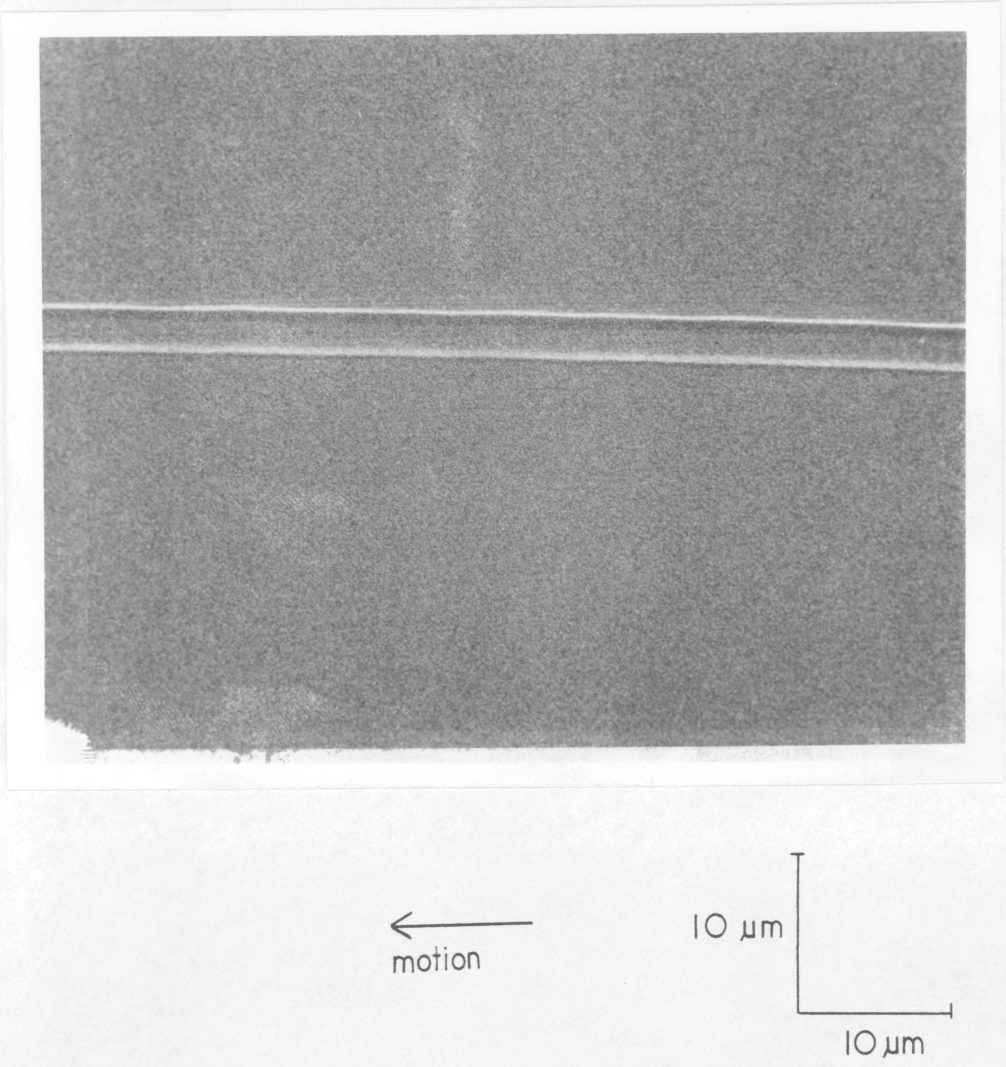

Figure 8. Photomicrograph showing the deformation of a thick polymer film on a smooth substrate by a profile meter stylus.

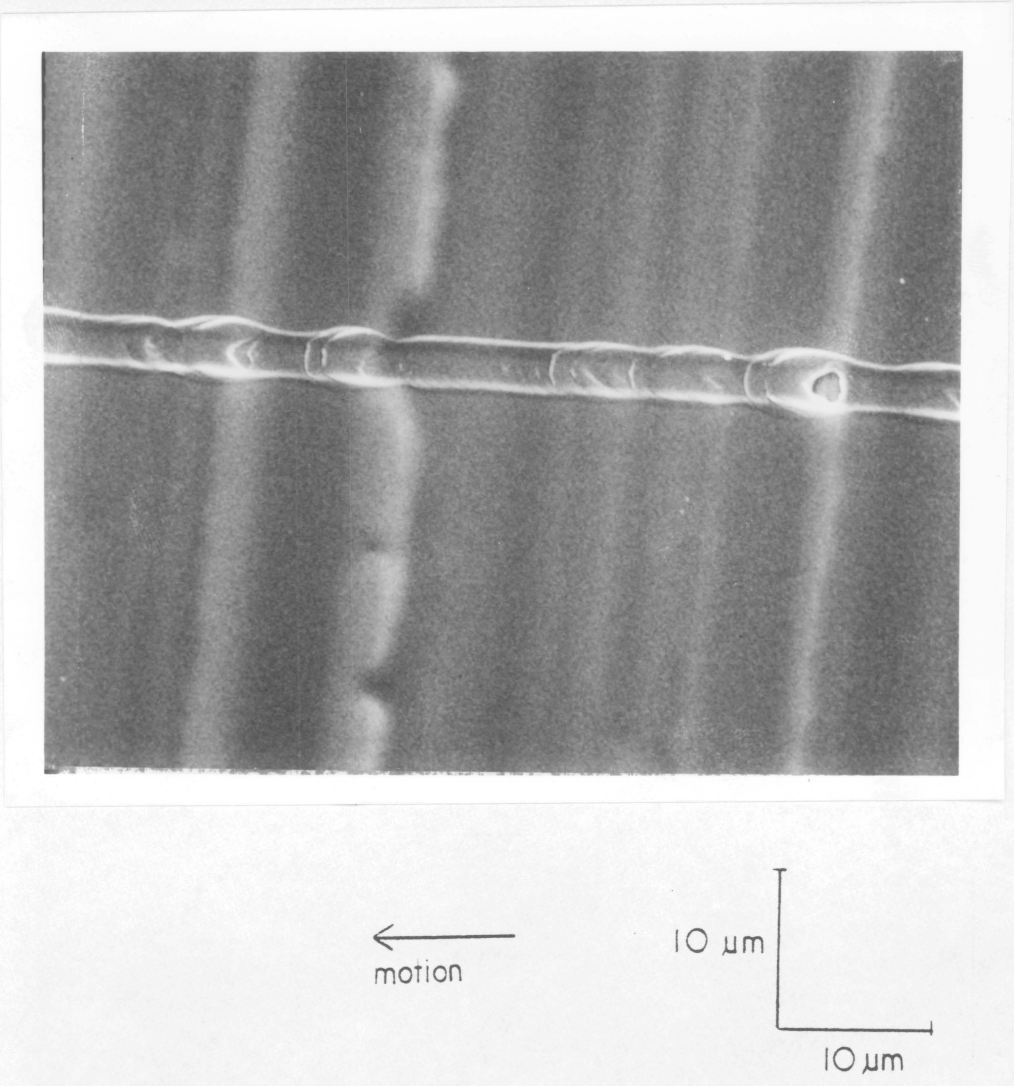

Figure 9. Photomicrograph showing the deformation of a thin polymer film on a rough substrate by a profile meter stylus.

resistance to deformation of the film is greater, thus the stylus does not indent as deeply.

5.1.2 FILM THICKNESS MEASUREMENTS

Figure 10 shows plots of the average film thickness as measured by ellipsometry versus the polymer solution concentration used to deposit the film on the substrate. The plots, prepared using the "Statistical Analysis Systems" (SAS) package [34], with 95 percent confidence limits, show that polysulfone results in a significantly greater film thickness than polystyrene when prepared with the same solution concentrations. As can be seen, a second-order function, almost linear, gives a good approximation of the relationship between film thickness and solution strength.

5.1.3 DEPTH OF STYLUS INDENTATION

The experimental data obtained from the micrographs and input to the SAS program are shown in Appendix F. Figure 11 shows the first-order effect of stylus speed on the mean depth of penetration of the stylus, measured on the micrographs. The confidence intervals are not shown on the plot, but the analysis, using the Tukey test [35,36], showed that the depth of indentation for the fastest stylus traversing speed is significantly less than at the lower two speeds. The linear curve fits the data points well, showing the general effect of stylus speed. Also, it was

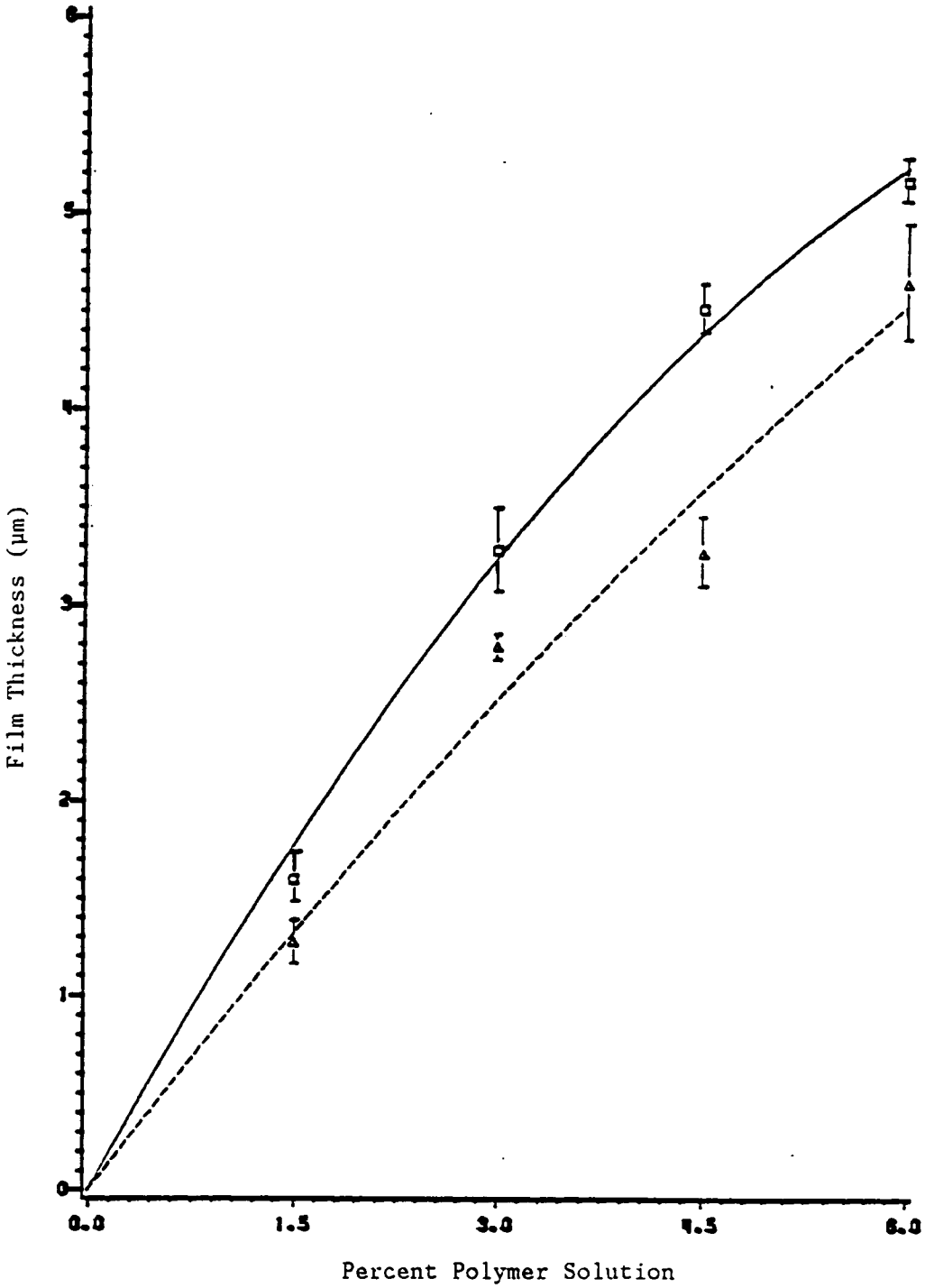

Figure 10. Polymer film thickness as a function of the solution concentration used to deposit the film.
(——□) PSF, (-----△) PS

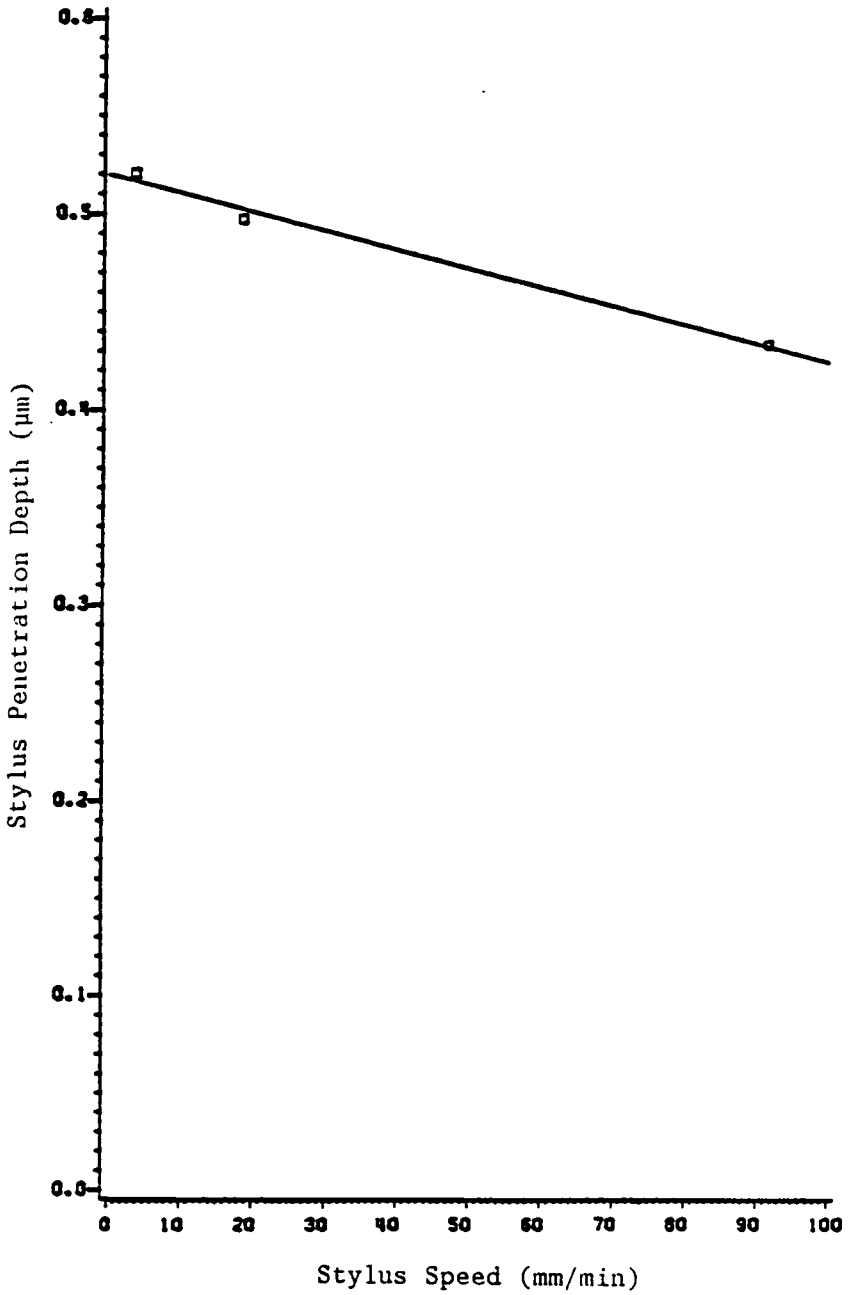

Figure 11. Effect of stylus traversing speed on stylus indentation of a polymer film.

found that the effect of stylus speed was no different for the two polymers in this study.

The first-order effect of substrate roughness on the stylus indentation depth is illustrated in Figure 12. The analysis revealed that the depth of indentation is significantly greater for the roughest substrate surface than for the three smoother substrates which are not statistically different from one another. Thus, it appears that the depth of indentation increases as the substrate roughness increases, but this effect does not prevail over the entire substrate roughness range.

The first-order effect of film thickness could not be assessed since the two polymers did not result in the same film thickness when prepared with the same solution concentrations. More preliminary work should have been performed by varying the solution concentrations to insure that comparable film thicknesses were obtained for the two polymers, discounting the effect of solution strength. In any event, the effect of polymer solution concentration on the depth of indentation is illustrated in Figure 13. Exponential functions have been fit through the data points since the depth of indentation must be zero when the film thickness is zero. Notice that the film thicknesses chosen lie near the flat portions of the exponential curves, in the range of steady-state indentation. If some thinner films had been chosen, the process of assessing the effect of film thickness would have been simplified. The SAS analysis showed that the only significant differences were that the stylus indents more deeply into a film prepared with a 6 percent than a 3 percent solution.

The depth data were also analyzed to find the second-order effects on the mean value of stylus penetration depth of polymer and film thick-

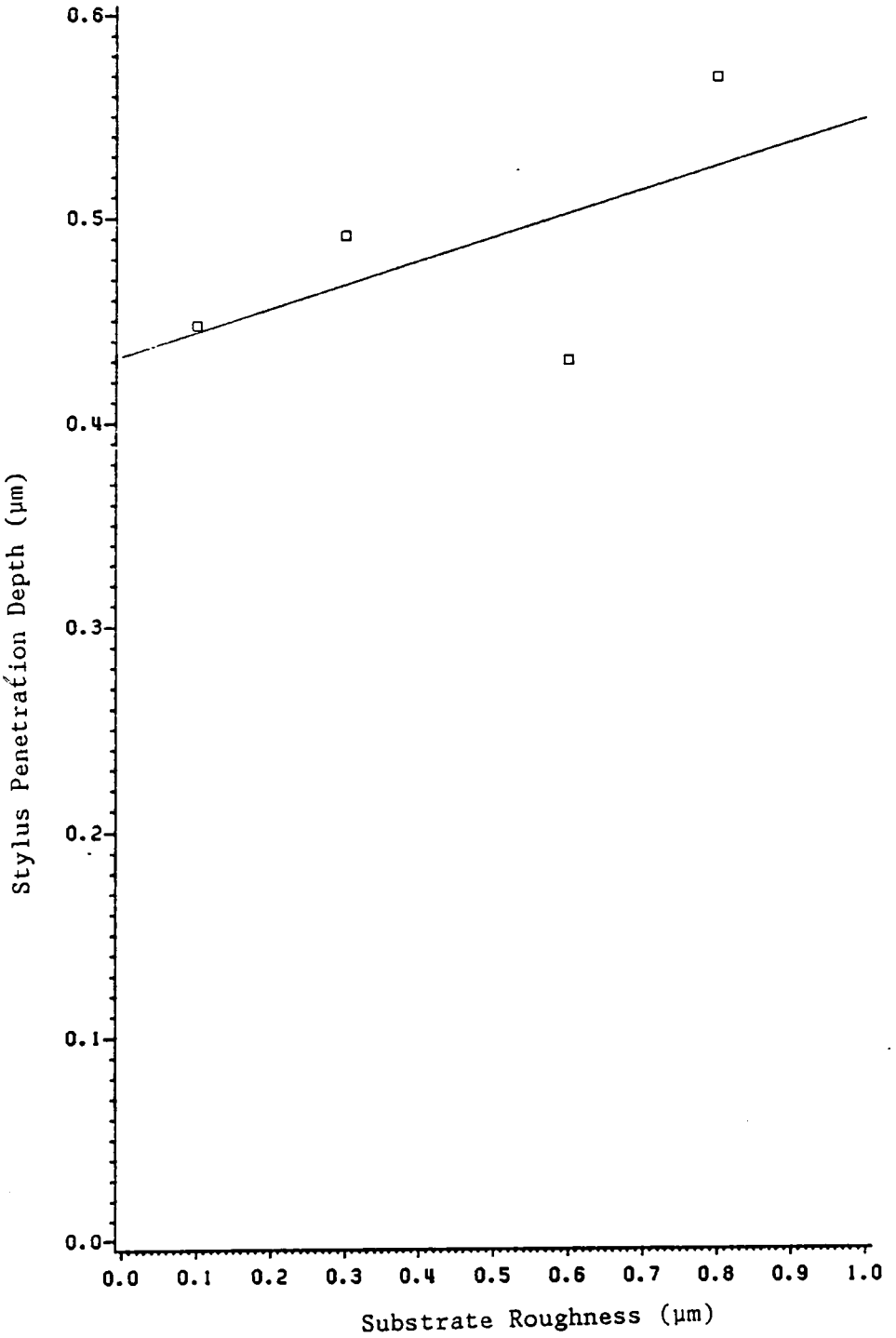

Figure 12. Effect of substrate roughness on stylus indentation of a polymer film.

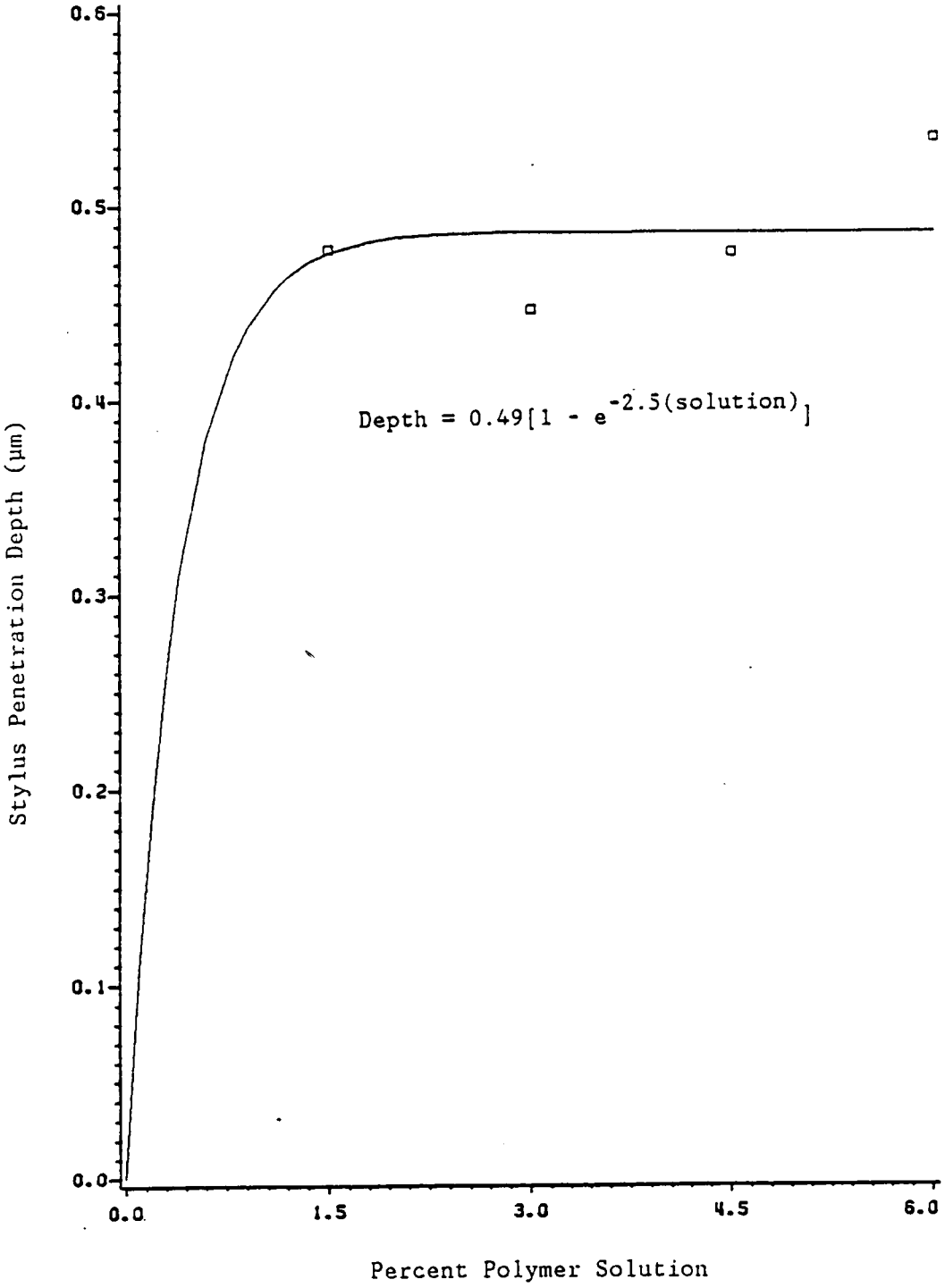

Figure 13. Effect of polymer solution concentration on stylus penetration of a polymer film.

ness. The statistical analysis showed that the data are not significantly different in most cases. For polysulfone, none of the mean depths are significantly different from one another. For polystrene, only the mean stylus indentation depths corresponding to the upper and lowermost film thicknesses are significantly different.

The second-order effects of substrate roughness and stylus traversing speed are presented in Figure 14. The curves are not intended to show significance in the data, but to show the general trend of the effects of these two independent variables. Notice that the slope of the straight line corresponding to a substrate roughness of 0.8 μm has a higher negative value than the other lines. This would suggest that the effect of stylus speed on the depth of indentation is greater for a rough substrate than a smooth substrate. The lines for the three smoother substrates are essentially parallel, meaning that substrate roughness and stylus speed jointly have little effect for lower substrate roughnesses.

The joint effects of stylus speed and film thickness are shown in Figure 15. As shown in the figure, the slopes of the straight lines through the data become progressively less negative as the film thickness, represented by the polymer solution concentration, increases. This suggests that the effect of stylus speed on the depth of indentation decreases as the film thickness increases.

5.1.4 VARIATION OF THE STYLUS INDENTATION DEPTH

The arithmetic average deviation of the depth of penetration from the mean depth (D_a) is also of importance to this study. If this deviation

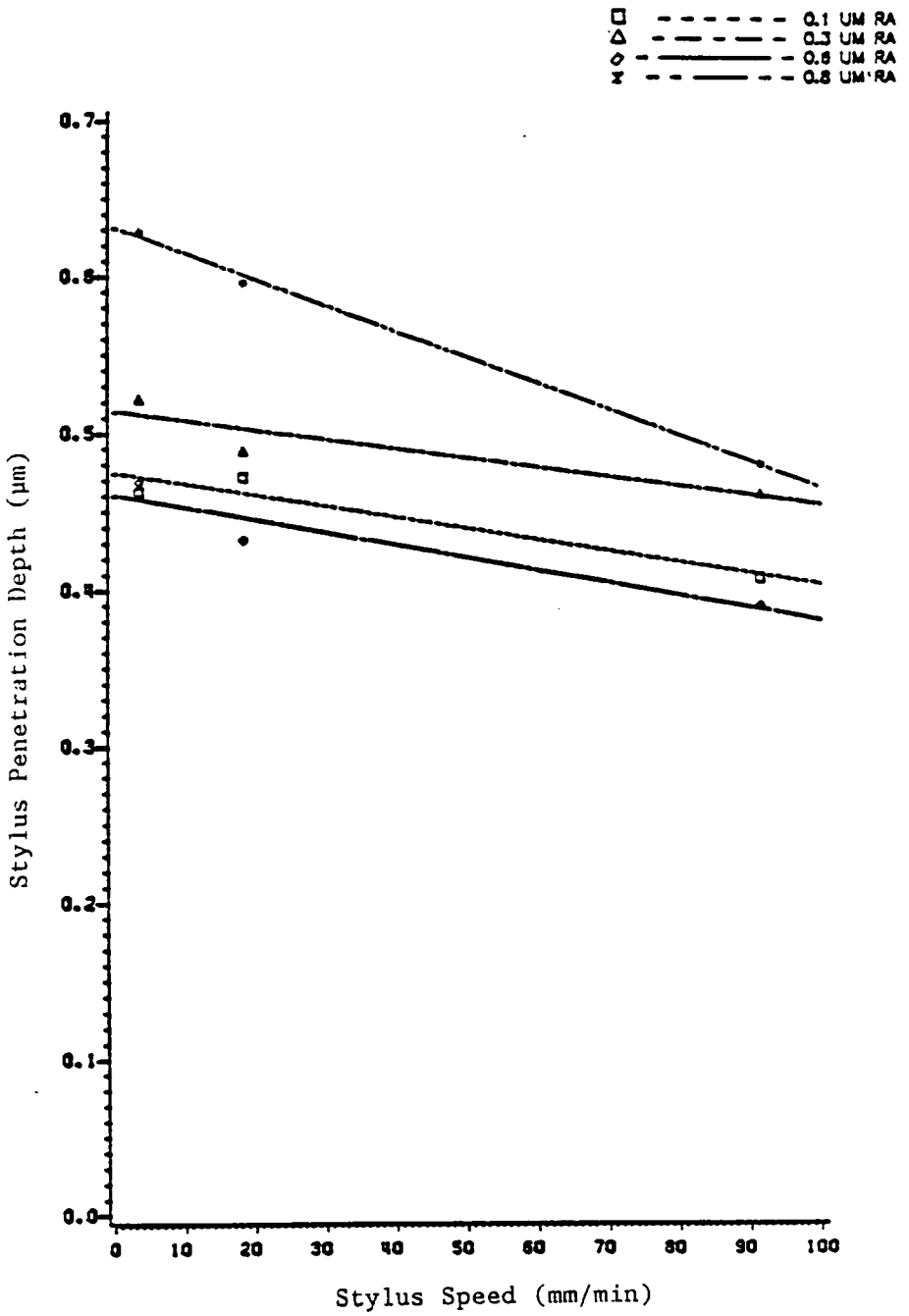

Figure 14. Effects of stylus speed and substrate roughness on stylus indentation depth.

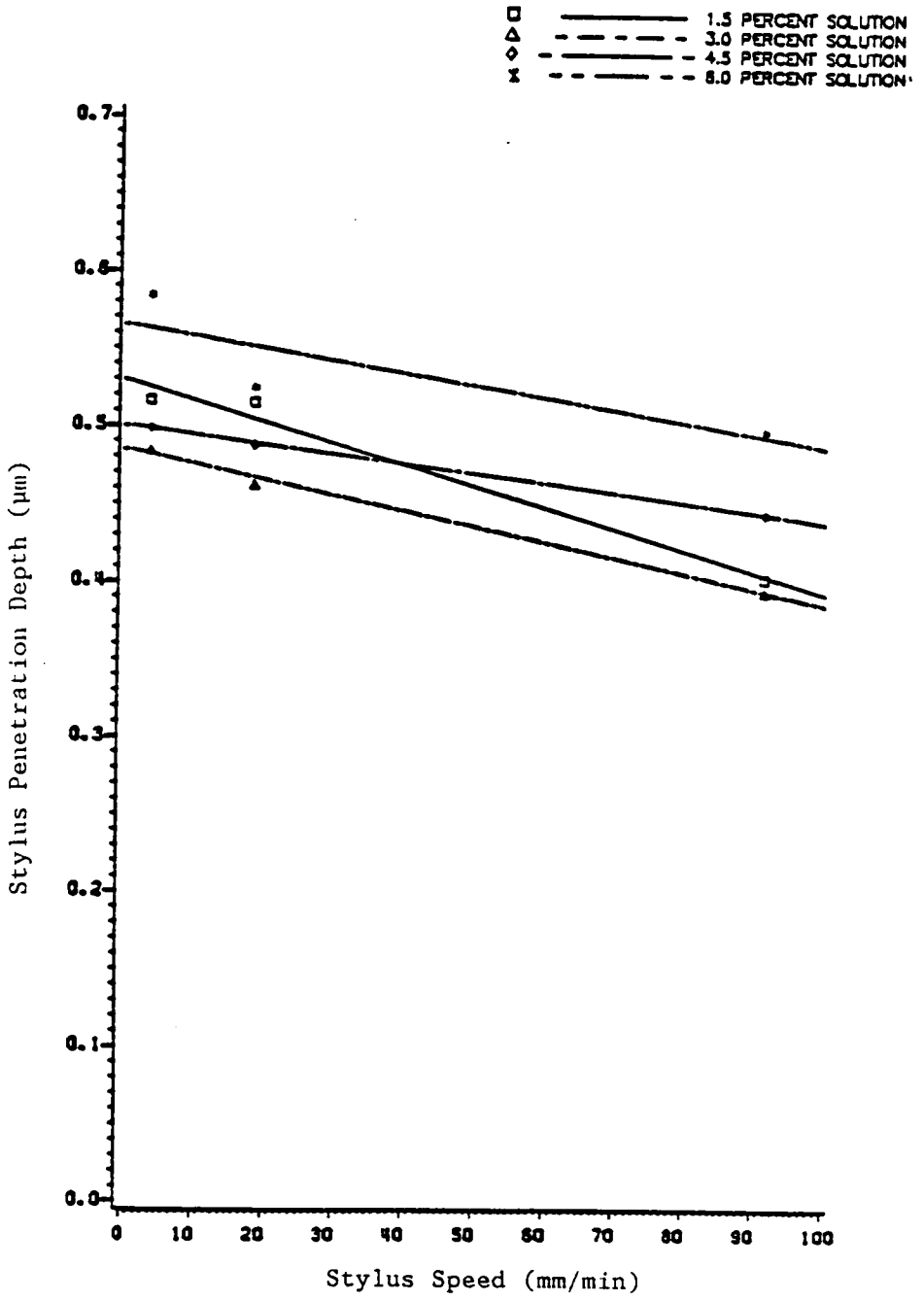

Figure 15. Effects of stylus speed and percent polymer solution on stylus indentation depth.

is small, the reading the profile meter obtains for the film surface roughness is very close to the actual value. As sketched in Figure 16, the stylus will indent the film surface more deeply as it accelerates up and over a peak and less deeply as it crosses through a valley in the surface. Also notice that as the stylus indents deeper, closer to the substrate, the substrate stiffness comes into effect, and the stylus will indent less. Thus, the acceleration and substrate effects counteract one another. This variation in the depth, relative to the film surface, thus results in an erroneous measurement of the film surface profile. The purpose of the analysis in this area is to determine the effect of the independent variables on the accuracy of the measurement obtained.

The first-order effect of substrate roughness on the value of the D_a is shown in Figure 17. A function which have a zero ordinate intercept has been fit through the data, since the film surface would be perfectly along with the substrate. The analysis by the SAS program showed that all the D_a values represented by the data points in the figure are significantly different except those points corresponding to nominal substrate roughnesses of 0.3 and 0.6 μm. Thus, one can be confident in stating that the variation of the depth of indentation increases as the roughness of the substrate increases.

Figure 18 shows the joint effect of substrate roughness and polymer on the variation of stylus penetration depth (D_a). Again, functions with a zero ordinate intercept have been fit through the data. The confidence intervals,represented by plus (+) signs, are large due to the averaging process, but, still, the means corresponding to the smoothest and roughest substrates are significantly different. Notice especially that the type

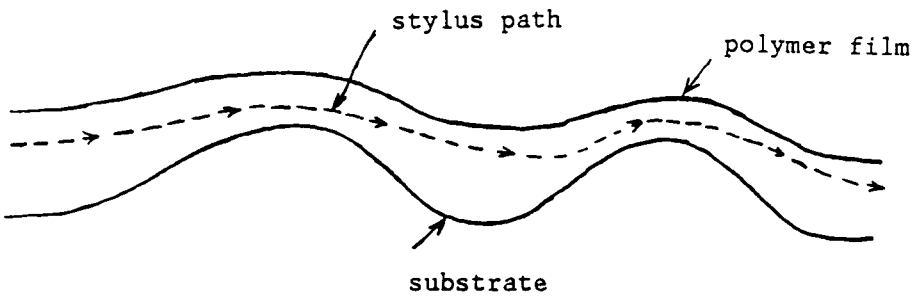

Figure 16. How the depth of indentation of the stylus changes as it traverses the polymer surface.

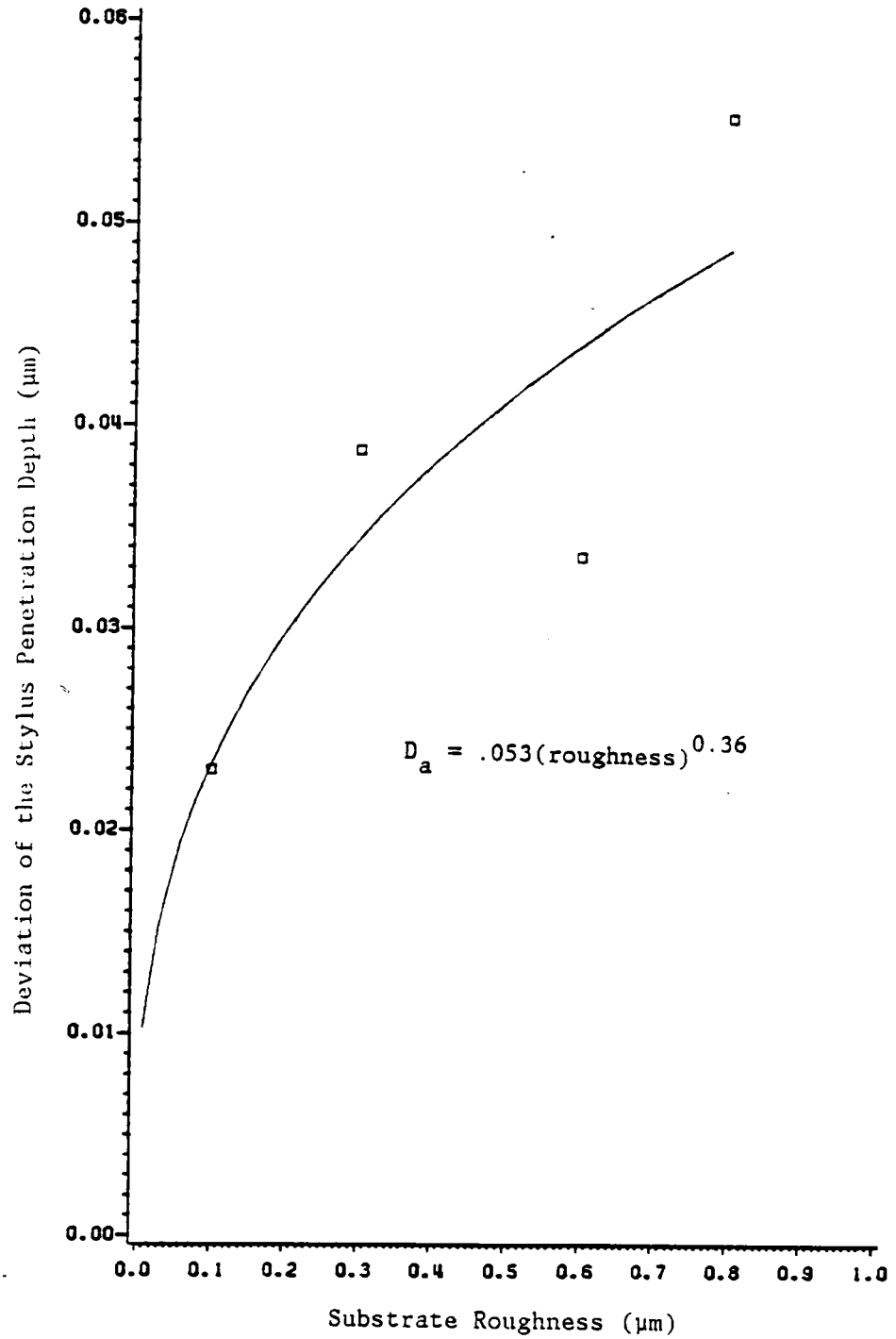

Figure 17. The effect of substrate roughness on the average deviation of the stylus penetration depth (D_a).

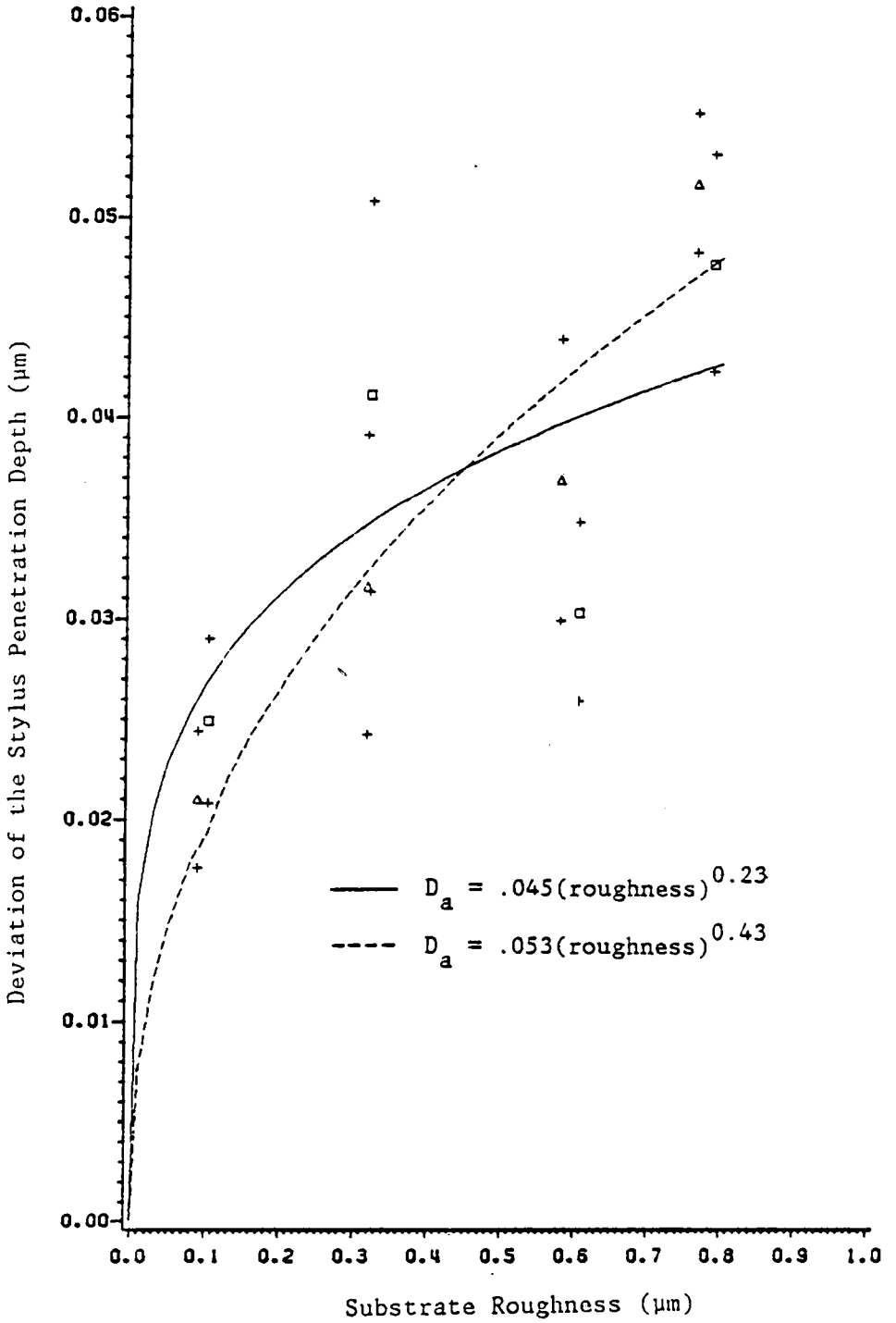

Figure 18. Variation in the stylus indentation depth as a function of the substrate roughness : (——□) PSF (-----△) PS

of polymer has no significant effect on the relation between substrate roughness and stylus indentation depth variation.

The effect of stylus speed on the variation of the stylus indentation depth is shown in Figure 19. The analysis revealed that the D_a value for a stylus speed of 91.4 mm/min is significantly less than the value at 3.6 mm/min. This illustrates the viscoelastic property of polymers. As the stylus speed increases, the strength of the material increases causing the stylus to follow the surface more closely. Further analysis showed that the effect of stylus speed is no different for the two polymers studied.

The first-order effect of film thickness on the D_a could not be assessed for the same reason which was stated when referring to the mean depth of indentation. In any event, the effect of polymer solution concentration can be assessed and is shown in Figure 20. Statistical analysis reveals that the variation of the stylus indentation depth decreases significantly as the film thickness increases due to using a higher solution concentration. The D_a values for solutions of 3, 4.5, and 6 percent are not significantly different from one another, but the value corresponding to a solution of 1.5 percent is statistically higher than the other three solution concentrations. Still, one must be cautious because these observations refer to solution concentrations, and the same solution concentration will not result in the same film thickness for two different polymers.

The SAS program calculated the effect of solution concentration on the mean value of the D_a. The results of these calculations are illustrated by the curves in Figure 21, with the 95 percent confidence limits

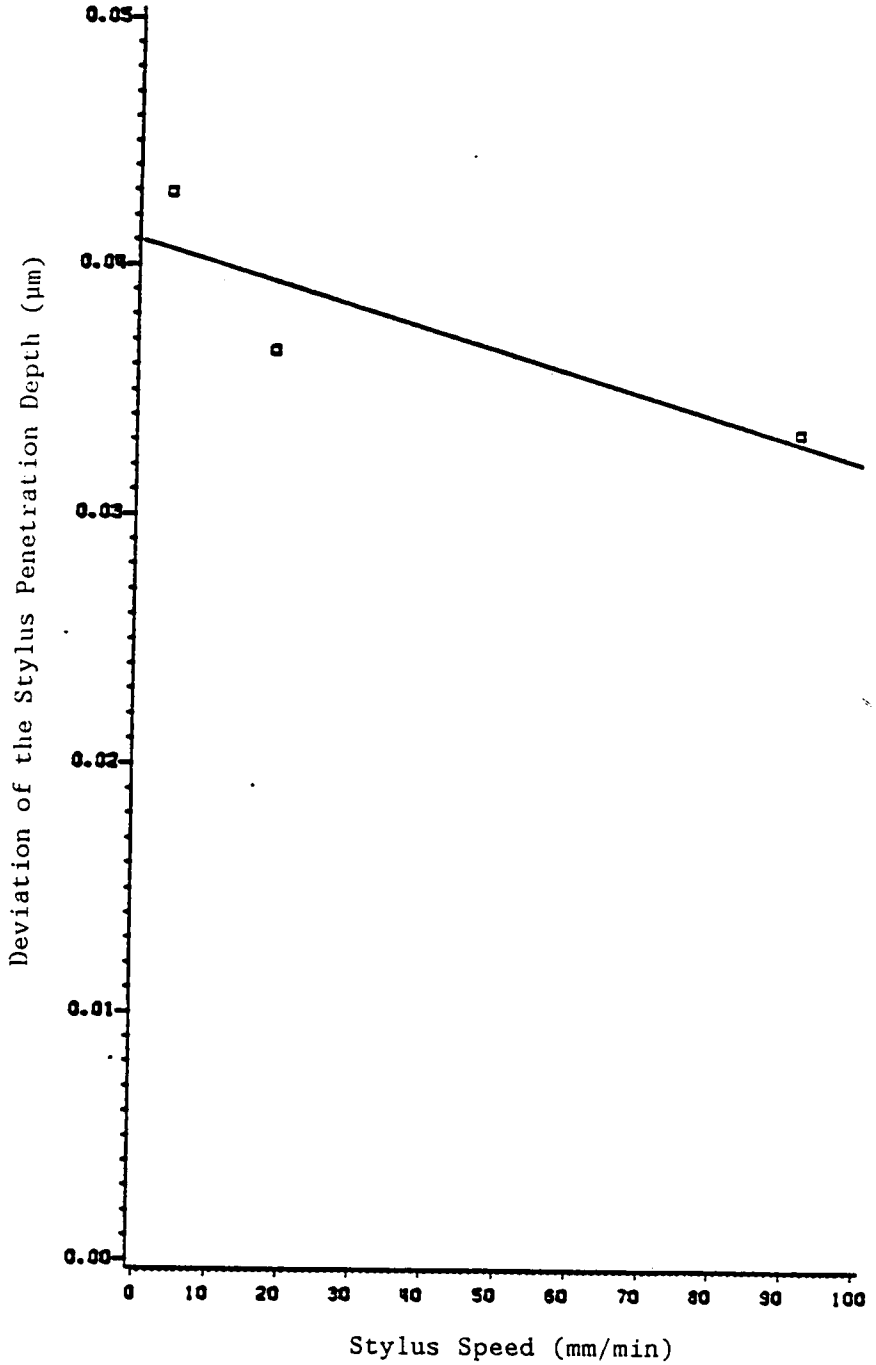

Figure 19. The effect of stylus traversing speed on the variation of the stylus penetration depth (D_a).

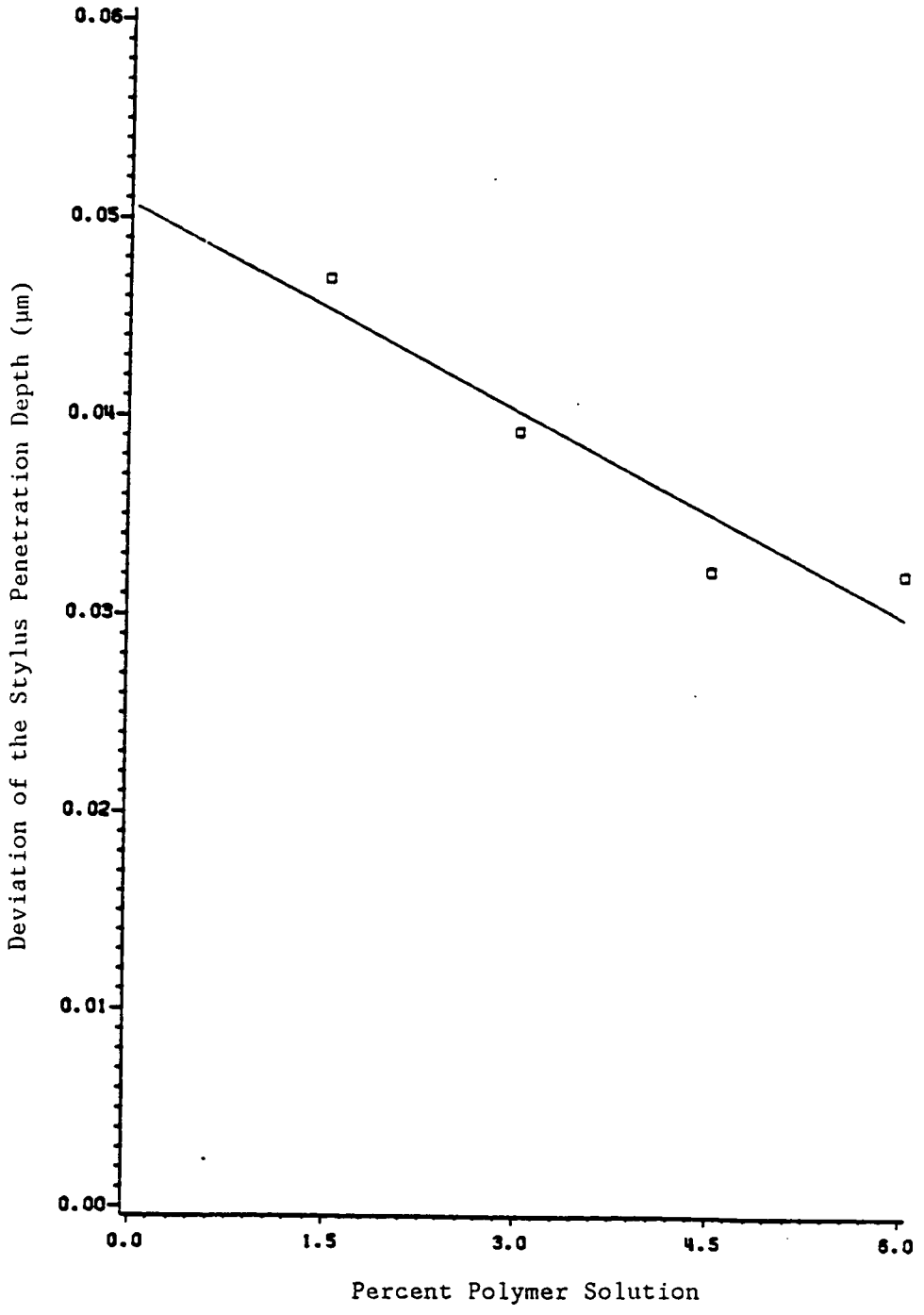

Figure 20. The effect of solution concentration on the variation of the stylus penetration depth (D_a).

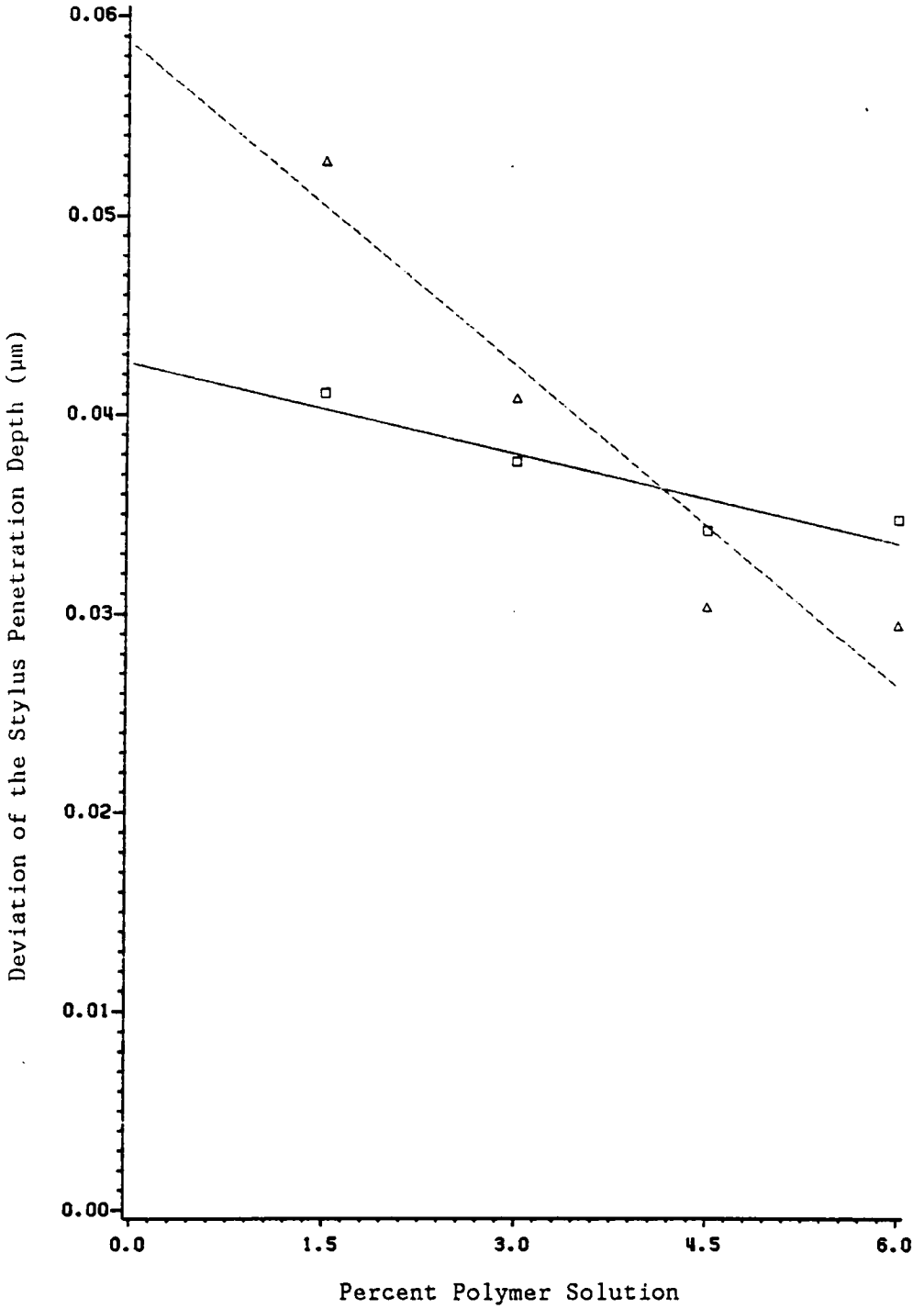

Figure 21. The average deviation of the stylus penetration depth as a function of polymer solution concentration: (——□) PSF, (-----△) PS

on the data points also shown. It is observed that the D_a is inversely related to the thickness of the polymer film, but this method of analysis yields large confidence intervals so no firm conclusions can be drawn.

The second-order effects of stylus speed and film thickness is represented by the least-squares fit lines in Figure 22. Notice that, as a general trend, the slopes of the lines become less negative as the thickness of the film increases. There seems to be little effect of stylus speed on the variation of the depth of indentation when the film thickness is large. The author recognizes that the hard substrate has a greater effect on the D_a than does the speed of the stylus, and as the film thickness increases the effect of the substrate decreases.

5.1.5 MEASURED FILM ROUGHNESS

Of great importance to the study of polymer film surfaces with a stylus-type profile meter is the measurement of roughness obtained when the stylus is traversed across the surface. One would expect the measured film roughness to correlate well to the substrate roughness, attenuated by the effect of the polymer film and the dynamic interaction of the stylus with the film. The correlation of the measured film roughness to the substrate roughness is shown in Figure 23. The slope of the line in the figure is about 0.89. This relation is the essentially the same for the two polymers studied. Notice that this is the measured value of the film roughness, not the actual value.

The original intended purpose of this thesis was to determine the actual polymer film surface roughness knowing the measured value obtained

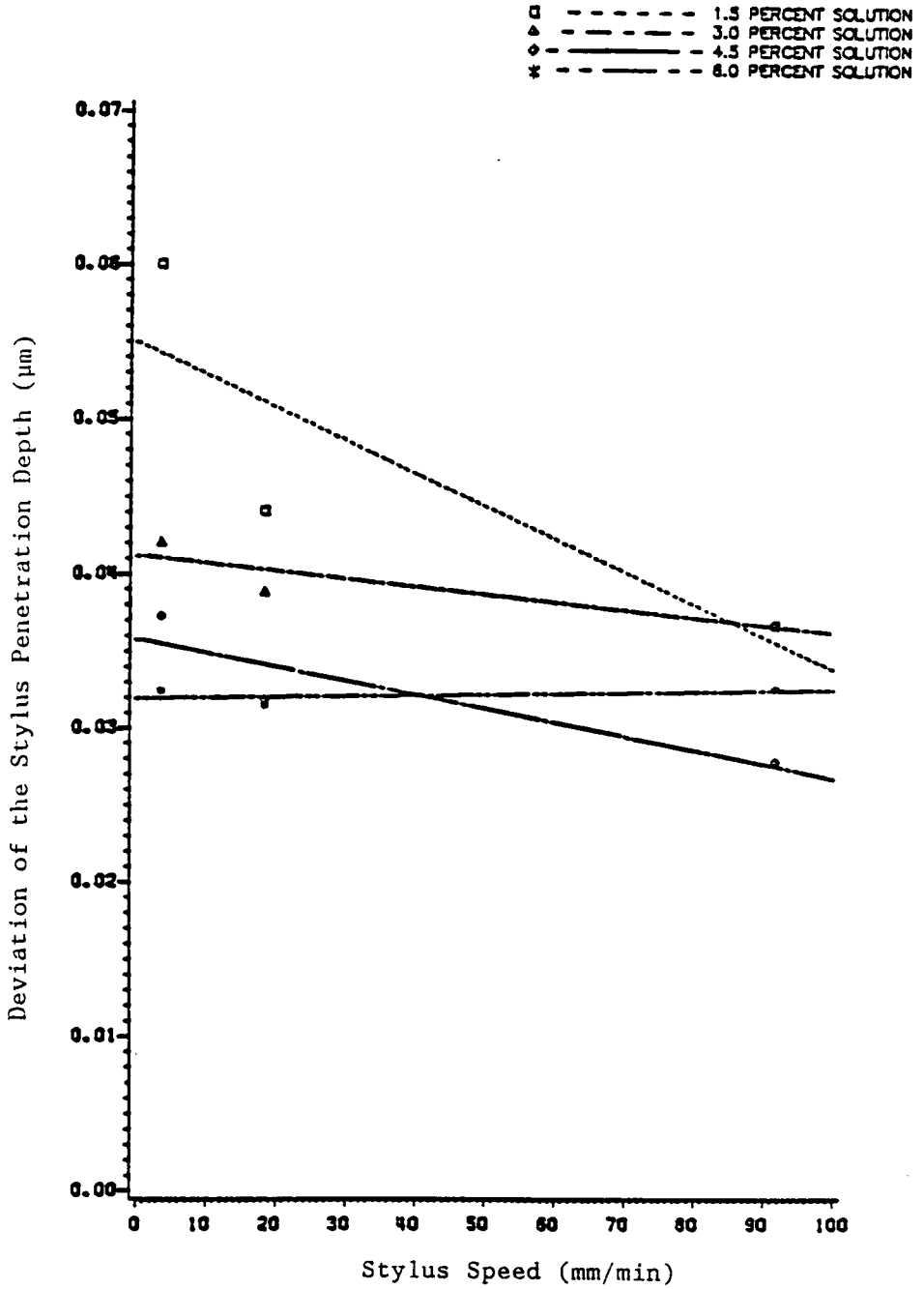

Figure 22. Effect of stylus speed and polymer solution concentration on the variation of the depth of stylus indentation.

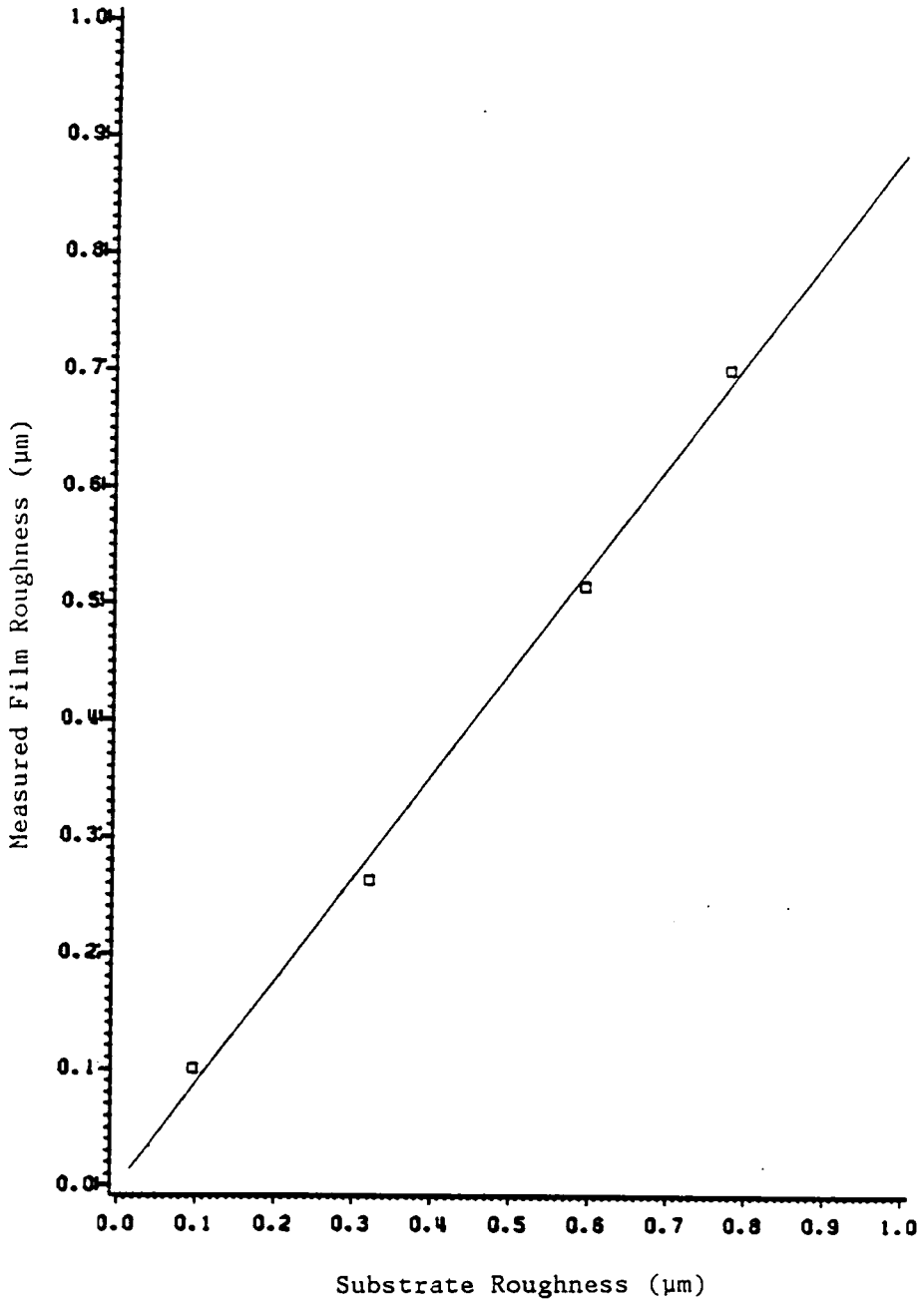

Figure 23. Effect of substrate roughness on the measured value of film surface roughness.

by the profile meter. However, to do so would require knowing far more information than is presently at our disposal.

One proposed method for estimating the roughness of the polymer film surface is to account for the amount which the stylus indentation depth varies as the measurement is taken. If this variation is zero, the measurement of the film surface roughness is exact, as far as variations with a wavelength greater than or equal to the sampling interval of the measurement process. If the phase relationship between the measured film profile and the depth data sampled from the micrographs were known, the actual film surface profile could be obtained by adding the depth of indentation to the corresponding elevation of the measured film profile. However, this phase relationship is not known and could not be controlled in the experiment.

The stylus traversing speed, as shown in Figure 24, has negligible effect on the measurement of film roughness. The slope of the line through the data has a very slight upward slope with stylus speed. This observation can be explained by the fact that the D_a decreases as the stylus speed increases. Instead of the stylus indenting more deeply as it crosses a peak, it follows the the surface more closely when the stylus is moving faster. Thus, the D_a is less and the measured film roughness is greater.

Another illustration of the effect of substrate roughness on the measured film roughness is shown in Figure 25. The four lines corresponding to the different substrate roughnesses are approximately parallel and horizontal, again showing that the speed has very little effect, and its effect does not change as the substrate roughness changes.

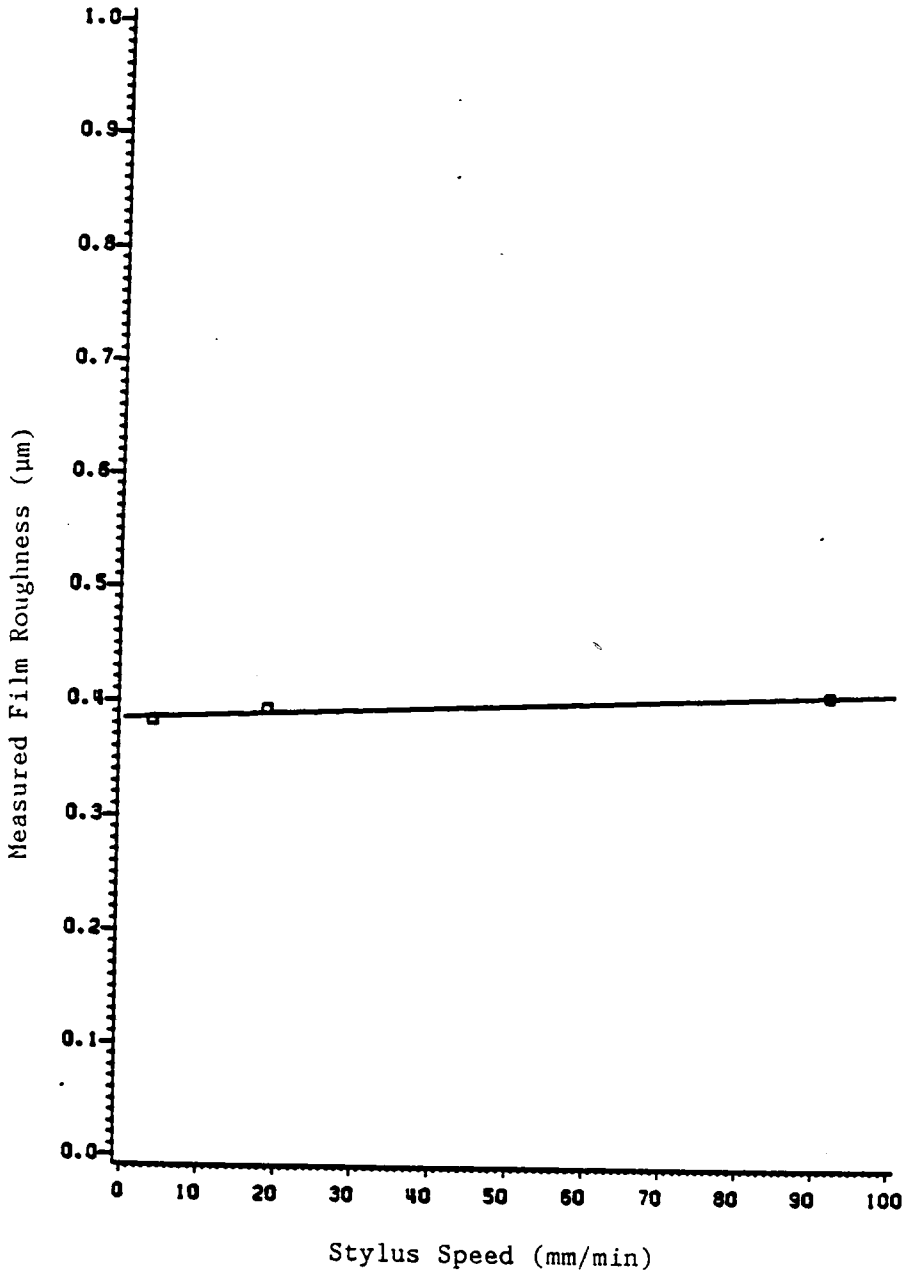

Figure 24. The effect of stylus speed on the measured value of film roughness.

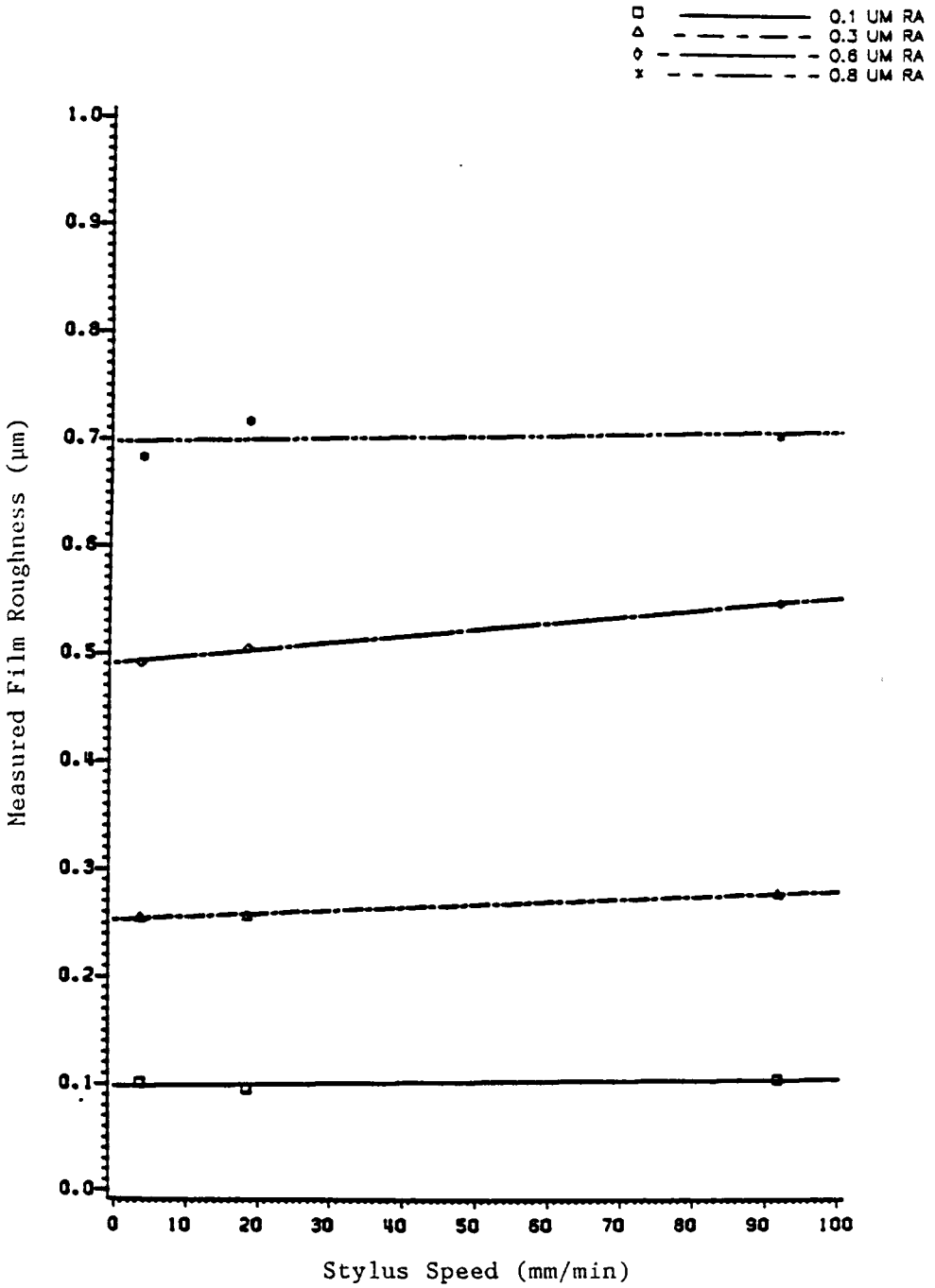

Figure 25. The effect of substrate roughness and stylus speed on the measured value of film roughness.

5.1.6 FREQUENCY ANALYSIS OF SURFACE PROFILES

The frequency components present in the surface profiles were determined by computing and plotting their Fourier transforms. The film and the substrate surface profiles were then compared by dividing the Fourier transform of the film surface profile by that of the substrate surface profile, obtaining a "transfer function." This gives a measure of the amount of attenuation of the measured surface roughness between the substrate and the film. Also, the technique can reveal what frequencies, in particular, are masked out by the application of a polymer film over the substrate. A quantitative measure of this attenuation factor was devised by calculating the area under the transfer function over the frequency range covered. This is not a true transfer function because no phase relationship between the film and substrate profiles is included. Perhaps, it is best defined as a "frequency response function", or FRF, depicting only amplitude response. Examples of these FRF curves are shown in Figure 26 through Figure 29, for polystrene films of four different thicknesses at the same stylus speed and substrate roughness. As the reader can see, there are many different situations which can be illustrated by similar figures, far too many to present in this text. These four figures will serve to illustrate the effect of film thickness on the FRF curves. The plots were constructed on semi-logarithmic scales, with the logarithm of the FRF amplitude shown on the vertical scale. Notice that as the film thickness increases, from Figure 26 to Figure 29, the attenuation of the FRF curve increases and the curve drops off more drastically at higher frequencies.

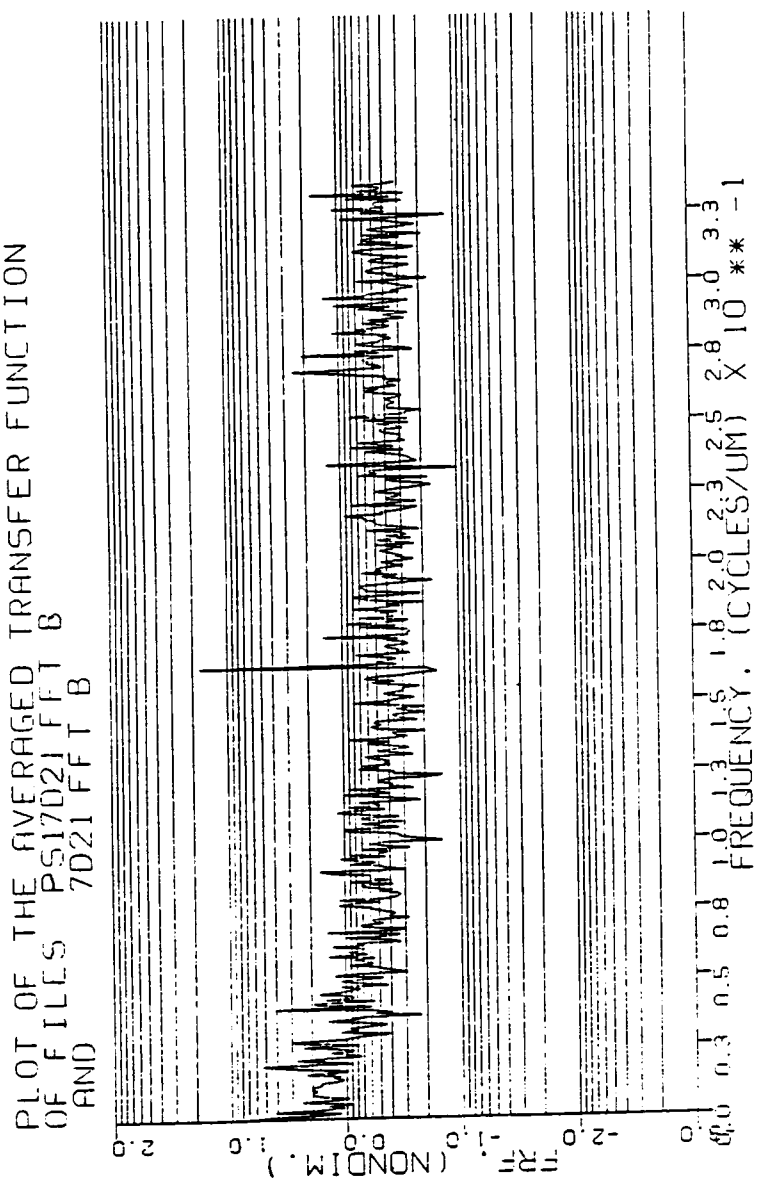

Figure 26. FRF plot between the film and substrate measured surface profiles for a 1.5 percent polystyrene film on a substrate with roughness 0.8 μm R_a Stylus speed = 18.3 mm/min.

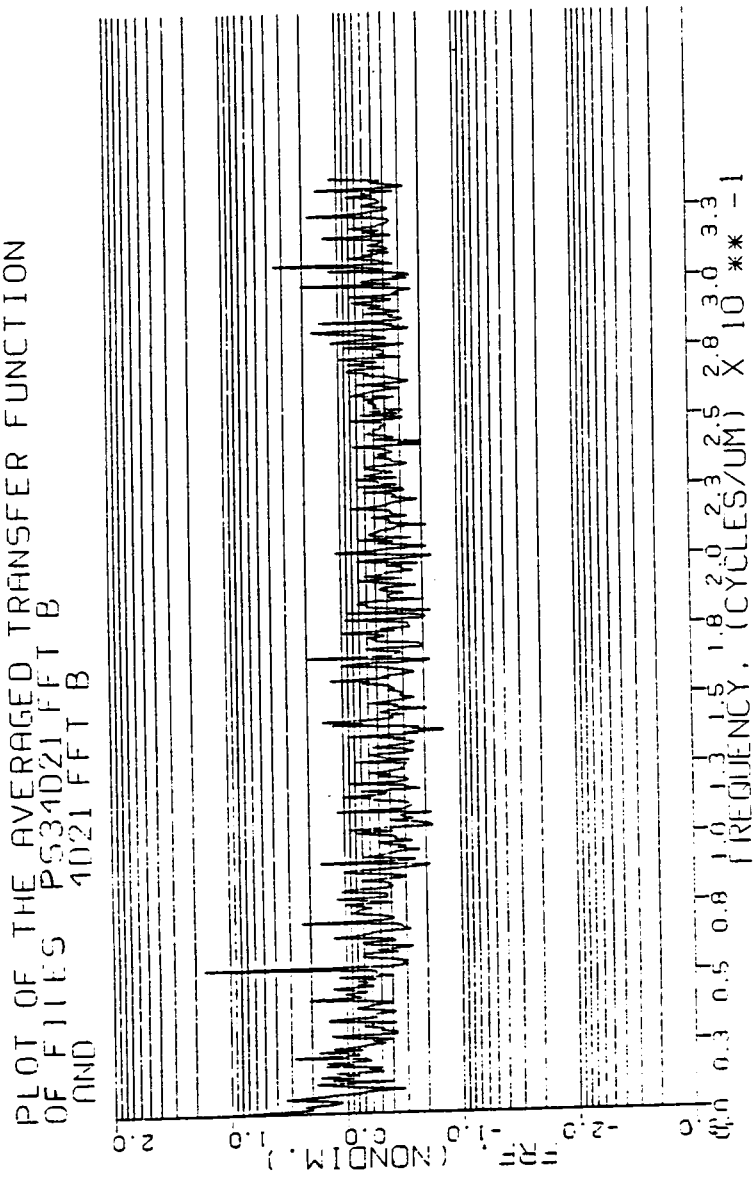

Figure 27. FRF plot between the film and substrate measured surface profiles for a 3 percent polystyrene film on a substrate with roughness 0.8 μm R_a Stylus speed = 18.3 mm/min.

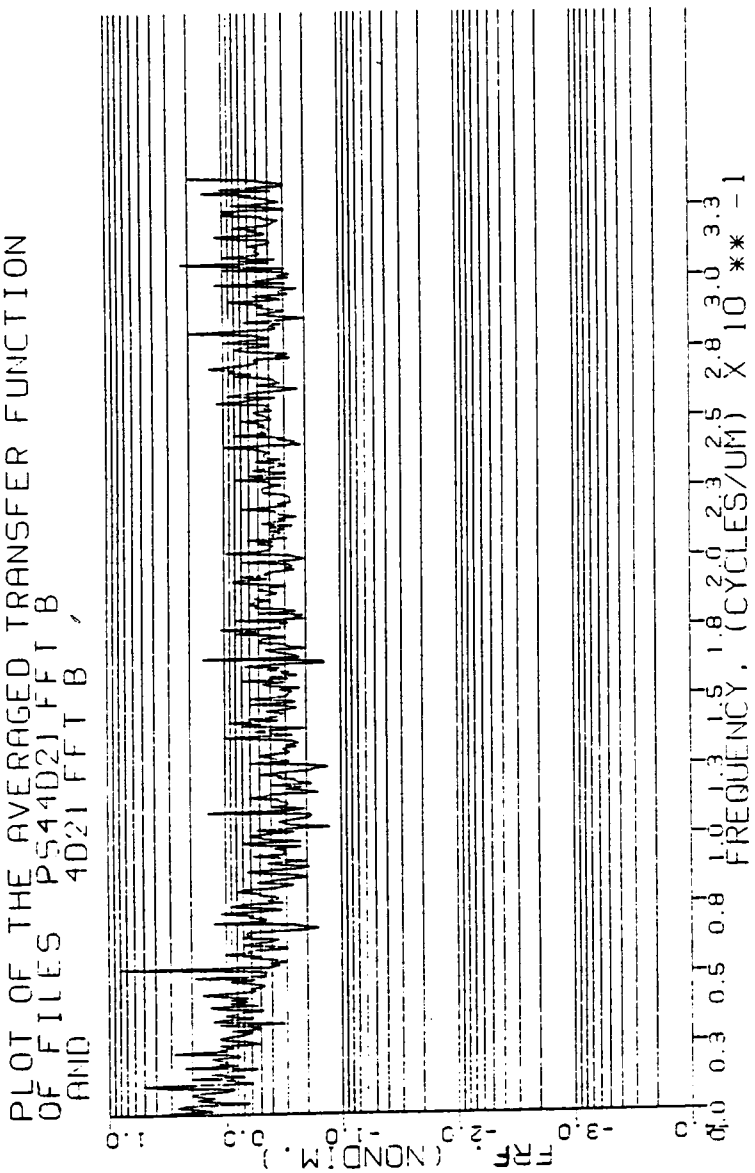

Figure 28. FRF plot between the film and substrate measured surface profiles for a 4.5 percent polystyrene film on a substrate with roughness 0.8 μm R_a Stylus speed = 18.3 mm/min.

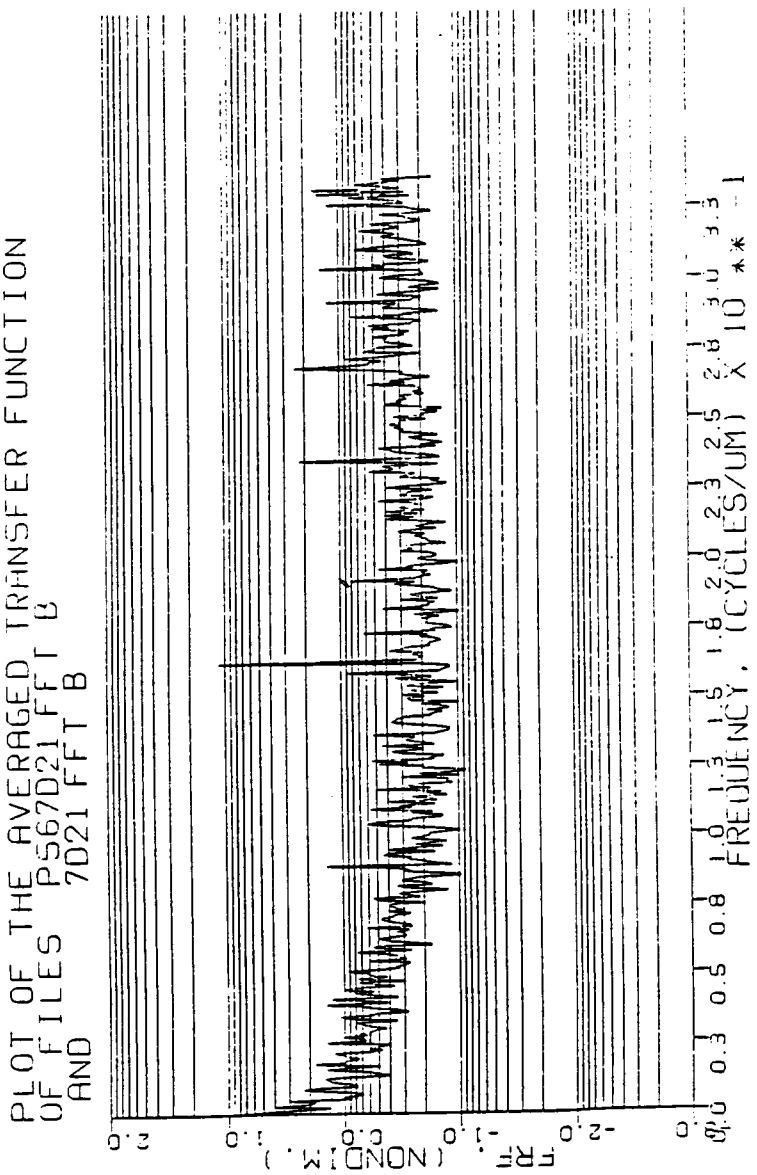

Figure 29. FRF plot between the film and substrate measured surface profiles for a 6 percent polystyrene film on a substrate with roughness 0.8 μm R_a Stylus speed = 18.3 mm/min.

The Fourier transforms do not cover the same frequency range for the traces taken at different stylus tracing speeds. Therefore, the areas under the corresponding FRF's cannot be directly compared. Thus, for comparison purposes, the areas were normalized by multiplying by two times the corresponding sample interval in μm. The quantity 1/[2 x (sample interval)] is equal to the Nyquist frequency of the sampling process, which is the frequency span of the FRF. If the two profiles are identical, the magnitude of the FRF is constant at unity over the entire frequency range. Thus, the area under the FRF curve, in this case, is equal to the Nyquist frequency, which indicates that there is no attenuation between the two profiles.

The SAS program was employed to calculate the mean value of the normalized area corresponding to each stylus traversing speed. The results of this operation are shown in Figure 30, with a straight line fit through the data. The area increases as the speed of the stylus increases. T-tests on the data reveal that the normalized area under the FRF curve for the fastest stylus speed is significantly higher than those for the lower two speeds, which are not significantly different. Further analysis showed that the type of polymer had no signifcant effect on the relation between the stylus speed and the area.

This observation reinforces the results found when discussing the variation of the stylus indentation depth. Figure 19 on page 53 shows that the variation of the depth to which the stylus indents the polymer film lessens as the speed increases. Thus, the stylus follows the surface more closely as the speed increases, and we find that there is less attenuation of the measured film profile, as shown in Figure 30. This re-

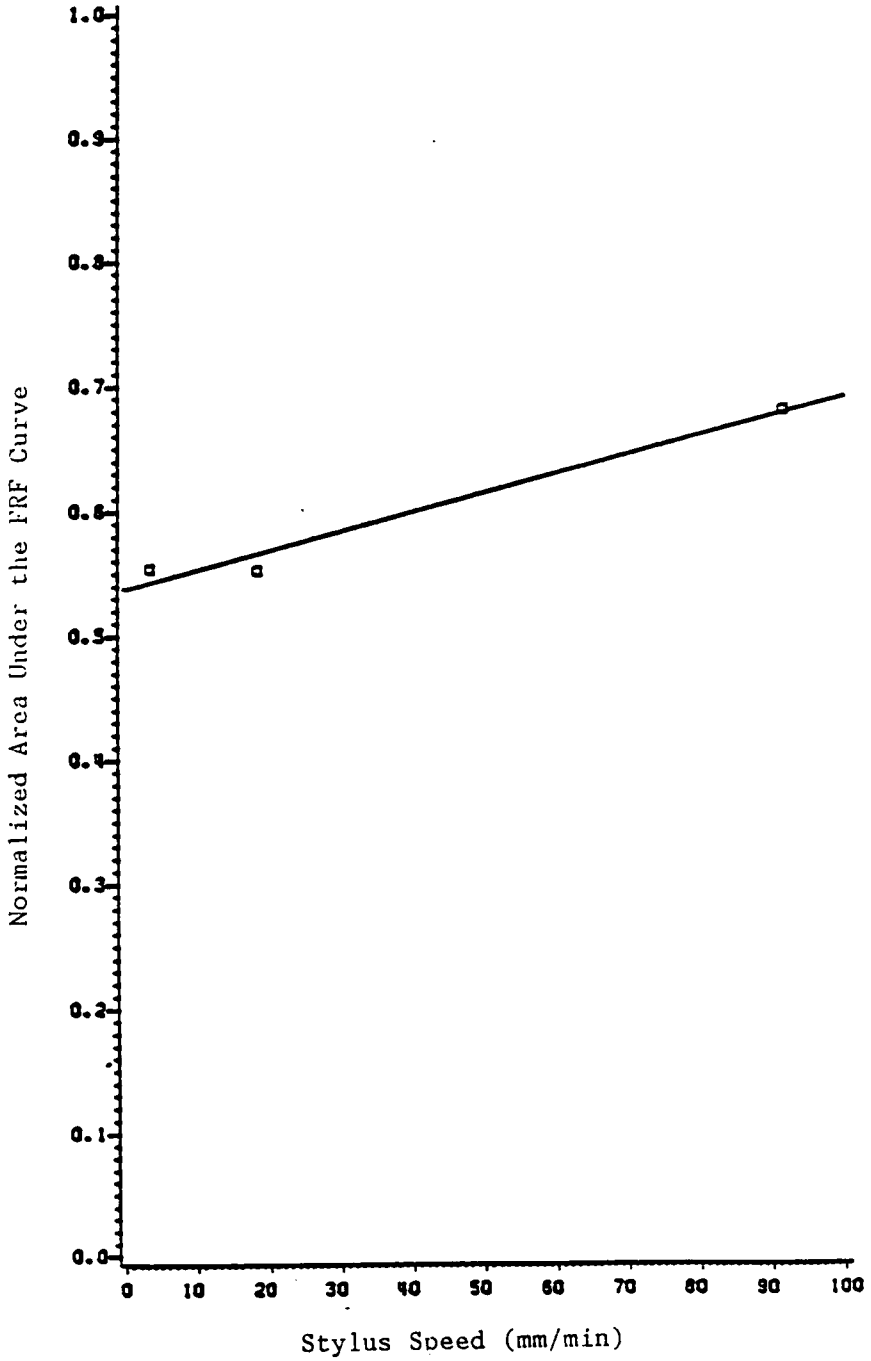

Figure 30. Effect of stylus speed on the normalized area under the FRF curve.

sult may be explained by the viscoelastic property of the polymers which provide more resistance to deformation as the strain rate increases.

It was found through analysis that the substrate roughness has negligible effect on the area under the FRF curve.

Several second-order effects on the FRF's may be inferred from the experimental results. The first to be presented is that of film thickness and the type of polymer. As shown in Figure 31, the slope of the line through the data for PSF has a greater negative value than does the line for PS. This may possibly be explained by that fact that PSF is 20 percent stronger in yield strength than PS. With a higher strength the stylus will follow the surface of the film more closely resulting in less attenuation of the measured profile in relation to the substrate profile.

The effects of film thickness and substrate roughness are illustrated in Figure 32. The slope of the straight lines through the data appears to increase slightly as the thickness, or concentration, increases. This suggests that the effect of substrate roughness is greater when the film is thicker. The figure also serves to reinforce the effect of film thickness that was shown previously. As the film thickness increases, the area under the FRF curve decreases, suggesting that the thicker films attenuate the frequency components more than the thinner films.

The final second-order effect on the FRF to be presented is of substrate roughness and stylus speed. Figure 33 shows the data plotted with straight lines fit through the points. Again, we notice a change in slope with substrate roughness. The figure shows that the effect of speed is greater when the substrate roughness is low. Stylus accelerations vary to a greater degree at a particular traversing speeds when

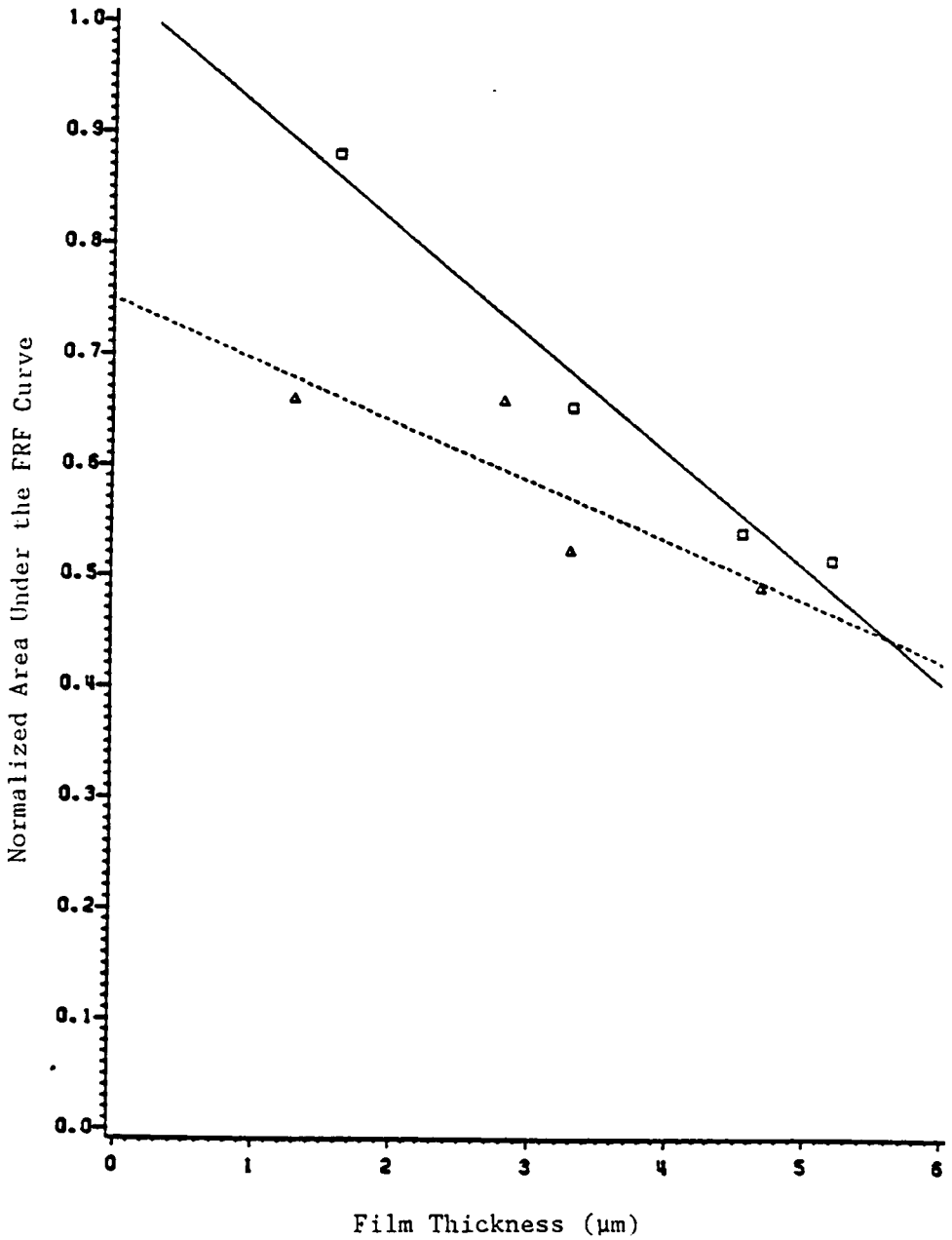

Figure 31. The effect of polymer and film thickness on the normalized area under the FRF curves: (——□) PSF, (-----△) PS

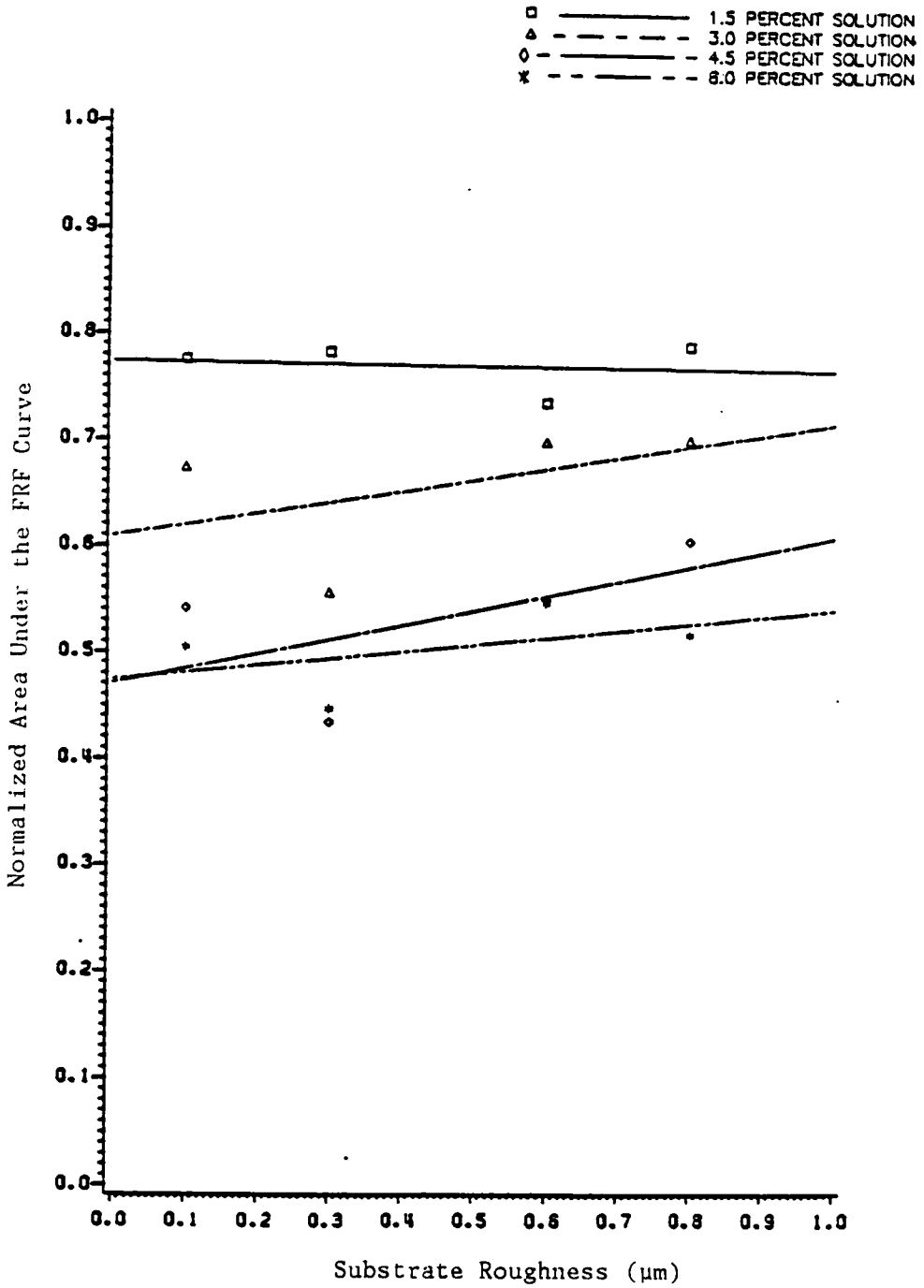

Figure 32. The effect of polymer solution concentration and substrate roughness on the normalized area under the FRF curves.

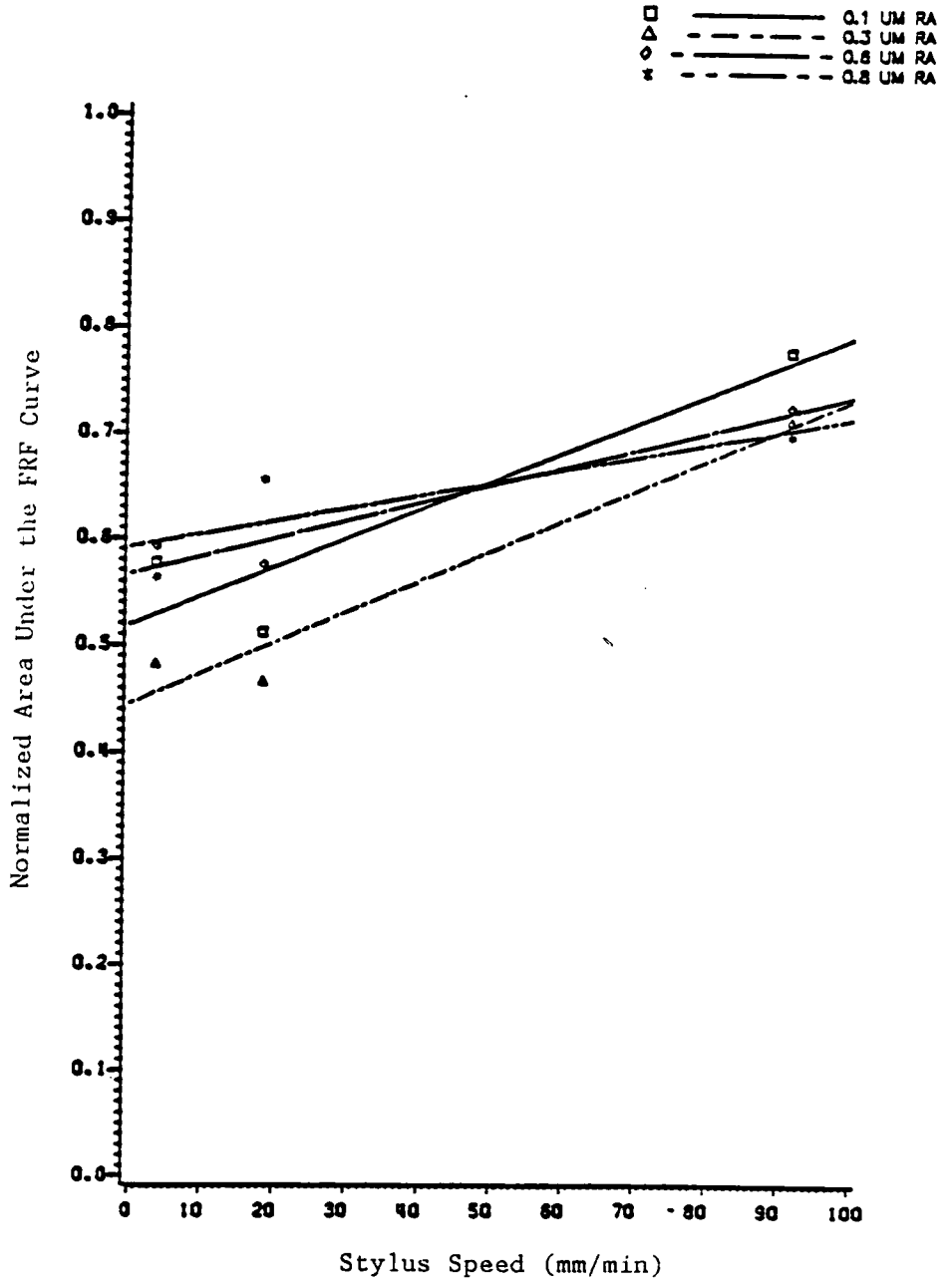

Figure 33. The effect of the substrate roughness and stylus speed on the normalized area under the FRF curves.

the substrate roughness is higher. Thus, these drastic variations in the acceleration forces cause the stylus not to follow the film surface as well when the substrate is rougher, resulting in a lower value of the normalized area.

5.2 THEORETICAL RESULTS

A Fortran computer program was written to find a solution to the plastic deformation problem of a profile meter stylus indenting a polymer film which has been disposited on a roughened substrate. The method of solution is called slip-line field theory, the theory and numerical methods of which have been discussed in detail in Appendix A and Chapter 4. The model assumes that the polymer is a semi-infinite body and thus the substrate has no effect on the system. Also, it is a static model, so it would most closely predict the depth of indentation when the stylus speed is relatively low and the film thickness is large. It was desired to find the load of the stylus on the film corresponding to a particular indentation depth. The plane-strain slip-line fields cooresponding to nine different indentation depths are shown in Figure 44 through Figure 52 in Appendix D; the fields are symmetric about the centerline of the stylus tip so only the right half of the fields are shown. Note that the figures are not all at the same scale. Also notice in the figures that the angle of indentation, θ, instead of the depth is given. The angle of indentation is measured counter-clockwise from the axis of symmetry about the center of curvature of the stylus tip. The tip of the stylus is approximately spherical in shape, so the depth and the angle

are directly related. The shape of the field at a particular indentation depth does not change as the yield strength of the material is varied, only magnitude of the stresses necessary to cause the plastic deformation change.

The computer program calculates the vertical forces on the stylus tip at each indentation depth. The forces are first calculated for an ideal rigid-plastic material which has a constant yield strength under all conditions. A family of curves of load versus indentation depth is shown in Figure 34, covering five different material yield strengths, from 55 to 75 MPa. The yield strength of the material is then modified for the effects of hydrostatic pressure and the slip-line field is recomputed. The resulting forces between the stylus and the film are presented versus the depth of indentation for several yield strengths in Figure 35. Notice that more force is required to indent the polymer when it is considered to be sensitive to hydrostatic pressure.

To compare the theoretical to the experimental results, we first use the fact that the force exerted by the stylus on the surface is 100 mgf (9.81×10^{-4} N). The length of the stylus is 2.5 μm. Thus, the force per unit of stylus length is 392 N/m. From reference [37], the yield strength in tension of polystyrene is 63.5 MPa. Then, referring to Figure 35, we find that the depth of indentation would be about 0.50 μm. This point is shown on the figure and it is in good agreement with the steady-state value of the exponential curve in Figure 13 on page 44.

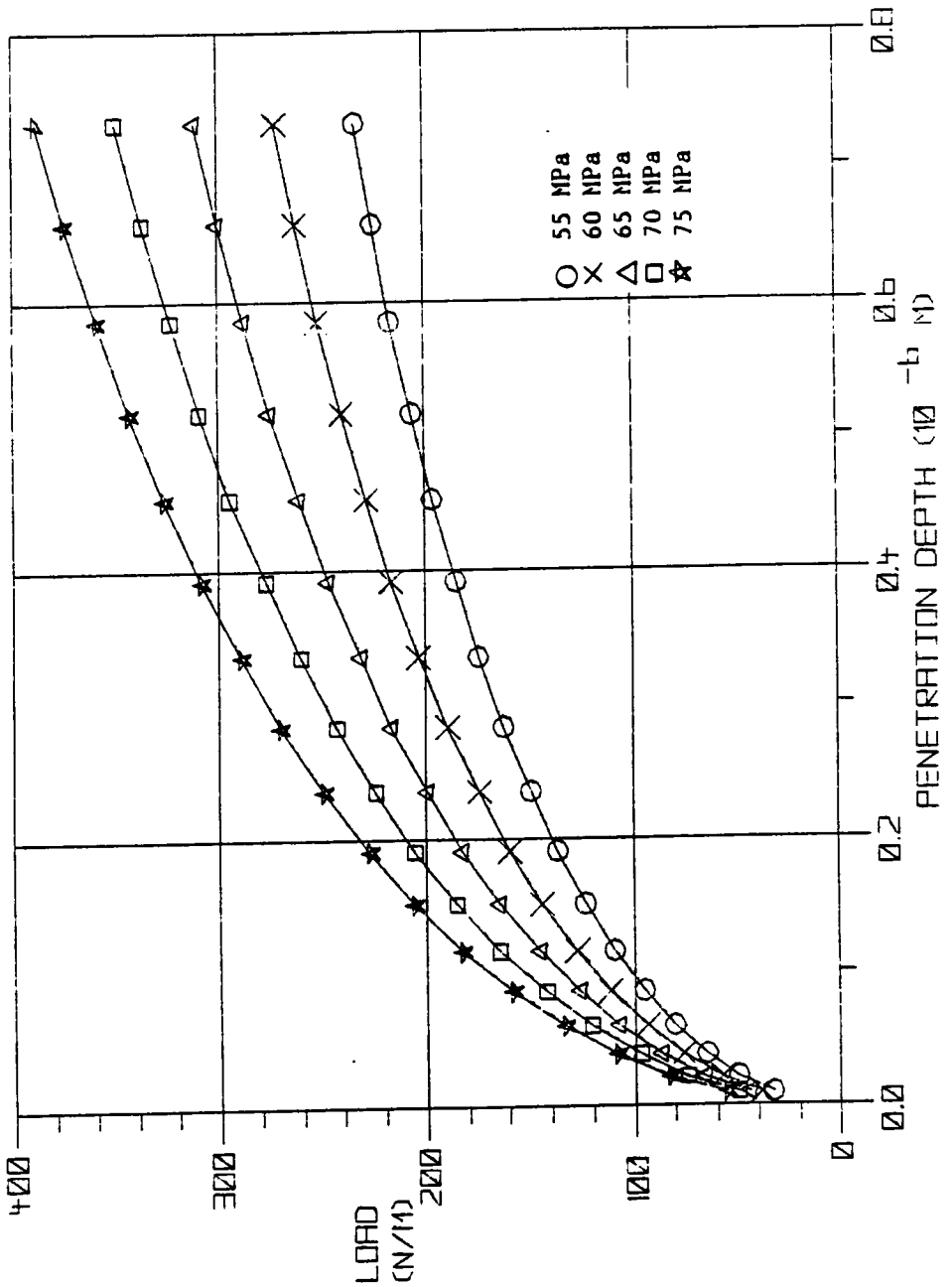

Figure 34. The force between the stylus tip and a rigid-plastic material as a function of the depth of indentation for several material yield strengths.

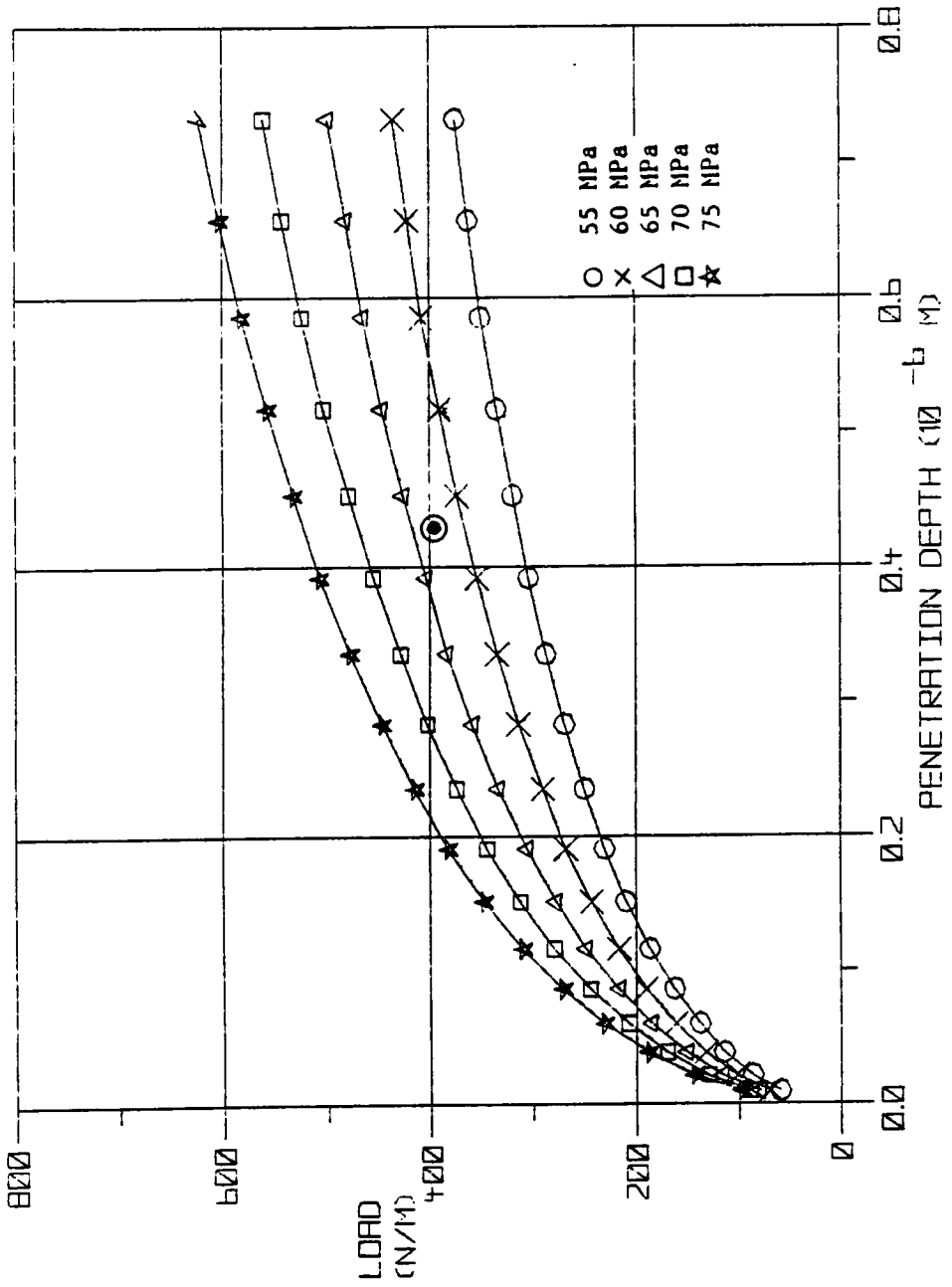

Figure 35. The force between the stylus tip and a polymer whose properties change with pressure as a function of the depth of indentation for several material yield strengths.

6.0 DISCUSSION

6.1 FILM THICKNESS AND POLYMER PROPERTIES

Figure 10 illustrates the effect of the polymer solution concentration on the thickness of the resulting film when deposited on a metal substrate. Notice that the thickness of the polysulfone (PSF) film is significantly greater than the polystrene (PS) film for the same solution concentration. Several factors, such as density, molecular weight, and solution viscosity, may have an effect on the thickness of the resulting films. The density of PS is less that of PSF [37]. However, the molecular weight of the polysulfone polymer used was between 40,000 and 50,000 g/mole, while the polystyrene had a molecular weight of about 190,000. The relative viscosities of the prepared solutions is not known. These facts can be counteracting, but it seems that the viscosity has a greater effect on the resulting film thickness.

There is considerable scatter in the data, due mainly to deficiencies in the measurement technique. The method of ellipsometry used to measure the thickness of the films is valid, for the particular instrument, in the range 2×10^{-4} μm to 6 μm. The film thicknesses studied were in the upper end of this thickness range where erroneous measurements could be obtained.

Also, the method requires that the films be extremely smooth. If the surface is not smooth, much of the laser light shone on the polymer surface by the ellipsometer will be scattered, possibly causing an erroneous

measurement of the film thickness. The smoothest possible films for measurement were prepared by using ferrotype plates for substrates. Still, the casting process, using a doctor's blade, results in films that are not the smoothest attainable, due to uneven solvent evaporation. Other methods, such as spin casting, give much smoother, yet thinner films, for the same solution concentrations. Thus, in any experiment of this type, it is essential that the polymer films to be studied are prepared using a very high quality and consistent process. Any roughness of the polymer film surface should be caused only by the roughened substrate. Extensive premilinary experimentation should be performed to verify this fact.

6.2 DEPTH OF PENETRATION

The effects of the independent variables of film thickness, substrate roughness, stylus traversing speed, and type of polymer have been presented in the preceding chapter. The depth to which the profile meter stylus indents the two different polymer films is not significantly different. One would expect the stylus to indent more deeply into the material with the lower yield strength. References [37,38] give the strength of PSF as 20 percent greater than that of PS. An explanation for the above observations may be as follows. When the films where deposited on the substrates, it was desired to perform the required work in a minimum elasped time, to mimimize the effect of time on the properties of the polymers being studied. The yield strength of most polymers increases with the amount of time between preparation and testing [39].

All the substrates were coated with films in approximately seven hours. Regretfully, the order of film casting was not randomized, with PSF first followed by PS. Fortunately, seven hours is not a significant amount of time so this factor does not have a great effect on the results.

The next step in the experimental work was to collect surface profiles on the polymer films over the roughened substrates. At this step it is postulated that the discrepancy in the depth of indentation data was generated. Nine days of total time were required to collect all of the data. Again, the author regrets that the order of data taking was not randomized during this procedure either. However, the error is more damaging in this case.

The data collection was performed on the PSF films first, requiring seven days to complete. The data for the PS films were collected on the eighth and ninth days. The author was aware of the effect of time on the properties of polymers, which is why he attempted to mimimize this preparation time. However, nine days is a significant amount of time, and, as a result, the polystyrene films were allowed to cure longer than the polysulfone films. Thus, it is believed that the effect of time on the strength was greater for the PS films than for the PSF films. If the order of collection had been randomized, one may have observed the expected results. On the other hand, if the order had not been randomized and the elasped time of data collection had been, say, about forty-eight hours, the difference in curing time would have been less, and more satisfactory results may have been obtained.

The data show that the depth of indentation is not significantly affected by the thickness of the polymer film. One would expect the stylus

to indent further into the surface as the film thickness increases. The strength of the polymers studied is more than one order of magnitude less than the strength of the steel substrates. When the films are thin, the hard substrate greatly affects the penetration of the stylus. This influence should decrease as the thickness increases and the properties of the polymer itself begins to govern the system. To illustrate this hypothesis, an exponential curve is fit through the data in Figure 13. It appears that the thickness of the films were all in the upper part of the thickness range where the substrate has little effect on the mean indentation depth. If a wider thickness range had been investigated, down to much thinner films, the exponential behavior may have actually been observed.

Figure 11 shows that the depth of indentation of the stylus into the film is inversely related to the traversing speed. The fastest stylus speed results in a significantly lower mean indentation depth than the slower two speeds. As the speed of the stylus increases the viscous damping property of the polymer comes into greater effect, the resistance to deformation increases, and thus, the stylus indents less [40].

The effect of substrate roughness on the depth of indentation of the stylus is much more difficult to assess. The results (see Figure 12) show that the depth of indentation is significantly greater on the roughest substrate than the three smoother substrates. The data depicted in the figure is the mean indentation depth. The depth varies about this mean as the stylus traverses the surface. The rougher substrates have tall sharp peaks while the peaks of the smoother substrates have been ground off. The stylus indents the surface of the film more deeply as it crosses

over a peak and it indents less as it moves over a valley in the surface. Thus, since there are more tall peaks on the rougher substrates, the mean indentation depth increases as the substrate roughness increases.

The variation of the depth of indentation of the stylus (D_a) is the most important parameter studied in this thesis. When the first photomicrographs from SEM sessions were observed, the immediately apparent characteristic of the stylus/film interaction was the variation in the depth of indentation. This variation is due to changes in acceleration forces and film thickness, on a microscopic scale, as the stylus traverses the surface. Because of these factors, there is a phase difference between the actual and measured film surface profiles and hence the measured surface could be an accurate representation of the polymer film surface topography. Unfortunately, there is no practical method of determining this phase shift unless an independent, non-contacting method was used to determine the film topography.

The depth of indentation and the variation of the depth were measured from the micrographs by sampling at discrete intervals along the stylus track in the film. The data were then fed into the SAS program which calculated the mean value of the D_a for each film thickness, and also for each speed and nominal substrate roughness. It is shown in Figure 21 that the D_a is inversely related to the thickness of the polymer film over the substrate, but again the confidence intervals limit definite conclusions. The D_a, like the depth, should be related to the strength of the polymer. If the strength is high, the D_a should be low. However, it was found that there were no significant differences between the two polymers studied.

Figure 19 shows the D_a versus the stylus traversing speed. The figure shows the the D_a vaule for the slowest speed is significanly greater than for the fastest speed. The effect is not drastic, though, for the following reason. effect of stylus speed on the D_a. As the speed of the stylus increases, the strain rate increases, and the polymer film is more resistant to deformation. On the other hand, with higher stylus speed, the acceleration forces vary to a greater degree, so the stylus will be forced to indent farther. These two effects are counteracting but the acceleration forces have less effect on the interaction.

The D_a increases with an increase in the substrate roughness as shown in Figure 18, even though only a few significant differences are present to justify this statement. This is essentially what was expected. As the stylus is traversed across the surface being measured, it climbs over peaks and through valleys. The taller the peaks, the higher the acceleration forces on the stylus and thus it will indent further as it climbs over a peak as compared to a smoother surface. The result is an overall higher value of D_a if the substrate roughness is higher.

6.3 FREQUENCY ANALYSIS OF PROFILES

Of great interest in this thesis is the effect the presence of a polymer film over a roughened substrate has on the measurement of surface roughness. When a polymer film is deposited on a substrate, the film fills in the valleys of the substrate surface profile. In so doing, the film is thicker in the valleys than on the peaks. (This, of course, occurs on a microscopic scale.) Thus, in effect, the film masks over the

underlying substrate. Then, when the stylus instrument is used to estimate the surface roughness, the resulting measurement is lower than that of the substrate roughness. Another effect of this masking of the substrate is the attenuation of certain frequency components of the surface profile. When the film is deposited, small peaks on the substrate are smoothed over by the presence of the film. Thus, amplitudes of high frequency components in the substrate surface profile are attenuated by the presence of the film. This phenomenon can be seen in Figure 26 through Figure 29 which show different frequency response functions between the film and substrate surface profiles. The amplitude of the FRF curve is lower over the frequency range and the curve drops off at a faster rate when the films are thicker.

The FRF curves are effected by stylus speed in the same manner as is the variation of the depth of indentation. As shown in Figure 30, higher stylus speeds result in less attenuation of the FRF curve. The stylus follows the surface of the film more closely when the stylus is traversed faster.

6.4 MEASURED FILM ROUGHNESS

The surface profile obtained when the stylus is traversed across the polymer film surface is referred to here as the measured film roughness. This is not the actual film roughness due to the dynamic interaction between the film and the stylus. The relationship between the measured film roughness and the actual film roughness can be dependent upon several effects. These effects are shown in the sketches of Figure 36. Since

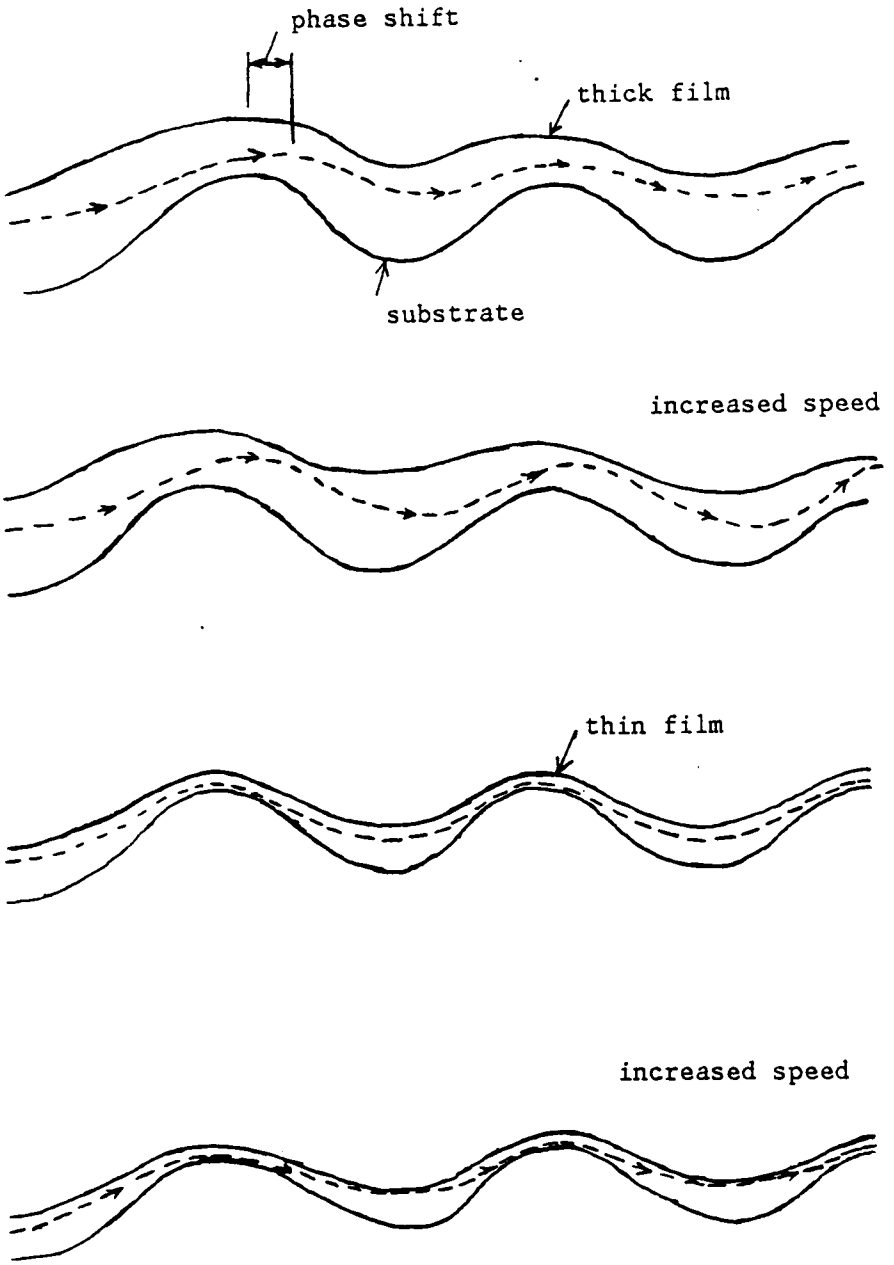

Figure 36. Measuring the film surface profile.

the stylus/film/substrate is a dynamic system and there is mass present, there will be a phase shift between the measured profile and the substrate profile. If the film is thick and the stiffness of the substrate has little effect, the phase shift will be large and the measured surface profile could be very close to the actual profile, excepting the phase shift. With an increase in stylus speed, the accelerations will be higher and the result could be a measurement higher than the actual profile.

If the film is thin, on the other hand, the substrate will affect the behavior. First, the phase shift will be less due to the higher stiffness of the system. As the stylus begins to accelerate up a peak and indents deeper, the substrate stiffness will limit this indentation. Hence, the measurement of the film surface will be relatively accurate. However, with an increase in speed, the acceleration of the stylus will predominate and the stylus will plow through the film over the peak, resulting in a lower reading than the actual.

6.5 THEORETICAL MODEL OF THE STYLUS/FILM INTERACTION

A slip-line field model was developed to theoretically estimate the depth to which the stylus indents a polymer film. The model gives the researcher an approximation of the shape of the plastically deformed region beneath the stylus tip. The model does not account for the effect of the underlying substrate, an assumption which greatly simplifies the analysis. Also, the proposed model is a static case, so the effect of strain rate is not accounted for. It has been found that the model gives a good estimate of the mean indentation depth when the film thickness is

large, and the effect of hydrostatic pressure is included. Considerably more work could be performed on this model to account for the highly dynamic interaction between the stylus and the polymer film.

7.0 CONCLUSIONS

The major purpose of this thesis was to determine how to measure the roughness of polymer films on hard substrates using a stylus-type profile meter. Generally, it was found that the measured profile will be an accurate representation of the polymer film surface topography if the variation in the depth of penetration of the stylus is minimized. This may be accomplished by using the highest of the stylus traversing speeds when measuring the surface.

1. The depth of indentation decreases with a increase in stylus traversing speed. As the speed increases, the rate of deformation increases and the viscoelasticity of the polymer causes higher resistance and thus the stylus indents less. The depth of penetration was significantly greater on the roughest substrate than the three smoother substrates and the depth was more sensitive to variation in speed on the roughest substrate than for the other substrates (see Figure 14).

2. Film thickness was found to have no significant effect on the mean depth of indentation, probably due to the fact that the film thicknesses chosen for the study were in the of the thickness range where the substrate stiffness has little effect on the indentation depth.

3. The effects of the independent variables on the variation of the stylus indentation depth were also studied. It was found that the depth of indentation varies more when the film thickness is small. This fact is due mainly to the lower acceleration forces because the film has masked over the substrate.

4. The stylus indentation depth varies less as the speed increases. At faster speeds, the film provides more resistance to deformation and the stylus follows the film surface more closely. Thus, it is suggested that a fast stylus speed setting be used to obtain a more accurate measurement of the film surface.

5. The variation of the depth increases as the substrate roughness increases because the film cannot withstand the higher acceleration forces present when the substrate is rougher.

6. The roughness values of the film surface profiles were studied and it was found that the measured film roughness correlates linearly with the substrate roughness, the film roughness being 89 percent of the substrate roughness.

7. Frequency response functions between the substrate and film surface profiles were also studied in depth. To quantitatively measure the effects of the independent variables on the FRF curves, the area under the curve was calculated. The greater the area, the less the attenuation between the substrate and the film. It was found that the area

increased with stylus speed, again since the stylus follows the film surface more closely at higher speeds. The substrate roughness was found to have negligible effect, while the area decreases drastically as the film thickness increases. This proves that the film masks over the substrate roughness, attenuating the amplitudes, especially at high frequencies.

8. The slip-line field model of a stylus indenting a polymer film gives a very accurate estimate of the mean indentation depth.

8.0 RECOMMENDATIONS

The author would like to make several recommendations to any researcher interested in pursuing the subject of this thesis further or any other work involving the use of polymer films, where it is essential that the properties of the films be well known and controlled. These recommendations are based on experiences gained by the author in the pursuance of this work.

1. In order to obtain more confident data, more SEM observation should be made on more stylus tracks. In this work, only one stylus track was observed for each of the ninety-six (96) possible situations. However, one should expect to invest considerable funds in this expanded work.

2. The film thickness effect on the depth of indentation and the measured film roughness was not as great as expected. With the polymers studied, the same solution concentrations did not result in the same film thicknesses, and all the work in this thesis was performed with polymer solutions of 1.5, 3, 4.5, and 6 percent in solvent (chloroform). Thus, actually, there is only an effect of solution concentration instead of film thickness, the intended independent variable. In any work of this type concerning polymer films on substrates, it is essential that the film thicknesses be carefully controlled. Preliminary work should be performed with different

solutions so that the relationship between film thickness and solution concentration is well known for all polymers involved. These steps will ensure that better final results are obtained.

3. Along the same lines as above, a different film casting technique should be used to obtain smoother films and ones that can be assured to be uniform in thickness over their entire surface. The technique of using a doctor's blade does not allow uniform solvent evaporation, and the resulting films are not smooth nor uniform. All roughness of the film should result only from the presence of the underlying substrate. Extensive preliminary experimentation should be performed to ensure that the casting procedure is of high quality and consistency.

4. Polymeric materials for study should be chosen which have considerably different mechanical properties. Also, in choosing these polymers, it is helpful if abundant literature is available on the properties and behavior of the material. This was not the case with polysulfone, which is a relatively new material.

5. Also, to obtain better results, the film thickness range should be made as wide as possible. Another reason why the film thickness effects were low is because all the thicknesses were in the upper end of the range where the substrate has little effect on the stylus/film interaction. If the thickness range had been made larger, down to

much thinner films, more discernible effects of film thickness would have been observed.

6. The slip-line model of the stylus indenting a film gave good estimates of the mean stylus indentation depth. The model is a static case so the effects of strain-rate were not included in the analysis. Granted, considerably more time could be invested in expanding the model to account for the dynamic action of the stylus indenting the film.

REFERENCES

1. Hill, R., The Mathematical Theory of Plasticity, Oxford University Press, London, 1950.

2. Johnson, W., R. Sowerby and R. D. Venter, Plane Strain Slip Line Fields for Metal Deformation Processes, Pergamon Press, Oxford, 1982.

3. Spencer, G. C., Introduction to Plasticity, Chapman & Hall Ltd., London, 1968.

4. Hoffman, O. and G. Sachs, Introduction to the Theory of Plasticity for Engineers, McGraw-Hill Book Co., New York, 1953.

5. Gopinathan, V., Plasticity Theory and its Applications in Metal Forming, Wiley Eastern Limited, New Delhi, 1982.

6. Johnson, W., "Some Slip-Line Fields for Swaging or Expanding, Indenting, Extruding and Machining of Tools with Curved Dies," Journal of the Mechanics and Physics of Solids, vol. 11, Pergamon Press, Oxford, 1963, pp. 345-355.

7. Shield, W. B. and P. L. B. Oxley, "On the Plastic Flow of Metals Under Conditions of Axial Symmetry," Proceeding of the Royal Society, Series A, vol. 233, 1955, pp. 267-287.

8. Palmer, W. B and P. L. B. Oxley, "Mechanics of Orthogonal Machining," Proceedings of the Institute of Mechanical Engineers, vol 173, no. 24, 1959, pp. 623.

9. Lockett, F. J., "Indentation of a Rigid-Plastic Material by a Conical Indenter," Journal of the Mechanics and Physics of Solids, vol. 11, Pergamon Press, Oxford, 1963, pp. 345-355.

10. Hill R., E. H. Lee, and S. J. Tupper, "The Theory of Wedge Indentation of ductile materials," Proceedings of the Royal Society, A, vol. 188, 1947, p. 273.

11. Shield, R. T., "The Plastic Indentation of a Layer by a Flat Punch," Quarterly Journal of Applied Mechanics, vol. 13, 1955, p. 27.

12. Mulhearn, T. O., "The Deformation of Metals by Vickers-Type Pyramid Indenters," Journal of the Mechanics and Physics of Solids, vol. 7, 1958, p. 85.

13. Ishinsky, A. J., Journal of Applied Mathematics and Mechanics, (U.S.S.R.), vol. 8, p. 233, English translation by D. Tabor, Ministry of Supply, A. R. D., 1947, Theoretical Translation No. 2/47.

14. Argon, A. S. and M. I. Bessonov, "Plastic Flow in Glassy Polymers," Polymer Engineering and Science, vol. 17, no. 3, March, 1977, pp. 174-182.

15. Shigley, J. E., Mechanical Engineering Design, 3rd ed., McGraw-Hill Book Company, 1977, pp. 169,170.

16. Ward, I. M., Mechanical Properites of Solid Polymers, John Wiley and Sons, New York, 1983.

17. Matsushige, K., S. V. Radcliffe and E. Baer, "The Mechanical Behavior of Polystyrene Under Pressure," Journal of Materials Science, Vol. 10, 1975, pp. 833-845.

18. Ainbinder, S. B., M. G. Laka and I. Y. Maiors, "Effect of Hydrostatic Pressure on Mechanical Properties of Plastics," Mekhanika Polimerov, vol. 1, no. 1, 1965, pp. 65-75.

19. Rabinowitz, S., I. M. Ward and J. S. C. Parry, "Effect of Hydrostatic Pressure on the Shear Yield Behavior of Polymers," Journal of Materials Science, vol. 5, 1970, pp. 29-39.

20. Hong, S., Chung, S. Y. and R. F. Fedors, "Molecular Deformation and Stress-Strain Behavior of Poly(bisphenol-A-diphenol sulfone)," Journal of Applied Physics, vol. 54, no. 10, 1983, pp. 5592-5597.

21. Robeson, L. M., A. G. Farnham and J. E. McGrath, "Dynamic Mechanical Characteristics of Polysulfone and other Polyarylethers," Molecular Basis of Transitions and Relaxations, D. J. Meier, Ed., Gordon and Breach, New York, 1978, pp. 405-425.

22. Fried, J. R. and H. Kalkanoglu, "Multiple Secondary Relaxations of Bisphenol A Polysulfone," Journal of Polymer Science: Polymer Letters Edition, vol. 20, 1982, pp. 381-383.

23. McCrum, N. G., B. E. Read and G. Williams, Anelastic and Dielectric Effects in Polymeric Solids, John Wiley and Sons, London, 1967.

24. Cooley, J. W. and J. W. Tukey, "An Algorithm for the Machine Calculation of Complex Fourier Series," Mathematics of Computation, vol. 19, 1965, pp. 297-301.

25. Singleton, R. C., "On Computing the Fast Fourier Transform," Communications of the ACM, vol. 10, no. 10, October, 1967, pp. 647-654.

26. Newland, D. E., An Introduction to Random Vibrations and Spectral Analysis, Longman Group Ltd., New York, 1975, p. 33.

27. Anonymous, "Surface Texture (Surface roughness, Waviness, Lay)," American National Standards Institute, ANSI B46.1-1978.

28. R. H. Muller, "Principles of Ellipsometry," Advances in Electrochemistry and Electrochemical Engineering, Tobins and Delahay, editors, vol.9,

29. R. M. A. Azzam and N. M. Bashara, Ellipsometry and Polarized Light, North-Holland Publishing Co., New York, 1977.

30. R. J. Archer, "Manual of Ellipsometry," Gaertner Scientific Corporation, 1201 Wrightwood Ave., Chicago, IL 60614

31. Rothen A., "General Theory and Operating Instructions for the Ellipsometer," O. C. Rudolph & Sons, Inc., 1 Rudolph Road, P. O. Box 100, Nanders, NJ.

32. F. L. McCrackin, E. Passaglia, R. R. Stromberg, and H. L Steinberg, "Measurement of the Thickness and Refractive Index of Very Thin Films and the Optical Properties of Surfaces by Ellipsometry," Journal of Research of the National Bureau of Standards, A. Physics and Chemistry, vo. 67A, no. 4, July-August, 1963.

33. James, M. C., G. M. Smith and J. C. Wolford, Applied Numerical Methods of Digital Computation, 2nd ed., Harper and Row Publishers, New York, 1977.

34. Ray, A. A.,ed.,SAS User's Guide: Statistics, SAS Institute Inc., Cary, North Carolina, 1982.

35. Hinkle, D. E., W. Wiersma and S. G. Jurs, Applied Statistics for the Behaviorial Sciences, Rand McNally College Publishing Co., Chicago, 1979.

36. Snedecor, G. W. and W. G. Cochran, Statistical Methods, 7th ed., Iowa State University Press, 1980.

37. Harper, C. A.,ed.,Handbook of Plastics and Elastomers, McGraw-Hill Book Company, New York, 1975.

38. Thomas, H. L., "Polysulfones Make Strong, Stable Molded Articles," Industrial Research and Development, vol. 23, no.10, Sept. 1981, pp. 138-141.

39. Tant, M. R. and G. L. Wilkes, "An Overview of the Nonequilibrium Behavior of Polymer Glasses," Polymer Engineering and Science, vol.21, no.14, October, 1981.

40. Bueche, A. M. and Flom, D. G., Wear, vol. 2, p. 168, 1959.

41. Popov, E. P., Mechanics of Materials, 2nd ed., Prentice-Hall, Englewood Cliffs, New Jersey, 1976.

42. Fenton, R. G. and B. Durai Swamy, "Plane-Strain Plastic Flow of Strain-Rate Sensitive Materials," Journal of Engineering Materials and Technology, July, 1974, pp. 238-240.

43. Fenton, R. G. and B. Durai Swamy, "Slip-Line Field Solution of Extrusion of Strain-Rate Sensitive Materials," International Journal of Machine Tool Design and Research, vol. 15, Pergamon Press, Oxford, 1975, pp. 105-115.

44. Mabie, H. H. and F. W. Ocvirk, Mechanisms and Dynamics of Machinery, 3rd ed., John Wiley and Sons, New York, 1978.

APPENDIX A. THEORETICAL BACKGROUND

This appendix will discuss the theory and analytical techniques employed in the solution of the problem of a stylus indenting a polymer film. The theory of plastic flow as pertaining to an ideal rigid-plastic material will be discussed. The governing equations of the theory will be presented in a Cartesian coordinate system and then the equations will be rewritten to refer to a curvilinear coordinate system, the slip-lines. Since the behavior of polymers under stress is quite different from that of metals, the equations of plastic flow will be further modified to account for the effects of hydrostatic pressure and strain rate on the yield strength of polymeric materials.

A.1 GENERAL THEORY OF PLASTIC FLOW

This section will present the governing equations of plastic flow of a rigid-plastic solid. In elastic deformation, the stress is proportional to the amount of strain imposed on the body. In plastic deformation, the stress is proportional to rate of straining, or the strain increment, instead of the total strain. A rigid-plastic solid is a hypothetical material which is rigid when stressed below the yield point, but will flow with no increase in stress when the yield point is reached. Hence, it is assumed that the elastic modulus is infinitely large. These assumptions can lead to an estimate of the plastic strains and stresses if the plastic part of the total strain is much greater than the elastic part.

The method of derivation of strain-displacement relations and equilibrium equations is identical for elastic and plastic deformation. Stress and strain are related by Hooke's law for elastic deformation. For plastic deformation, a method must be devised to relate the stress to the strain-rate or the strain increment.

A.1.1 STRAIN-DISPLACEMENT RELATIONS

First, let's define a right-handed Cartesian coordinate system x_i, where i=1,2,3. Consider an infinitesimal element of material which has a projection OACB onto the x_1-x_2 plane, as shown in Figure 37. After being subjected to normal and shear strains, the element is displaced and deformed to the position O'A'C'B'. Let du_i, i=1,2,3, represent the infinitesimal displacements of a particle in the x_i directions in time dt, then the incremental strain tensor $d\varepsilon_{ij}$ for time dt is [2]

$$d\varepsilon_{ij} = \tfrac{1}{2}\{ \frac{\partial(du_i)}{\partial x_j} + \frac{\partial(du_j)}{\partial x_i} \} . \qquad (1)$$

Then, the rate of deformation tensor, or strain-rate tensor, is

$$e_{ij} = \frac{de_{ij}}{dt}$$

$$e_{ij} = \tfrac{1}{2}\{\frac{\partial}{\partial x_j}(\frac{du_i}{dt}) + \frac{\partial}{\partial x_i}(\frac{du_j}{dt})\} , \qquad (2)$$

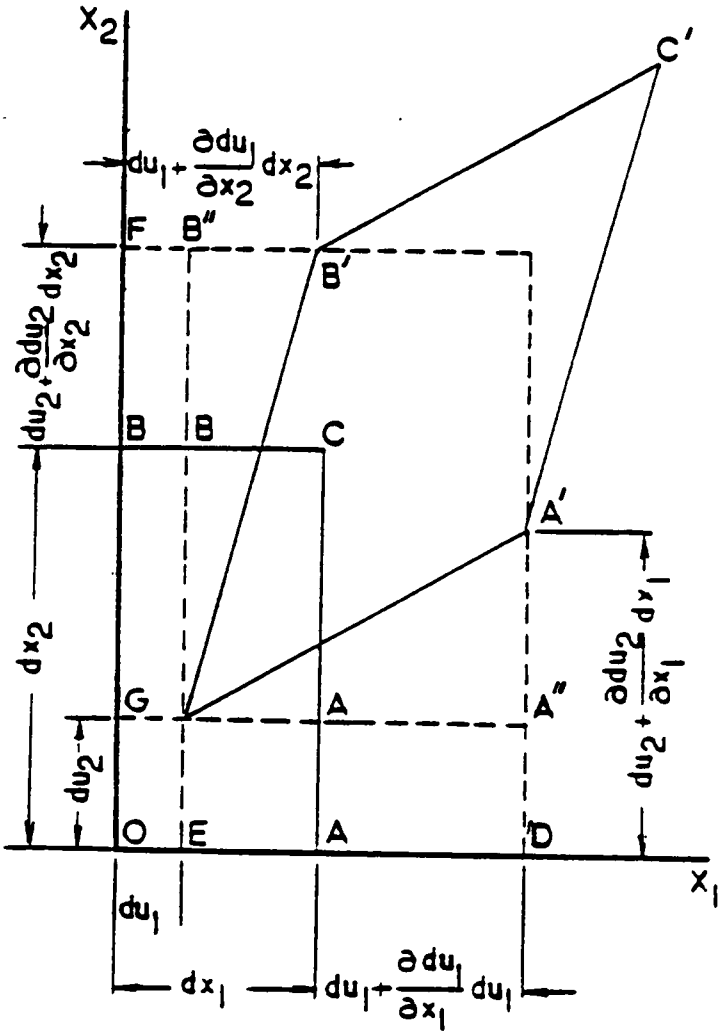

Figure 37. Derivation of strain-displacement relations.

where t is time or a parameter which varies proportionally with time. Defining the velocity of a particle with current position vector x_i as

$$v_i = \frac{du_i}{dt} , \tag{3}$$

the strain rate tensor, Equation 2, can be rewritten in terms of velocities:

$$e_{ij} = \tfrac{1}{2}\left(\frac{dv_i}{dx_j} + \frac{dv_j}{dx_i}\right) . \tag{4}$$

A.1.2 EQUILIBRIUM EQUATIONS

Consider a differential element of length dx_1, dx_2, dx_3 as shown in Figure 38. By summing the forces on the element in the three coordinate directions, three equations of equilibrium can be written [5]:

$$\begin{aligned}
\frac{\partial \sigma_{11}}{\partial x_1} + \frac{\partial \sigma_{12}}{\partial x_2} + \frac{\partial \sigma_{13}}{\partial x_3} &= 0 \\
\frac{\partial \sigma_{21}}{\partial x_1} + \frac{\partial \sigma_{22}}{\partial x_2} + \frac{\partial \sigma_{23}}{\partial x_3} &= 0 \\
\frac{\partial \sigma_{31}}{\partial x_1} + \frac{\partial \sigma_{32}}{\partial x_2} + \frac{\partial \sigma_{33}}{\partial x_3} &= 0 ,
\end{aligned} \tag{5}$$

where the stresses σ_{ij} are normal stresses if i=j and are shear stresses if $i \neq j$. Equation 5 are derived under the assumption that no body forces or moments are acting on the element.

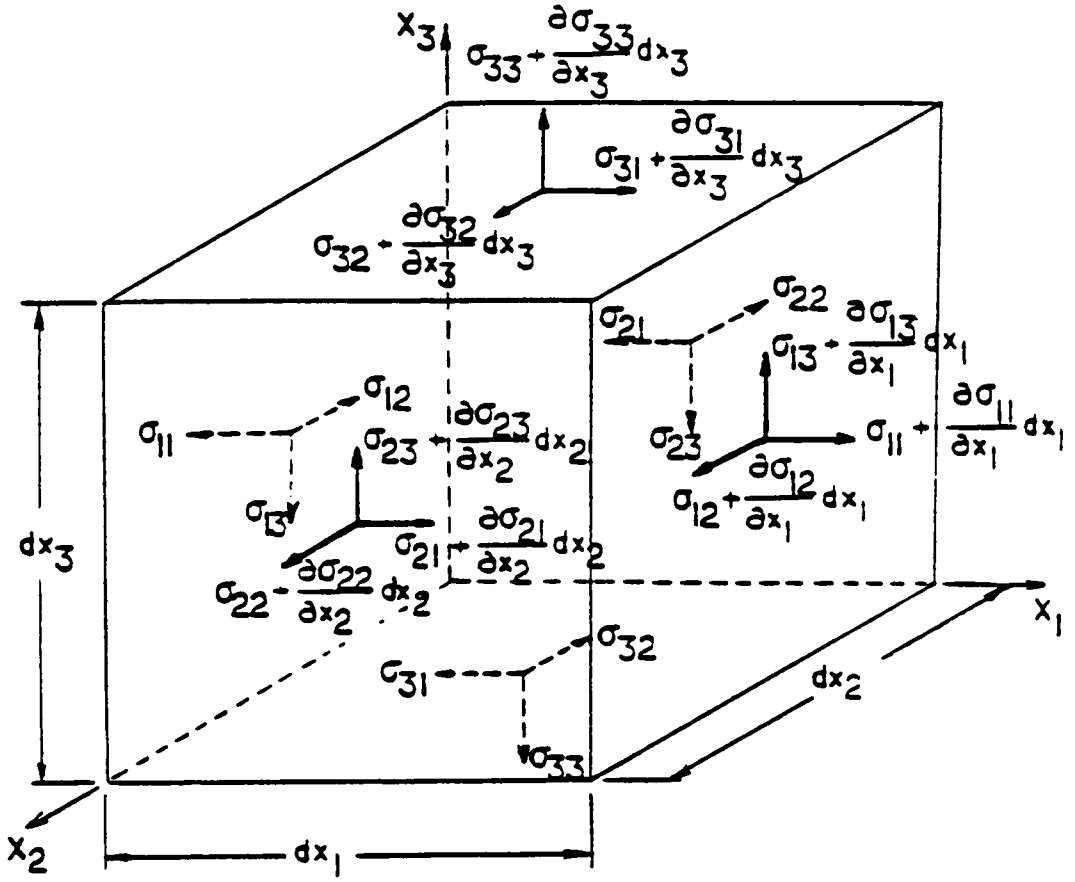

Figure 38. Stresses acting on an element of material.

A.1.3 DEVIATORIC STRESSES

At this time, it advantageous to define two stress components which are useful in the analysis of plastic deformation. The hydrostatic stress is a normal stress acting equally on the faces of a three-dimensional element and is defined by

$$p = \frac{1}{3}(\sigma_{11} + \sigma_{22} + \sigma_{33}) \quad . \tag{6}$$

The application of this hydrostatic stress causes only elastic deformation and no plastic deformation. When the hydrostatic stress tensor is substracted from the stress tensor, the deviatoric stress tensor is obtained: [5]

$$\sigma'_{ij} = \begin{bmatrix} \sigma_{11} - p & \sigma_{12} & \sigma_{13} \\ \sigma_{21} & \sigma_{22} - p & \sigma_{23} \\ \sigma_{31} & \sigma_{32} & \sigma_{33} - p \end{bmatrix} \quad . \tag{7}$$

In shorthand form, the deviatoric stress tensor is

$$\sigma'_{ij} = \sigma_{ij} + p\delta_{ij} \quad , \tag{8}$$

where,

$$\delta_{ij} = 1 \quad \text{for } i = j$$
$$= 0 \quad \text{for } i \neq j \quad .$$

δ is defined as the Kronecker delta. [5]

A.1.4 YIELD CRITERION

When a real body is subjected to external forces, it deforms. If the forces are low such that there is only a distortion of the crystal lattice, the body will return to its original dimensions when the load is released and the deformation is called elastic. If the load is increased further, a stage will be reached when the body will not return to its original dimensions. This deformation is called plastic. Hence, a criterion is needed to predict the onset of plastic yielding.

Many yield criteria have been proposed. The most popular yield criterion, and the one employed in this thesis, was proposed by von Mises [15]. It is assumed that the material is homogeneous and isotropic. That is, the material properties do not vary from point to point and are independent of the coordinate system choosen.

The general form of a yield criterion should be:

$$f(\sigma_{ij},\varepsilon_{ij}) = K \quad , \tag{9}$$

where K is a material constant. Until yielding occurs the material behaves elastically. Therefore, by Hooke's law,

$$\varepsilon_{ij} \propto \sigma_{ij} \ . \tag{10}$$

Then, the yield criterion becomes [5]

$$f(\sigma_{ij}) = K \ . \tag{11}$$

From these bases, von Mises' criterion in terms of stress components is

$$(\sigma_{11} - \sigma_{22})^2 + (\sigma_{22} - \sigma_{33})^2 + (\sigma_{33} - \sigma_{11})^2 + 6(\sigma_{12}^2 + \sigma_{23}^2 + \sigma_{31}^2) = 6k \tag{12}$$

where k is the yield shear strength.

A.1.5 STRESS-STRAIN RELATIONS

In elastic deformation, the strains are proportional to the stress. However, in plastic deformation the stresses are proportional to the strain increment or the strain rate. In 1871 Levy, and later in 1913, von Mises, proposed a general relationship between the strain increments and the stresses in plastic deformation. In differential form this relationship is [5]

$$d\varepsilon_{ij} = d\lambda \, \sigma'_{ij} \ , \tag{13}$$

where λ is a scalar quantity, a plasticity modulus of sorts. It is not a material constant and it varies as the deformation continues. Differentiating Equation 13 with respect to time yields

$$\frac{de_{ij}}{dt} = \frac{d\lambda}{dt} \sigma'_{ij}$$

$$e_{ij} = \dot{\lambda} \sigma'_{ij} \quad , \tag{14}$$

where the symbol $\dot{}$ represents differentiation with respect to time. Equation 14 is the proportionality relation between stress and strain-rate. In matrix form, the Levy-Mises equations (Equations 13) are

$$\begin{bmatrix} d\varepsilon_{11} & d\varepsilon_{12} & d\varepsilon_{13} \\ d\varepsilon_{21} & d\varepsilon_{22} & d\varepsilon_{23} \\ d\varepsilon_{31} & d\varepsilon_{32} & d\varepsilon_{33} \end{bmatrix} = d\lambda \begin{bmatrix} \sigma_{11} - p & \sigma_{12} & \sigma_{13} \\ \sigma_{21} & \sigma_{22} - p & \sigma_{23} \\ \sigma_{31} & \sigma_{32} - p & \sigma_{33} - p \end{bmatrix} \tag{15}$$

From Equation 15, we can write

$$d\varepsilon_{11} = d\lambda(\sigma_{11} - p) \ .$$

Inserting Equation 6 yields

$$d\varepsilon_{11} = d\lambda \left[\sigma_{11} - \frac{1}{3}(\sigma_{11} + \sigma_{22} + \sigma_{33}) \right] \tag{16}$$

$$d\varepsilon_{11} = \frac{2}{3} d\lambda \left[\sigma_{11} - \frac{1}{2}(\sigma_{22} + \sigma_{33}) \right].$$

Similarily,

$$\begin{aligned} d\varepsilon_{22} &= \frac{2}{3} d\lambda \left[\sigma_{22} - \frac{1}{2}(\sigma_{11} + \sigma_{33}) \right] \\ d\varepsilon_{33} &= \frac{2}{3} d\lambda \left[\sigma_{33} - \frac{1}{2}(\sigma_{11} + \sigma_{22}) \right] \\ d\varepsilon_{12} &= d\lambda \, \sigma_{12} \\ d\varepsilon_{23} &= d\lambda \, \sigma_{23} \\ d\varepsilon_{31} &= d\lambda \, \sigma_{31} \, . \end{aligned} \tag{17}$$

A.2 PLANE PLASTIC FLOW / SLIP-LINE FIELD SOLUTION

A.2.1 STRESS EQUATIONS

A state of plane plastic strain occurs when the flow is everywhere parallel to a certain plane, say the (x_1, x_2) plane, and motion of material is independent of the distance from that plane, in the x_3 direction. Thus, under conditions of plane strain,

$$\begin{aligned} e_{33} &= \varepsilon_{33} = d\varepsilon_{33} = 0 \\ \sigma_{23} &= 0 \\ \sigma_{31} &= 0 \\ \frac{\partial}{\partial x_3} &= 0 \, . \end{aligned} \tag{18}$$

From Equation 17, we can write

$$\sigma_{33} = \frac{1}{2} (\sigma_{11} + \sigma_{22}) \quad . \tag{19}$$

Inserting Equation 19 into von Mises' criterion, Equation 12, yields

$$\left(\frac{\sigma_{11} - \sigma_{22}}{2}\right)^2 + \sigma_{12}^2 = k^2 \quad . \tag{20}$$

The three-dimensional equilibrium equations, Equation 5, reduce to the following for the case of plane strain:

$$\frac{\partial \sigma_{11}}{\partial x_1} + \frac{\partial \sigma_{12}}{\partial x_2} = 0$$

$$\frac{\partial \sigma_{21}}{\partial x_1} + \frac{\partial \sigma_{22}}{\partial x_2} = 0 \quad . \tag{21}$$

Referring to the Mohr's circle diagram in Figure 39, if the σ_{11} and σ_{22} stress planes are rotated by an angle ϕ so they coincide with the maximum shear stress planes, the normal and shear stresses acting on the resulting planes are

$$\sigma_{12}(\phi) = k \tag{22}$$

$$\sigma_{11}(\phi) = \sigma_{22}(\phi) = -p = \frac{1}{2}(\sigma_{12} + \sigma_{22}) \quad .$$

Then the stresses acting in the x_i coordinate system can be written in the form

$$\sigma_{11} = -p + k \sin 2\phi$$

$$\sigma_{22} = -p - k \sin 2\phi \tag{23}$$

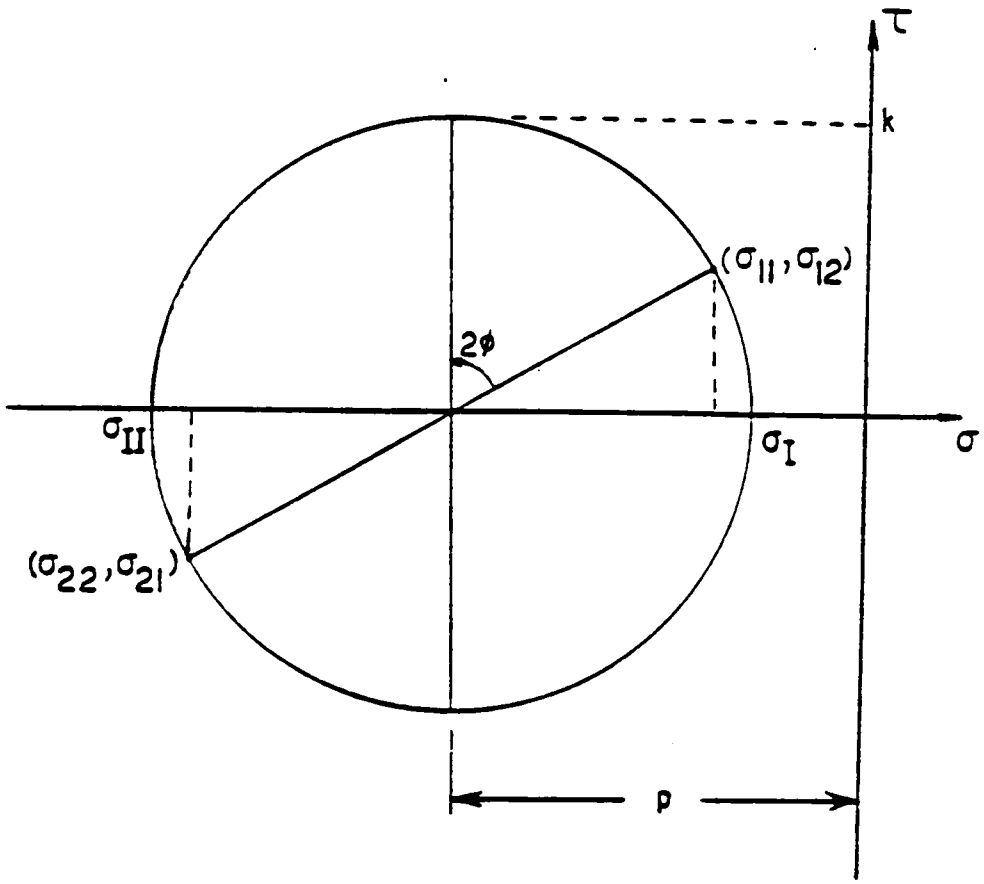

Figure 39. Mohr's circle of stress showing location of maximum shear stress planes

$$\sigma_{12} = k \cos 2\phi \ .$$

Differentiating Equation 23 with respect to x_1 and x_2 and substituting the resulting equations into the equilibrium equations, Equation 21, yields [2]

$$- \frac{\partial p}{\partial x_1} - 2k \cos 2\phi \frac{\partial \phi}{\partial x_1} - 2k \sin 2\phi \frac{\partial \phi}{\partial x_2} = 0$$

$$- \frac{\partial p}{\partial x_2} - 2k \sin 2\phi \frac{\partial \phi}{\partial x_1} + 2k \cos 2\phi \frac{\partial \phi}{\partial x_2} = 0 \ . \qquad (24)$$

Equations 25 are hyperbolic and solving by the method of characteristics [2], it is found that

$$\frac{\partial x_2}{\partial x_1} = \tan\phi$$

$$\frac{\partial x_2}{\partial x_1} = \tan\left(\phi + \frac{\pi}{2}\right) \ . \qquad (25)$$

The above equations show that the two families of characteristics form an orthogonal network. Members of the family corresponding to the angle ϕ from the x_1 axis are called α-lines and those in the $(\phi + \pi/2)$ direction are called β-lines. The α- and β-lines correspond to the directions of maximum shear stress. The directions of α- and β-lines are defined such that the direction of algebraically greater principal stress lies in the first and third quadrants of the (α,β) coordinate system.

The stress solution, also by the method of characteristics, reveals that

$$p + 2k\phi = k = C1 = \text{constant along an } \alpha\text{-line}$$
$$p - 2k\phi = k = C2 = \text{constant along a } \beta\text{-line.} \qquad (26)$$

A.2.2 VELOCITY EQUATIONS

Since it is assumed that the material is rigid, the incompressibility relation is

$$\varepsilon_{11} + \varepsilon_{22} + \varepsilon_{33} = 0 \ ,$$

or,

$$e_{11} + e_{22} + e_{33} = 0 \quad . \qquad (27)$$

In terms of velocities, and recalling that $e_{33} = 0$, combining Equation 4 and Equation 27 yields,

$$\frac{\partial v_1}{\partial x_1} + \frac{\partial v_2}{\partial x_2} = 0 \quad . \qquad (28)$$

Recalling Mohr's circle of stress, the location of the maximum shear stress planes is defined by [41]

$$\cot 2\phi_1 = \frac{2\sigma_{12}}{\sigma_{11} - \sigma_{22}} \quad ,$$

where ϕ_1 is measured from the positive x_1 direction. From Mohr's circle of strain, the planes of maximum shear strain, or strain-rate,are located by

$$\cot 2\phi_2 = - \frac{e_{12}}{e_{11} - e_{22}} \quad .$$

In an isotropic material, the principal axes of stress and strain rate coincide, or $\phi_1 = \phi_2$, hence,

$$\frac{2\sigma_{12}}{\sigma_{11} - \sigma_{22}} = \frac{\frac{\partial v_1}{\partial x_2} + \frac{\partial v_2}{\partial x_1}}{\frac{\partial v_1}{\partial x_1} - \frac{\partial v_2}{\partial x_2}} = \tan 2\phi \quad , \tag{29}$$

where Equation 29 has been rewritten using Equation 4. The isotropy equation is then [2]

$$\frac{\partial v_1}{\partial x_2} + \frac{\partial v_2}{\partial x_1} = -\left[\frac{\partial v_1}{\partial x_1} - \frac{\partial v_2}{\partial x_2}\right] \cot 2\phi \quad . \tag{30}$$

Equation 28 and Equation 30 are hyperbolic and the solution yields

$$dv_1 + \tan\phi \, dv_2 = 0 \text{ on an } \alpha\text{-line} \qquad (31)$$
$$dv_1 - \cot\phi \, dv_2 = 0 \text{ on a } \beta\text{-line.}$$

If U and V are the velocity components in the α- and β- directions, respectively,

$$v_1 = U\cos\phi - V\sin\phi$$
$$v_2 = U\sin\phi + V\cos\phi \; . \qquad (32)$$

Substituting into Equation 31 gives

$$dU - V\,d\phi = 0 \text{ on an } \alpha\text{-line}$$
$$dV + U\,d\phi = 0 \text{ on a } \beta\text{-line.} \qquad (33)$$

These are Geringer's equations which essentially state that the rate of extension along any slip-line is zero for an ideal rigid-plastic materal since the material has no elastic strain component. [1]

A.3 HENCKY'S FIRST THEOREM

Figure 40 shows an element of a slip-line field net. The region ABCD is bounded by two α-lines AB and DC and two β-lines AD and BC. The difference in hydrostatic pressure, p, between the points A and C can be found through Equation 26:

$$p_C - p_A = (p_C - p_D) + (p_D - p_A) = 2k(2\phi_D - \phi_C - \phi_A)$$

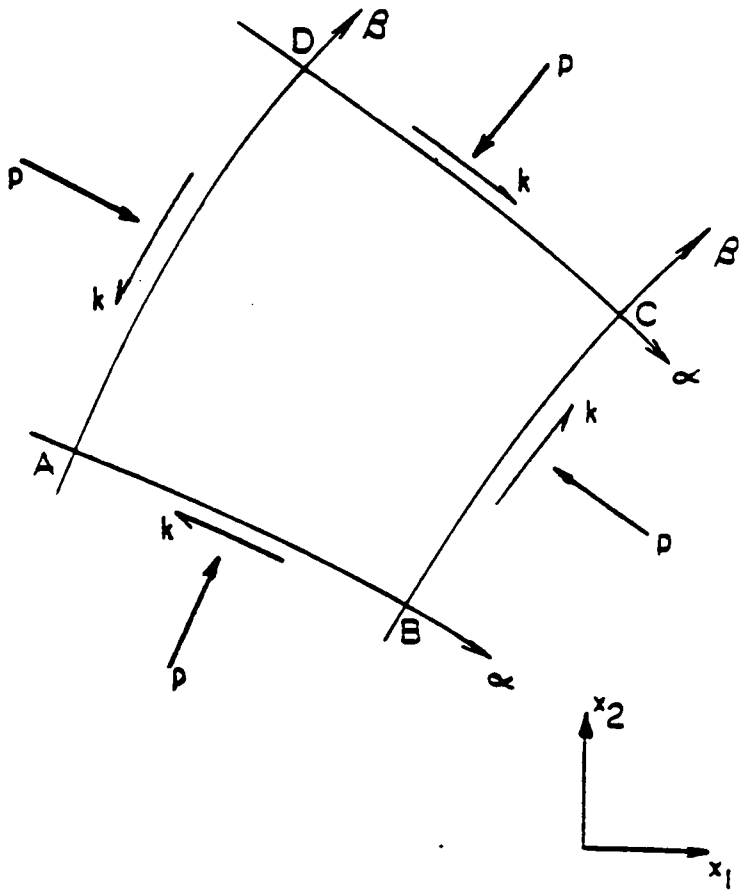

Figure 40. An element of a slip-line field net.

$$p_C - p_A = (p_C - p_B) + (p_B - p_A) = 2k(\phi_C - \phi_A - 2\phi_B) \ . \qquad (34)$$

Hence,

$$\begin{aligned} \phi_D - \phi_A &= \phi_C - \phi_B \\ \phi_C - \phi_D &= \phi_B - \phi_A \ . \end{aligned} \qquad (35)$$

Equation 35 is Hencky's first theorem which states that "the angle between two slip-lines of one family, where they are cut by a slip-line of the other family, is constant along their length. In other words, if we pass from one slip-line to another of the same family, along any intersecting slip-line, the angle turned through and the change in pressure are constant." [1]

A.4 CALCULATION OF SLIP-LINE FIELDS

This section will develop a method for the solution of problems of plane plastic flow of a rigid-plastic solid [1,2]. The method consists of using the finite difference forms of the equations derived in the preceding section. The method essentially consists of replacing an element of slip-line by a straight line that makes an angle ϕ for an α-line and $(\phi+\pi/2)$ for a β-line from the positive x_1 direction, where ϕ is the mean of the values of ϕ at the ends of the element.

For ease of notation, the following discussion will refer to an (x,y) two-dimensional coordinate system, where the x-axis corresponds to the

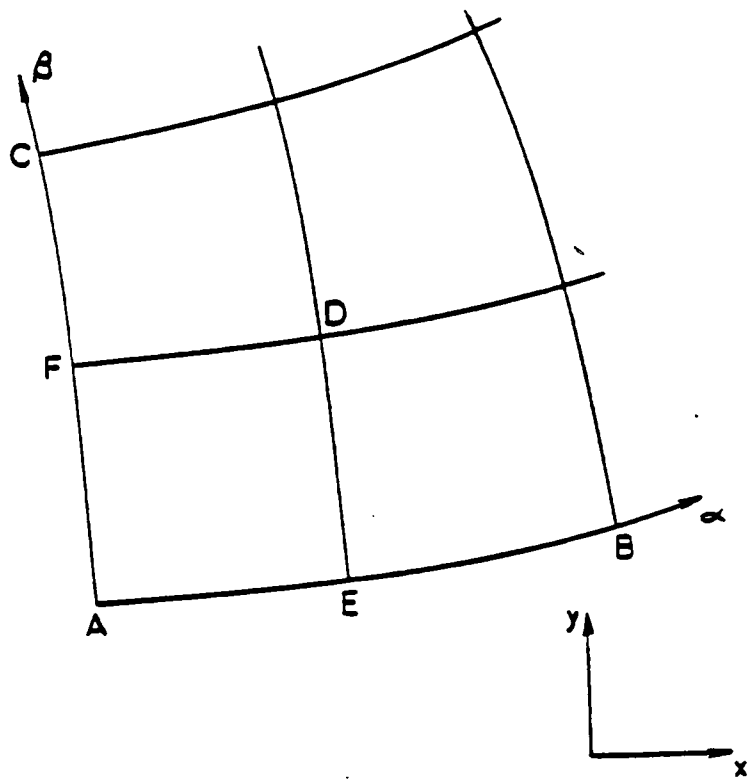

Figure 41. Slip-line net illustrating the first boundary value problem.

x_1-direction, and so forth. The simplest situation that arises in the construction of slip-line fields is called the "first boundary-value problem." Referring to Figure 41, if the α-line AB and the β-line AC are given the region bounded by the slip-lines AB, AC, the β-line through B and the α-line through C can be obtained numerically. Since the coordinates and the slip-line inclinations at points E and F are known, the point D, which is the intersection of the α-line through F and the β-line through E, can be found. By Hencky's first theorem, Equation 35,

$$\phi_D = \phi_E - \phi_A + \phi_F \ , \tag{36}$$

and the coordinates of point D can be approximated by the finite difference forms of Equation 25:

$$\begin{aligned} y_D - y_F &= (x_D - x_F) \tan\tfrac{1}{2}(\phi_D + \phi_F) \ , \\ y_D - y_E &= (x_D - x_E) \cot\tfrac{1}{2}(\phi_D + \phi_E) \ . \end{aligned} \tag{37}$$

The hydrostatic pressure at point D can be calculated by either of the following equations, which are finite difference forms of Equation 26:

$$\begin{aligned} p_D &= p_F + 2k(\phi_F - \phi_D) \quad \text{along an } \alpha\text{-line} \\ p_D &= p_E - 2k(\phi_E - \phi_D) \quad \text{along a } \beta\text{-line.} \end{aligned} \tag{38}$$

The procedure is repeated sequentially to obtain the coordinates and the phi-values of the other points in the field. The smaller the values $|\phi_E$

$- \phi_A|$ and $|\phi_F - \phi_A|$, the more accurately can be calculated the coordinated of the slip-line field nodal points by Equation 37, and thus the faster the convergence if an iterative technique must be employed.

If the normal components of velocity are known along the given slip-lines, that is V is known along AB and U is known along AC, the tangential components of velocity along these slip-lines can be found by applying Geringer's equations. The velocity components at the previously calulated point D can be found through the finite difference forms of Geringer's equations, Equation 33, by solving the two equations simultaneously for UD and VD,

$$U_D - U_F = \tfrac{1}{2}(V_D + V_F)(\phi_D - \phi_F)$$

$$V_D - V_E = \tfrac{1}{2}(U_D + U_E)(\phi_D - \phi_E) \quad . \tag{39}$$

Another situation which may arise and is of interest in this thesis is called the "third boundary-value problem."
This occurs when a slip-line OA and a curve OB, along which ϕ is known, are given as illustrated in Figure 42. First assume that the angle between the tangent to OA and OB at O is acute. It is desired to find the point D on the curve OB. At a point C on slip-line OA, a straight line is constructed in the β-direction to intersect OB at D'. Since the curve OB is known, the value of ϕ at D' can be calculated. Another straight line is then drawn through point C at an angle $(\phi+\pi/2)$ to intersect OB at D'', where $\phi = \tfrac{1}{2}(\phi_C + \phi_{D'})$. This procedure is repeated until the de-

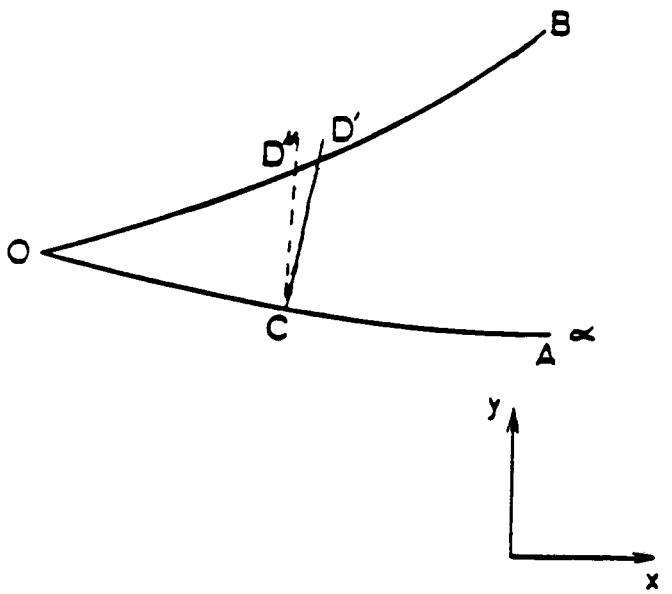

Figure 42. Slip-line net illustrating the third boundary value problem.

sired accuracy is reached. If the value of ϕ is constant along OB, this iterative process is not required.

A.5 PLANE-STRAIN PLASTIC FLOW OF VARIABLE FLOW STRESS MATERIALS

This section will present a numerical technique based on a modified form of Hencky's equations and Geringer's equations to solve plane-strain flow problems for materials which are sensitve to strain-rate and hydrostatic pressure. Hencky's theorem, Equation 26, has found extensive use for solving plane-strain flow problems for ideal rigid-plastic materials. Palmer and Oxley [8] modified these equations to solve flow problems of materials with variable flow stress. The equations they developed are of the form:

$$\begin{aligned} &\frac{\partial p}{\partial s_1} + 2k\frac{\partial \phi}{\partial s_1} - \frac{\partial k}{\partial s_2} = 0 \quad \text{on an } \alpha\text{-line} \\ &\frac{\partial p}{\partial s_2} - 2k\frac{\partial \phi}{\partial s_2} - \frac{\partial k}{\partial s_1} = 0 \quad \text{on a } \beta\text{-line} , \end{aligned} \tag{40}$$

where s_1 and s_2 are distances measured along the α- and β-lines, respectively. These equations found very limited application when first introduced due to computational difficulties. With the advent of the high-speed digital computers, Fenton and Durai Swamy [42,43] introduced the numerical procedures presented in this section.

If the flow stress is a function of the strain-rate and the hydrostatic pressure, i.e. k=k(e,p), Equation 40 and Geringer's equations Equation 33 are sufficient to solve plane flow problems of this more realistic material.

The procedure begins by calculating the slip-line field for the ideal rigid-plastic material using the methods developed in the previous section, Equations 37,38, and 39. The strain-rate components are then

$$e_\alpha = \frac{\partial U}{\partial s_1} - V\frac{\partial \phi}{\partial s_1}$$

$$e_\beta = \frac{\partial V}{\partial s_2} + U\frac{\partial \phi}{\partial s_2}. \tag{41}$$

The hydrostatic pressure is then calculated at the slip-line field nodal points using Equation 38. Knowing the relationship of the flow stress to the strain-rate and the hydrostatic pressure, a new flow stress distribution can be calculated throughout the field. Using Figure 40 as a reference, a new slip-line field is calculated using the variable flow-stress equation which is obtained by integrating Equation 40 and substituting into Equation 34. A first-order finite difference approximation of the resulting equation is

$$\begin{aligned}
&-(k_C + k_D)(\phi_C - \phi_D) + \frac{(CD)}{2}\left[\left(\frac{\Delta k}{\Delta s_2}\right)_D + \left(\frac{\Delta k}{\Delta s_2}\right)_C\right] \\
&+ (k_D + k_A)(\phi_D - \phi_A) + \frac{(AD)}{2}\left[\left(\frac{\Delta k}{\Delta s_1}\right)_D + \left(\frac{\Delta k}{\Delta s_1}\right)_A\right] \\
&= (k_C + k_B)(\phi_C - \phi_B) + \frac{(BC)}{2}\left[\left(\frac{\Delta k}{\Delta s_1}\right)_B + \left(\frac{\Delta k}{\Delta s_1}\right)_C\right] \\
&- (k_B + k_A)(\phi_B - \phi_A) + \frac{(AB)}{2}\left[\left(\frac{\Delta k}{\Delta s_2}\right)_A + \left(\frac{\Delta k}{\Delta s_2}\right)_B\right] .
\end{aligned} \tag{42}$$

The notation, CD, AD, BC, and AB, represents distances between the nodal points measured along the slip lines. For example, by geometry:

$$CD = [(x_D - x_C)^2 + (y_D - y_C)^2]^{1/2} \quad . \tag{43}$$

Also, Δ represents an incremental change in the quantity of interest.

The difference between any two consecutive flow stress distributions is

$$E_k = [\frac{1}{m+1} \sum_{i=1}^{m} (k_i^j - k_i^{j+1})^2]^{1/2} \quad , \tag{44}$$

where m is the total number of nodal points in the field and k_{ij} is the computed flow-stress at the nodal point i after the jth iteration. The iterative process is continued until E_k becomes satisfactorily small. Fenton and Durai Swamy found that the value of E_k becomes less than 2 percent after three iterations in their work.

APPENDIX B. COMPUTER PROGRAMS

```
C    Program   "S L I P":
C    This program calculates the slip-line field associated with
C    the indentation of a polymer film by a profile meter stylus.
C    The user inputs yield strength of the material and the angle
C    to which the stylus penetrates the surface. The program
C    outputs the x- and y-coordinates, the slip-line inclinations,
C    the hydrostatic pressure, the flow velocities,
C    the flow stress at the nodal points of the field, and the
C    pressure and vertical forces exerted on the stylus tip.
C    These results are stored in files 11 through 18, respectively.
C    The program can also be asked to calculate the load versus
C    angle of indentation for several yield strengths and the data
C    are stored in any file of the users choosing (best to use
C    files 40 and above).
C
C
C    NOMENCLATURE
C      X,Y = The cartesian coordinates of the nodal points
C      PHI = The inclination of the alpha-line to the positive X-dir
C      P   = The hydrostatic pressure at the nodal points
C      U,V = The flow velocities in the alpha- and beta-directions,
C            respectively, at the nodal points
C      YS  = the flow stress at the nodal points
C      YSS = yield strength of the material in shear
C      RS = the radius of the stylus tip = 2.5E-6 m
C      PSI = In generating an involute, it is the angle to which the
C            string has been unwrapped
C      INV = the involute function of ANG
C      R   = THE DISTANCE FROM THE ORIGIN TO A POINT ON THE
C            SLIP-LINE ABC
C      THE = the angular increment between the nodal points on the
C            indentation cavity AD
C      FORCE = the normal force on a nodal point on the cavity AD
C      FORCEY = the vertical component of FORCE
C      A   = the incremental area at a nodal point along the cavity AD
C      SIG = the normal stress at a nodal point on the cavity AD
C      THETA = the angle of indentation of the stylus tip which
C              has a half angle of 45 degrees.
C      PCOR = the hydorstatic pressure along the slip-line CD,
C             adjacent of the coronet
C      BD  = the length of the slip-line BD and the radius of the
C            circular fan BDC
C      FAN = the angular span of the circular fan BDC
C      NFAN = the number of angular increments in the
C             circular fan BDC
C      EK = the error in the successive flow stress distributions
C      SUBROUTINE KCONVG - calculates the flow stress for a particular
C            hydrostatic pressure, assuming a linear relationship
C            between the two parameters
C      SUBROUTINE VARIK - solves the nonlinear variable flow stress
C            equations by an interative approach.
C
      DOUBLE PRECISION X(50,50),Y(50,50),PHI(50,50),U(50,50),V(50,50)
      DOUBLE PRECISION PSI(50),P(50,50),INV(50),R(50),YS(50,50),THE(50)
      DIMENSION FORCE(30),FORCEY(30),A(30),SIG(30)
```

```
      DOUBLE PRECISION RFAN,CONV,THETA,THETAD,PSIA,PCOR,THE,DTH,SQRT2
      DOUBLE PRECISION ANGO,BD,FAN,DFAN,THFAN,XX(50,50),YY(50,50)
      DOUBLE PRECISION ANGI,TN1,TN2,PH1,PH2,YS1(50,50),EK1,EK,BYS,DYS
C
C   INITIALIZE ALL VARIABLES.
C
      DATA PI,SPEED,RS,YSS/3.1415926535D0,1.0,2.5D-6,6.351D7/
      DATA SLOPE/1.875D-1/,IVARI/20/,ITHETA/0/
      DATA IYS/0/,DYS/0.5D7/,NTHETA/17/
      INTEGER FLAG,BFILE,BFILE2,BFILE3,BFILE4
      REAL*8 K
      NAB=16
      NFAN=10
      NI=NAB+NFAN
      RFAN=NFAN
      CONV=PI/180.
C
C   READ DATA FROM TERMINAL.
C
  997 WRITE(6,448)
  448 FORMAT(' CHOOSE THE DESIRED OPERATION BY NUMBER:',/,
     1       7X,'(1) Calculate all data for the slip-line field for',/,
     2       11X,'one material yield strength and one indentation ',
     3       'angle.',/,
     4       7X,'(2) Calculate on the load versus angle of ',/,
     5       11X,'indentation data for several yield strengths.')
      READ(5,*,END=997) NOPER
      IF(NOPER.EQ.2) GO TO 995
  996 WRITE(6,444)
  444 FORMAT(' Enter the angle of indentation of the stylus, ',/,
     1       'in degrees,',/,' and the yield strength.')
      READ(5,*,END=996) THETAD,YSS
      WRITE(6,445)
  445 FORMAT(/,' The angle of indentation is ',F4.1,/,
     1       ' The yield strength is ',E10.5,/)
      GO TO 994
  995 WRITE(6,446)
  446 FORMAT(' Enter (1) the beginning yield stength,',/,
     1       7X,' (2)the number of yield stengths to consider,',/,
     2       3X,' and (3) the file to begin storing the data.')
      READ(5,*,END=995) BYS,NYS,BFILE
      BFILE2 = BFILE + NYS - 1
      BFILE3 = BFILE + NYS
      BFILE4 = BFILE2 +NYS
      WRITE(6,449) BFILE,BFILE2,BFILE3,BFILE4
  449 FORMAT(' The load vs. angle data will be stored in files ',/,
     1       I2,' through ',I2,' for an ideal material ',/,
     2       ' and in files ',I2,' through ',I2,/,
     3       ' for a material sensitive to hydrostatic pressure.')
  992 IYS = IYS + 1
      YSS = BYS + (IYS - 1)*DYS
      WRITE(6,451) YSS
  451 FORMAT(' Yield strength = ',E10.5)
  993 ITHETA = ITHETA + 1
      RTH = ITHETA
```

```
C
C START WITH AN INDENTATION ANGLE OF 5 DEGREES AND INCREMENT BY
C 2.5 DEGREES UP TO 45 DEGREES.
C
      THETAD = 5. + (RTH - 1.) * 2.5
  994 THETA=THETAD*CONV
      PSIA=PI/4.
      PCOR=YSS*2.*COS(THETA)**2
      SQRT2=SQRT(2.)
      FLAG = 0
C
C   DEFINE THE SURFACE OF THE STYLUS
C
      THE(1)=0.0
      NABM1 = NAB-1
      RABM1 = NABM1
      DTH=THETA/RABM1
      DO 10 I=1,NAB
           X(I,I)=RS*DSIN(THE(I))
           Y(I,I)=-RS*DCOS(THE(I))
           PHI(I,I)=-PI/4.+THE(I)
           U(I,I)=SPEED*(SQRT2)
           YS(I,I) = YSS
           THE(I+1)=THE(I)+DTH
   10 CONTINUE
C
C   DEFINE SLIP-LINE ABC
C
      ANGO=DTAN(PSIA)-PSIA
      BD=(ANGO+PI/4.+THE(NAB)-1.)*RS/SQRT2
      FAN=PI/2.-THETA
      DFAN=FAN/RFAN
      THFAN=0.0
      DO 20 I=2,NI
           IF(I.GT.NAB) GO TO 21
           PSI(I)=DATAN(ANGO+PI/4.+THE(I))
           R(I)=RS/SQRT2/DCOS(PSI(I))
           INV(I)=DTAN(PSI(I))-PSI(I)
           ANGI=INV(I)-ANGO
           X(I,1)=R(I)*DSIN(ANGI)
           Y(I,1)=-R(I)*DCOS(ANGI)
           PHI(I,1)=-PI/4.+THE(I)
           V(I,1)=0.0
           U(I,1)=U(I-1,1)+0.5*(V(I,1)+V(I-1,1))*(PHI(I,1)-PHI(I-1,1))
           YS(I,1) = YSS
        GO TO 20
   21      THFAN=THFAN+DFAN
           X(I,1)=X(NAB,NAB)+BD*DSIN(THETA-PI/4.+THFAN)
           Y(I,1)=Y(NAB,NAB)-BD*DCOS(THETA-PI/4.+THFAN)
           PHI(I,1)=PHI(NAB,NAB)+THFAN
           V(I,1)=0.0
           U(I,1)=U(I-1,1)+0.5*(V(I,1)+V(I-1,1))*(PHI(I,1)-PHI(I-1,1))
           YS(I,1) = YSS
   20 CONTINUE
C
```

```
C  CALCULATE THE NUMBER OF NODAL POINTS IN THE FIELD.
C
      NODES=0
      DO 23 J=1,NAB
           DO 24 I=J,NI
                NODES = NODES +1
   24      CONTINUE
   23 CONTINUE
      WRITE(6,25) NODES
   25 FORMAT(2X,'THE TOTAL NUMBER OF NODAL POINTS IN THE FIELD IS ',I6)
C
CC CALCULATE COORDS, ANGLES, AND VELOCITIES AT THE NODAL POINTS
C
   92 FLAG = FLAG + 1
      DO 30 J=2,NAB
           JJ=J+1
           DO 40 I=JJ,NI
                IF (FLAG.GT.1) GO TO 93
                PHI(I,J)=PHI(I,J-1)+PHI(I-1,J)-PHI(I-1,J-1)
                TN1=DTAN((PHI(I,J)+PHI(I-1,J))/2.)
                TN2=DTAN((PHI(I,J)+PHI(I,J-1))/2.)
                Y(I,J)=(Y(I-1,J)+(X(I,J-1)-X(I-1,J))*TN1
     1                    +TN1*TN2*Y(I,J-1))
     2                    /(1.0+TN1*TN2)
                X(I,J)=X(I,J-1)-(Y(I,J)-Y(I,J-1))*TN2
                YS(I,J) = YSS
   93           PH1=PHI(I,J)-PHI(I,J-1)
                PH2=PHI(I,J)-PHI(I-1,J)
                U(I,J)=(U(I-1,J)+0.5*(V(I,J-1)+V(I-1,J)
     1                    -0.5*U(I,J-1)*PH1)*PH2)/(1.0+0.25*PH1*PH2)
                V(I,J)=V(I,J-1)-0.5*(U(I,J)+U(I,J-1))*PH1
   40      CONTINUE
   30 CONTINUE
C
CC
CC  CALCULATE THE HYDROSTATIC PRESSURE AND FLOW STRESS AT THE
CC  NODAL POINTS.
C
      FTOTAL = 0.0
      DO 50 J=1,NAB
           PCOR= YS(NI,J)
           P(NI,J) = PCOR
           DO 60 II=1,NI-J
                I=-II+NI
                P(I,J) = P(I+1,J) + 2.*YS(I,J)*(PHI(I+1,J)-PHI(I,J))
   60      CONTINUE
C
CC CALCULATE THE PRESSURE AND FORCES ON THE STYLUS TIP.
C
           SIG(J) = P(J,J) + YS(J,J)
           IF(J.GT.1) GO TO 64
           A(J) = (THE(J+1)/2. - THE(J)) * RS
         GO TO 66
   64      IF(J.EQ.NAB) GO TO 65
           A(J) = (THE(J+1) - THE(J-1))/2. * RS
```

```
          GO TO 66
   65       A(J) = (THE(J) - (THE(J) + THE(J-1))/2.) * RS
   66       FORCE(J) = A(J) * SIG(J)
            FORCEY(J) = FORCE(J) * COS(THE(J))
            FTOTAL = FTOTAL + FORCEY(J)
   50 CONTINUE
C
C  PRINT THE RESULTS.
C
C  ZERO ALL X,Y,PHI,U,V,P, AND YS NOT IN RANGE OF FIELD.
C
      DO 700 I=1,NI
           DO 701 J=1,NAB
                XX(I,J) = X(I,J)*1.0D+06
                YY(I,J) = Y(I,J)*1.0D+06
                IF(FLAG.EQ.3) GO TO 701
                IF(J.GT.I) GO TO 702
              GO TO 701
  702           X(I,J) = 0.
                Y(I,J) = 0.
                PHI(I,J) = 0.
                P(I,J) = 0.
                U(I,J) = 0.
                V(I,J) = 0.
                YS(I,J) = 0.
  701       CONTINUE
  700 CONTINUE
C
C     IF(NOPER.EQ.2) GO TO 998
      DO 705 IPRT=1,8
           IF (IPRT.EQ.1) WRITE(11,501) THETAD,FLAG
           IF (IPRT.EQ.2) WRITE(12,502) THETAD,FLAG
           IF (IPRT.EQ.3) WRITE(13,503) THETAD,FLAG
           IF (IPRT.EQ.4) WRITE(14,504) THETAD,FLAG
           IF (IPRT.EQ.5) WRITE(15,505) THETAD,FLAG
           IF (IPRT.EQ.6) WRITE(16,506) THETAD,FLAG
           IF (IPRT.EQ.7) WRITE(17,507) THETAD,FLAG
           IF (IPRT.EQ.8) WRITE(18,508) THETAD,FLAG
C
  501      FORMAT(2X,'X-COORDS AT SLIP-LINE FIELD NODAL POINTS:',
     $       '  THETA= ',F5.2,'  FLAG= ',I1,/)
  502      FORMAT(2X,'Y-COORDS AT SLIP-LINE FIELD NODAL POINTS:',
     $       '  THETA= ',F5.2,'  FLAG= ',I1,/)
  503      FORMAT(2X,'PHI VALUES AT NODAL POINTS:  THETA= '
     $       ,F5.2,'  FLAG= ',I1,/)
  504      FORMAT(2X,'HYDROSTATIC PRESSURE AT NODAL POINTS:  THETA= '
     $       ,F5.2,'  FLAG= ',I1,/)
  505      FORMAT(2X,'VELOCITY IN ALPHA-DIRECTION AT NODAL POINTS:',
     $       '  THETA= ',F5.2,'  FLAG= ',I1,/)
  506      FORMAT(2X,'VELOCITY IN BETA-DIRECTION AT NODAL POINTS:',
     $       '  THETA= ',F5.2,'  FLAG= ',I1,/)
  507      FORMAT(2X,'FLOW STRESS AT NODAL POINTS:  THETA= '
     $       ,F5.2,'  FLAG= ',I1,/)
  508      FORMAT(2X,'PRESSURE AND VERTICAL FORCES AT STYLUS NODAL',
```

```
     $     ,' POINTS:  THETA= ',F5.2,' FLAG= ',I1,/)
C
C
      IF (IPRT.EQ.8) GO TO 706
           DO 706 I=1,NI
                IF (IPRT.EQ.1) WRITE(11,509) (X(I,J),J=1,NAB)
                IF (IPRT.EQ.1.AND.FLAG.EQ.6) WRITE(30,511)
     $                                        (XX(I,J),J=1,NAB)
                IF (IPRT.EQ.2) WRITE(12,509) (Y(I,J),J=1,NAB)
                IF (IPRT.EQ.2.AND.FLAG.EQ.6) WRITE(31,511)
     $                                        (YY(I,J),J=1,NAB)
                IF (IPRT.EQ.3) WRITE(13,509) (PHI(I,J),J=1,NAB)
                IF (IPRT.EQ.4) WRITE(14,509) (P(I,J),J=1,NAB)
                IF (IPRT.EQ.5) WRITE(15,509) (U(I,J),J=1,NAB)
                IF (IPRT.EQ.6) WRITE(16,509) (V(I,J),J=1,NAB)
                IF (IPRT.EQ.7) WRITE(17,509) (YS(I,J),J=1,NAB)
  509           FORMAT(2X,12D10.3,/)
  511           FORMAT(2X,12F10.4,/)
  706      CONTINUE
  705 CONTINUE
  998 WRITE(18,509) (SIG(J),J=1,NAB)
      WRITE(18,509) (FORCEY(J),J=1,NAB)
      WRITE(18,510) FTOTAL
  510 FORMAT(2X,'TOTAL VERTICAL FORCE ON STYLUS IS',/,2X,12D10.3,/)
      IF(FLAG.EQ.1) WRITE(BFILE+IYS-1,512) THETAD,FTOTAL
      IF(FLAG.EQ.6) WRITE(BFILE3+IYS-1,512) THETAD,FTOTAL
  512 FORMAT(2X,F4.1,E10.3)
C
C  MODIFY YIELD STRENGTH DUE TO HYDROSTATIC PRESSURE
C  AND CALCULATE A NEW SLIP LINE FIELD.
C
      DO 70 J=1,NAB
           DO 80 I=J,NI
                CALL KCONVG(YSS,K,P,I,J,YS,THETA,SLOPE,PI,NOCON)
                IF(NOCON.EQ.2) WRITE(6,226) I,J
  226           FORMAT(2X,'SUBR. KCONVG DID NOT CONVERGE AFTER',
                ' 100 ITERS (',I2,',',I2,')',/)
                IF (FLAG.GT.1) GO TO 71
                YS(I,J)= K
   71           YS1(I,J) = K
   80      CONTINUE
   70 CONTINUE
C
C  CALCULATE THE ERROR IN THE COMPUTED FLOW STRESS DISTRIBUTION
C  AND CHECK FOR CONVERGENCE.
C
      IF (FLAG.EQ.1) GO TO 83
      EK1 = 0.0
      DO 81 J=1,NAB
           DO 82 I=J,NI
                EK1 = (YS1(I,J) - YS(I,J))**2 + EK1
                YS(I,J) = YS1(I,J)
   82      CONTINUE
   81 CONTINUE
      EK = SQRT(EK1/(NODES + 1))
```

```
      WRITE(18,230) EK,FLAG
  230 FORMAT(2X,' THE ERROR IN THE COMPUTED FLOW STRESS DISTRIBUTION IS
     1',D11.4,2X,' ON ITERATION #', I4,/)
      IF(FLAG.EQ.6) GO TO 999
C
   83 DO 90 J=2,NAB-1
            JJ=J+1
            DO 91 I=JJ,NI
                 CALL VARIK(X,Y,PHI,XD,YS,I,J,IVARI)
                 IF(NOCON.EQ.1) WRITE(6,222) I,J
  222            FORMAT('SUBROUTINE VARIK DID NOT CONVERGE. (I,J)='
     1           ,'(',I2,',',IS,')')
                 IF(NOCON.EQ.1) STOP
   91       CONTINUE
   90 CONTINUE
      GO TO 92
  999 IF(NOPER.EQ.1)STOP
      IF(ITHETA.LT.NTHETA) GO TO 993
      ITHETA = 0
      IF(IYS.LT.NYS) GO TO 992
      STOP
      END
```

```
C
C
C    THIS SUBROUTINE SOLVES THE VARIABLE FLOW STRESS EQUATIONS, THREE
C    NONLINEAR SIMULTANEOUS EQUATIONS.
C    AN ITERATIVE METHOD IS USED WHICH INVOLVES WRITING A TRUNCATED
C    TAYLOR SERIES EXPANSION FOR EACH OF THE THREE EQUATIONS.
C
      SUBROUTINE VARIK (X,Y,PHI,XD,YS,I,J,IVARI)
C
      DIMENSION X(50,50),Y(50,50),PHI(50,50),YS(50,50)
      DOUBLE PRECISION X,Y,PHI,XA,XB,XC,XD,YA,YB,YC,YD,PHA,PHB,PHC
      DOUBLE PRECISION PHD,YS,YSA,YSB,YSC,YSD,XBA,YBA,YSBA,XCA,YCA
      DOUBLE PRECISION YSCA,SQ1,SQ2,SQ3,SQ4,YSDB,YSDC,XDB,XDC,YDC
      DOUBLE PRECISION YDB,F1,F2,F3,F1DX,F1DY,F1DP,F2DX,F2DY,F2DP
      DOUBLE PRECISION F3DX,F3DY,F3DP,DEL,DEL1,DEL2,DEL3,A,B,C
      DOUBLE PRECISION XNEXT,YNEXT,PHNEXT,ERR1,ERR2,ERR3
      ITER=0
      XA=X(I-1,J-1)
      YA=Y(I-1,J-1)
      PHA=PHI(I-1,J-1)
      XB=X(I,J-1)
      YB=Y(I,J-1)
      PHB=PHI(I,J-1)
      XC=X(I-1,J)
      YC=Y(I-1,J)
      PHC=PHI(I-1,J)
      XD=X(I,J)
      YD=Y(I,J)
      PHD=PHI(I,J)
      YSA=YS(I-1,J-1)
      YSB=YS(I,J-1)
      YSC=YS(I-1,J)
      YSD=YS(I,J)
      XBA=XB-XA
      YBA=YB-YA
      YSBA=YSB-YSA
      XCA=XC-XA
      YCA=YC-YA
      YSCA=YSC-YSA
      SQ2=DSQRT(XCA**2+YCA**2)
      SQ4=DSQRT(XBA**2+YBA**2)
      YSDB=YSD-YSB
      YSDC=YSD-YSC
C
C  THE ITERATION BEGINS HERE
C
  999 ITER=ITER+1
      XDB=XD-XB
      YDB=YD-YB
      XDC=XD-XC
      YDC=YD-YC
C
C
      SQ1=DSQRT(XDC**2+YDC**2)
      SQ3=DSQRT(XDB**2+YDB**2)
```

```
C
C
C    ENTER THE VARIABLE FLOW STRESS EQUATIONS.
C
      F1=YSD*PHC-YSC*PHD+YSA*PHC-YSC*PHA+YSD*PHB-YSB*PHD+YSA*PHB-YSB*PHA
     1   +SQ1/2.*(YSCA/SQ2+YSDB/SQ3) + SQ2/2.*(YSDC/SQ1+YSBA/SQ4)
     2   -SQ3/2.*(YSBA/SQ4+YSDC/SQ1) - SQ4/2.*(YSCA/SQ2+YSDB/SQ3)
      F2=YDB + XDB/DTAN(0.5*(PHD+PHB))
      F3=YDC - XDC*DTAN(0.5*(PHD+PHC))
C
C
C    ENTER THE FIRST DERIVATIVES OF THE VARIABLE FLOW STRESS EQS.
C
C    F1DX = PARTIAL DERIVATIVE OF F1 WITH RESPECT TO X, AND SO FORTH
C
      F1DX=XDC/SQ1/2.*(YSCA/SQ2+YSDB/SQ3)-SQ1/2.*YSDB*XDB/SQ3**3
     1      -SQ2/2.*YSDC*XDC/SQ1**3 - XDB/SQ3/2.*(YSBA/SQ4+YSDC/SQ1)
     2      +SQ3/2.*YSDC*XDC/SQ1**3 + SQ4/2.*YSDB*XDB/SQ3**3
C
C
      F1DY=YDC/SQ1/2.*(YSCA/SQ2+YSDB/SQ3)-SQ1/2.*YSDB*YDB/SQ3**3
     1      -SQ2/2.*YSDC*YDC/SQ1**3 - YDB/SQ3/2.*(YSBA/SQ4+YSDC/SQ1)
     2      +SQ3/2.*YSDC*YDC/SQ1**3 + SQ4/2.*YSDB*YDB/SQ3**3
C
      F1DP=-2.*YSD-YSC-YSB
C
C
      F2DX=1./DTAN(0.5*(PHD+PHB))
C
      F2DY=1.0
C
      DS=DSIN(PHD+PHB)
      F2DP=-XDB/(DSIN(0.5*(PHD+PHB)))**2
C
C
      F3DX=-DTAN(0.5*(PHD+PHC))
C
      F3DY=1.0
C
      F3DP=-XDC/(DCOS(0.5*(PHD+PHC)))**2
C
C    CALCUATE THE DETERMINANTS TO SOLVE THE EQUATIONS BY CRAMER'S RULE.
C
      DEL1=-F1*(F2DY*F3DP-F2DP*F3DY) + F2*(F1DY*F3DP-F1DP*F3DY)
     1      - F3*(F1DY*F2DP-F1DP*F2DY)
C
      DEL=F1DX*(F2DY*F3DP-F2DP*F3DY) - F1DY*(F2DX*F3DP-F2DP*F3DX)
     1    + F1DP*(F2DX*F3DY-F2DY*F3DX)
C
      DEL2=F1*(F2DX*F3DP-F2DP*F3DX) - F2*(F1DX*F3DP-F1DP*F3DX)
     1      + F3*(F1DX*F2DP-F1DP*F2DX)
C
      DEL3=-F1*(F2DX*F3DY-F2DY*F3DX) + F2*(F1DX*F3DY-F1DY*F3DX)
     1      - F3*(F1DX*F2DY-F1DY*F2DX)
C
```

```
      A=DEL1/DEL
      B=DEL2/DEL
      C=DEL3/DEL
C
      XNEXT=XD+A
      YNEXT=YD+B
      PHNEXT=PHD+C
C
C  CHECK FOR CONVERGENCE
C
      IF(PHD.EQ.0.0) PHD = 0.15D-16
      ERR1=DABS(A/XD)
      ERR2=DABS(B/YD)
      ERR3=DABS(C/PHD)
C
      IF(ERR1.LE.0.05.AND.ERR2.LE.0.05.AND.ERR3.LE.0.05) GO TO 998
      IF(ITER.LT.IVARI) GO TO 997
      NOCON=1
      RETURN
  997 XD=XNEXT
      YD=YNEXT
      PHD=PHNEXT
      GO TO 999
C
  998 X(I,J)=XNEXT
      Y(I,J)=YNEXT
      PHI(I,J)=PHNEXT
C
      RETURN
      END
```

```
C
C  Subroutine 'K C O N V G'
C
C  Given the present yield strength at the nodal point, a
C  new yield strength is calculated knowing that the yield
C  strength is a linear function of the hydrostatic pressure
C
      SUBROUTINE KCONVG(YSS,K,P,I,J,YS,THETA,SLOPE,PI,NOCON)
      DOUBLE PRECISION YS,P,ERR,T,YSS
      REAL*8 K
      DIMENSION YS(50,50)
      PI=3.1415927
      N=0
      T=YSS+SLOPE*P
C     IF(I.EQ.10.AND.J.EQ.10) WRITE(1,1) N,T,K,P
    1 FORMAT(2X,I5,3(2X,E10.4))
      K=T
      RETURN
      END
```

```
C  PROGRAM  "S L I P L O T"
CC
CC THIS PROGRAM PLOTS THE SLIP-LINE FIELD FOR THE
CC FORTRAN PROGRAM 'SLIP.FOR;1'.
C
      DIMENSION X(40,40),Y(40,40),LAB1(8)
      DIMENSION LAB2(2),LAB2O(2),LAB3(5)
      DATA XMAX/0.0/,YMIN/0.0/
      DATA LAB1/84,72,69,84,65,32,61,32/,LAB3/32,68,69,71,83/
      PI=3.1415927
      I2=2
      NI=26
      NAB=16
      NFAN=10
C
CC READ SLIP-LINE FIELD COORDINATES FROM FILES 30 AND 31
C
      DO 2 I=1,NI
      READ(30,1) (X(I,J),J=1,NAB)
      READ(31,1) (Y(I,J),J=1,NAB)
    1 FORMAT(2X,12E10.3,/)
    2 CONTINUE
C
CC LOCATE THE POINTS THAT MAKE UP THE CORONET.
C
      X(NI+1,NAB+1) = 2.*X(NI,1) - X(NI,NAB)
      THETA = 180./PI*ATAN(X(NI,NAB)/-Y(NI,NAB))
      ITHETA = THETA
      LAB2(1) = ITHETA/10
      LAB2(2) = ITHETA - LAB2(1)*10
      CALL ASC(LAB2,LAB2O)
      IF(LAB2(1).EQ.0) I2=1
      IF(LAB2(1).EQ.0) LAB2O(1)=LAB2O(2)
      THETA=THETA*PI/180.
      AREA = THETA/2.*(ABS(Y(1,1)))**2 + Y(NI,NAB)*X(NI,NAB)/2.
      Y(NI+2,NAB+2) = Y(NI,NAB) + 2.*AREA/(X(NI+1,NAB+1)-X(NI,NAB))
      Y(NI+1,NAB+1) = Y(NI,NAB)
      X(NI+2,NAB+2) = X(NI,NAB)+ABS(Y(NI+2,NAB+2)-Y(NI,NAB))/TAN(THETA)
      X(NI+3,NAB+3) = X(NI+1,NAB+1)*3./2.-X(NI,1)/2.
C
CC FIND THE MAXIMUM AND MINIMUM VALUES OF X AND Y.
C
      DO 5 I=1,NI+3
      DO 6 J=1,NAB+3
      IF(X(I,J).GT.XMAX) XMAX = X(I,J)
      IF(Y(I,J).LT.YMIN) YMIN = Y(I,J)
    6 CONTINUE
    5 CONTINUE
C
CC SET UP THE TERMINAL WINDOW
C
      XMP1 = XMAX + 0.1*XMAX
      YMM1 = YMIN + 0.1*YMIN
      YM2 = YMM1 + (XMP1 + 0.5)*781./1024.
      CALL INITT(960)
```

```
      CALL DWINDO (-0.5,XMP1,YMM1,YM2)
C
CC  WRITE THE LABEL FOR THE PLOT
C
      CALL MOVEA(X(NI,NAB),Y(NI,NAB)-(YMIN-Y(NI+2,NAB+2))/2.)
      CALL ANSTR(8,LAB1)
      CALL ANSTR(I2,LAB2O)
      CALL ANSTR(5,LAB3)
C
CC  DRAW THE SLIP-LINE FIELD
C
      DO 3 J=1,NAB-1
      CALL MOVEA (X(J,J),Y(J,J))
      CALL DRAWA (X(J+1,J),Y(J+1,J))
      CALL DRAWA (X(J+1,J+1),Y(J+1,J+1))
      CALL DRAWA (X(J,J),Y(J,J))
      JJ=J+1
      DO 4 I=JJ,NI-1
      CALL MOVEA (X(I,J),Y(I,J))
      CALL DRAWA (X(I+1,J),Y(I+1,J))
      CALL DRAWA (X(I+1,J+1),Y(I+1,J+1))
      CALL DRAWA (X(I,J+1),Y(I,J+1))
      CALL DRAWA (X(I,J),Y(I,J))
    4 CONTINUE
    3 CONTINUE
C
CC  DRAW THE CORONET
C
      CALL MOVEA(X(NI,1),Y(NI,1))
      CALL DRAWA(X(NI+1,NAB+1),Y(NI+1,NAB+1))
      CALL DASHA(X(NI,NAB),Y(NI,NAB),3)
      CALL DRAWA(X(NI+2,NAB+2),Y(NI+2,NAB+2))
      CALL DRAWA(X(NI+1,NAB+1),Y(NI+1,NAB+1))
C
CC  LABEL SELECTED POINTS
C
      CALL MOVEA(-X(2,2),Y(2,1))
      CALL ANMODE
      CALL ANCHO(65)
      CALL MOVEA(X(NAB,1)-X(2,2),2.*Y(NAB,1)-Y(NAB,3))
      CALL ANCHO(66)
      CALL MOVEA(X(NI,1)+X(2,2),Y(NI-2,1))
      CALL ANCHO(67)
      CALL MOVEA(X(NI,NAB),Y(NI,NAB)+Y(1,1)-Y(2,1))
      CALL ANCHO(68)
      CALL MOVEA(X(NI+2,NAB+2),Y(NI+2,NAB+2)-Y(2,1)+Y(1,1))
      CALL ANCHO(69)
      CALL MOVEA(X(NI+1,NAB+1),Y(NI+1,NAB+1)+Y(1,1)-Y(2,1))
      CALL ANCHO(70)
C
CC  DRAW THE FREE SURFACE
C
      CALL MOVEA(X(NI+1,NAB+1),Y(NI+1,NAB+1))
      CALL DRAWA(X(NI+3,NAB+3),Y(NI+1,NAB+1))
C
```

```
C  DRAW THE LINE OF SYMMETRY
C
      CALL MOVEA(X(1,1),Y(NI+2,NAB+2))
C
      CALL DASHA(X(1,1),YMIN,2)
      CALL FINITT(0,767)
      STOP
      END
C
C  SUBROUTINE 'A S C':  USED TO CONVERT NUMBERS TO ASCII FORMAT.
C
      SUBROUTINE ASC(IN,OUT)
      DIMENSION IN(2)
      INTEGER OUT(2)
      IST=48
      DO 10 I=1,2
          OUT(I)=IST+IN(I)
   10 CONTINUE
      RETURN
      END
```

APPENDIX C. CONSTRUCTION OF A SLIP-LINE FIELD FOR STYLUS INDENTATION.

C.1 CALCULATION OF THE CAVITY SURFACE AD

The surface of the cavity is assumed to be cylidrical in shape with radius R. Thus, placing the origin at the center of curvature and letting the slip-line field reside in the 4th quadrant of the (x,y) coordinate system, the coordinates of nodal points along the cavity surface are calculated by

$$X_i = R \sin\theta_i \tag{45}$$

$$Y_i = -R \cos\theta_i \ , \tag{46}$$

where θ_i is measured counter-clockwise from the negative y-axis. The inclination of the α-lines at the nodal points is given by

$$\phi_i = -\frac{\pi}{4} + \theta_i \ . \tag{47}$$

C.2 CALCULATION OF THE SLIP-LINE ABC

The construction of the slip-line ABC is shown in Figure 43. The straight β-lines in the region ABD intersect the cavity surface at 45 degrees. These lines are then tangential to a circle of radius $R/\sqrt{2}$, concentric with the cavity surface. From Hill [1], the α-lines in the region ABD are then involutes of that circle. The nodal points along the

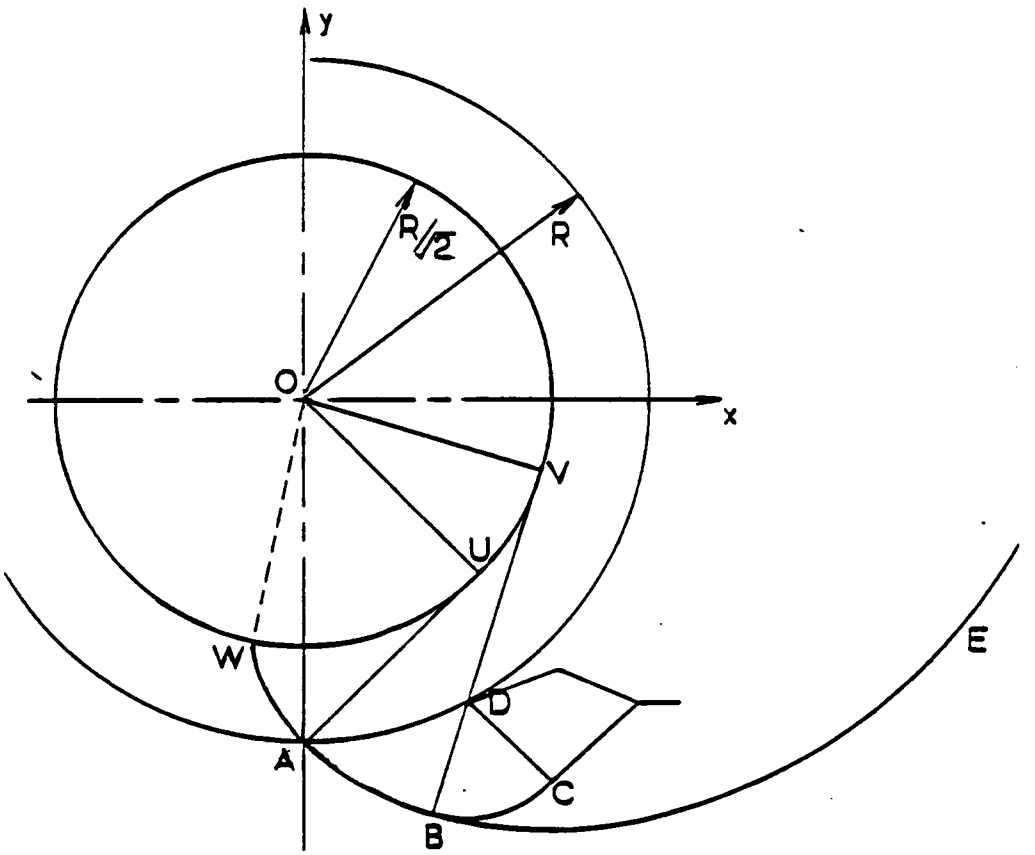

Figure 43. Construction of the slip-line field with involutometry.

α-line ABC from point A to point B are calculated by involutometry [44]. The α-lines in the region BCD are circular arcs with the center of curvature at point D. The inclination of the α-line at point A, ϕ_A, is π/4. <WOA is defined as the involute funtion of ϕ_A, inv $\phi_A = \tan\phi_A - \phi_A$. From the principle of generating an involute by unwinding a taut string from the circumference of a circle, the arc WV is equal to the length BV. Therefore,

$$<WOV = \frac{\text{arc } WV}{OV} = \frac{BV}{OV} = \tan\phi_B = \frac{BV}{R/\sqrt{2}} \tag{48}$$

$$<WOV = <WOA + \frac{\pi}{4} + \theta_D \ , \tag{49}$$

where θ_D is defined as above. The length BV is then

$$BV = <WOV \frac{R}{\sqrt{2}} = (<WOA + \frac{\pi}{4} + \theta_D)\frac{R}{\sqrt{2}} \ . \tag{50}$$

The length of the β-line BD is then

$$BD = BV - \frac{R}{\sqrt{2}} = (<WOA + \frac{\pi}{4} + \theta_D - 1)\frac{R}{\sqrt{2}} \tag{51}$$

BD is the radius of curvature of the circular arc BC. Next, let <WOj denote the involute function at the jth point on the involute AB, where point A is the the 1st point:

$$<WOj = <WOA + \frac{\pi}{4} + \theta_i \tag{52}$$

The distance from the origin to the jth nodal point is then

$$r_j = \frac{R}{\sqrt{2}\cos(<WOj)} \quad . \tag{53}$$

The coordinates of the point along the slip-line from A to B are

$$x_j = r_j \sin(<WOj - <WOA) \tag{54}$$

$$y_j = -r_j \cos(<WOj - <WOA) \tag{55}$$

$$\phi_j = -\frac{\pi}{4} + \theta_i \ , \tag{56}$$

where i and j index in unison.

APPENDIX D. SLIP-LINE FIELDS FOR STYLUS INDENTATION OF A POLYMER FILM

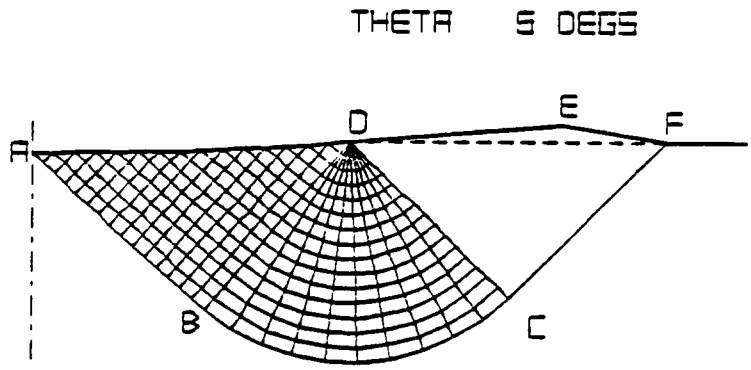

Figure 44. Slip-line field for stylus indentation angle of 5 degrees.

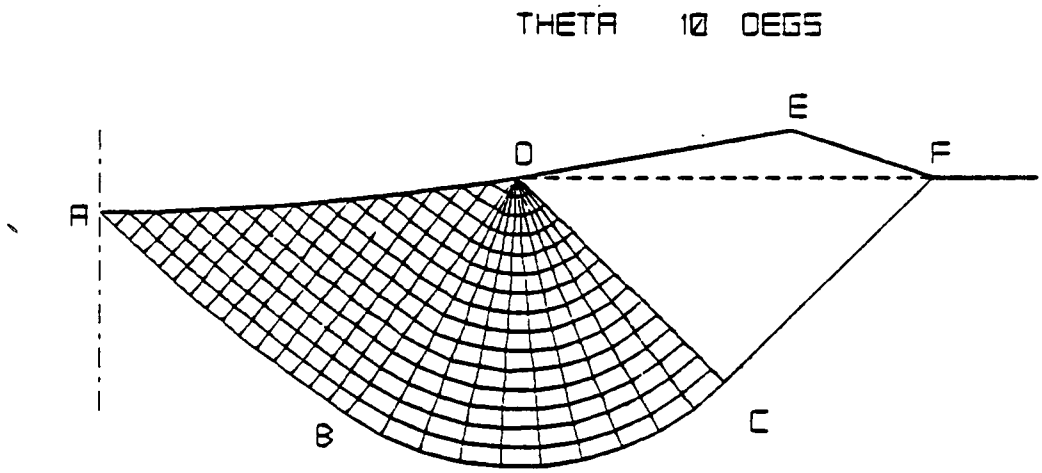

Figure 45. Slip-line field for stylus indentation angle of 10 degrees.

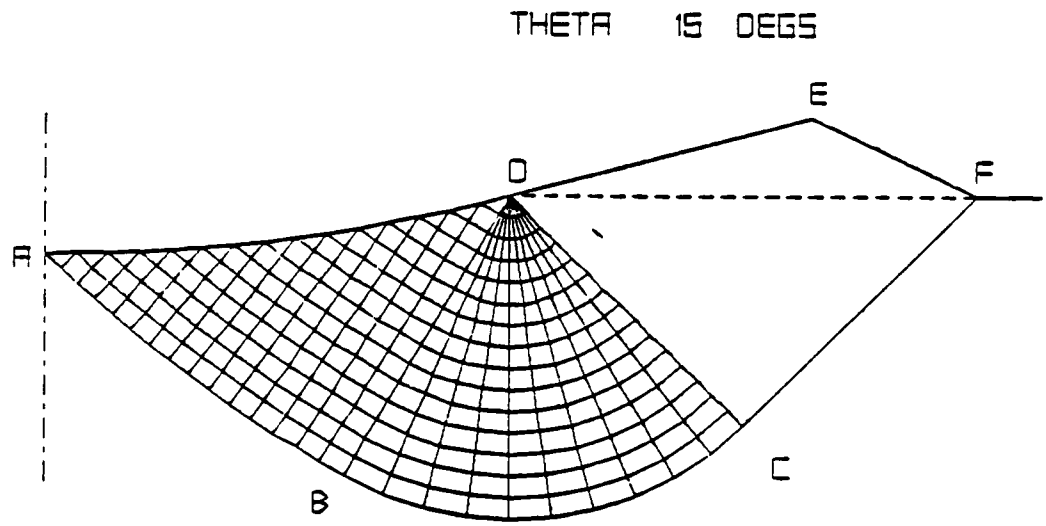

Figure 46. Slip-line field for stylus indentation angle of 15 degrees.

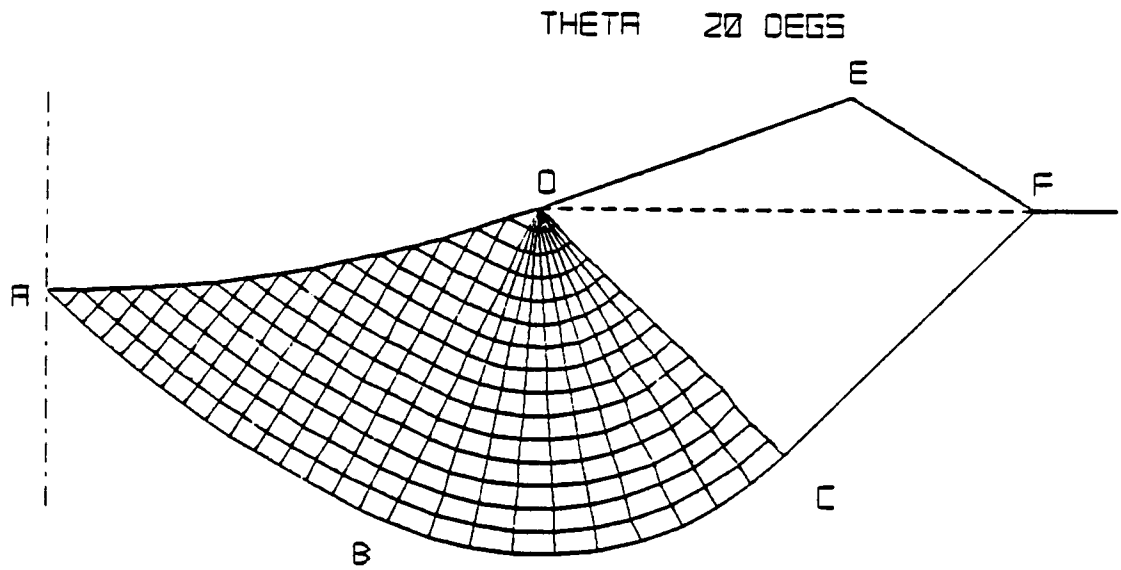

Figure 47. Slip-line field for stylus indentation angle of 20 degrees.

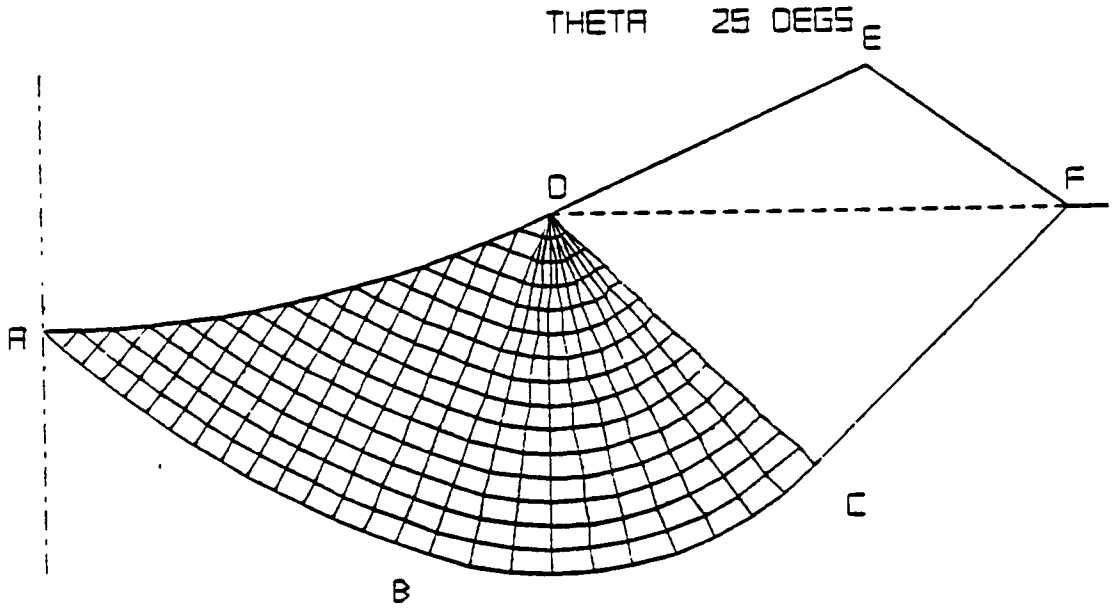

Figure 48. Slip-line field for stylus indentation angle of 25 degrees.

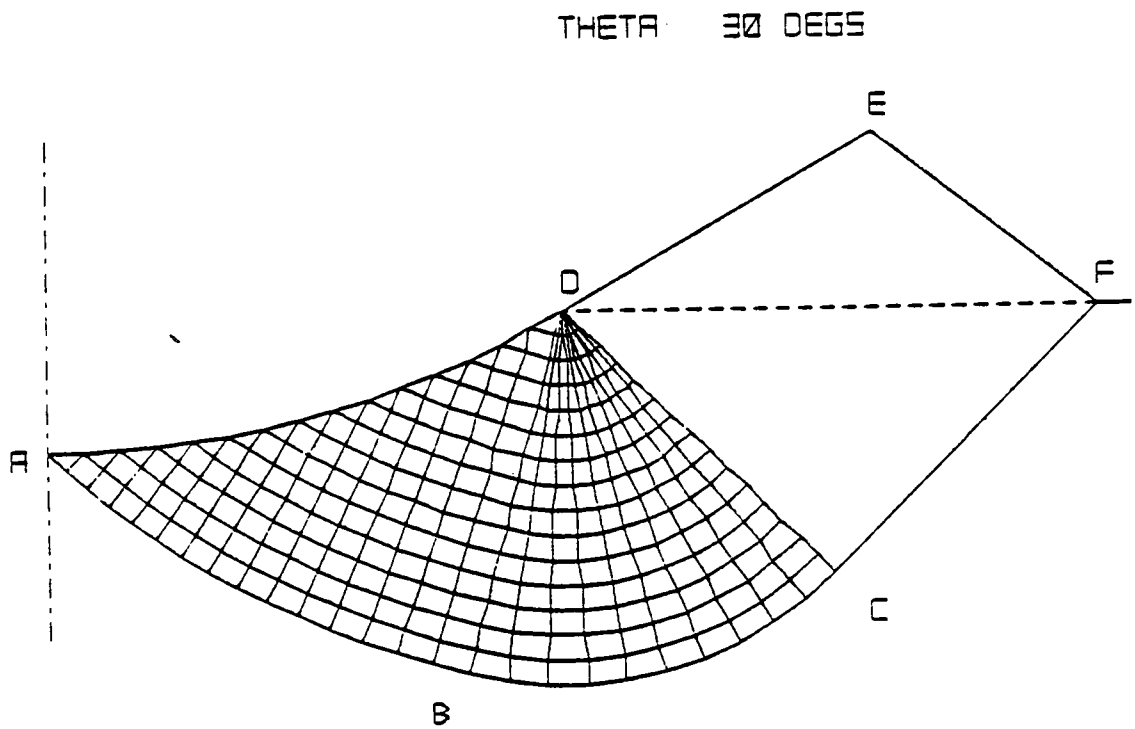

Figure 49. Slip-line field for stylus indentation angle of 30 degrees.

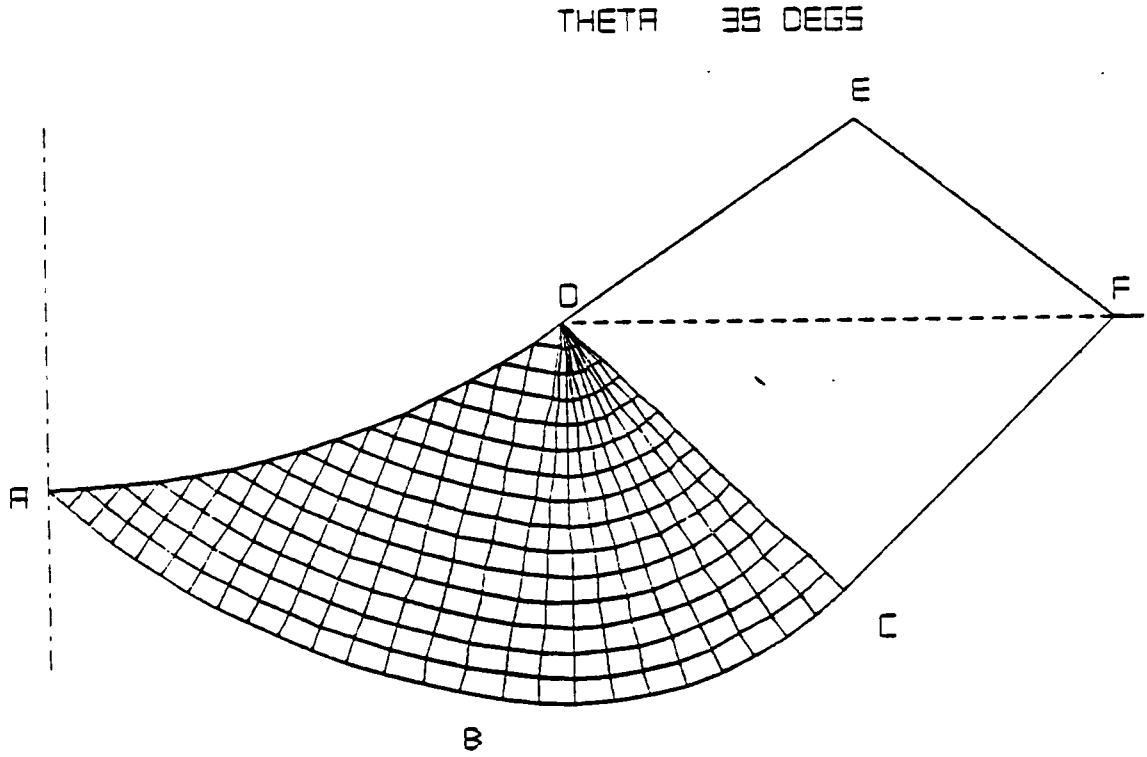

Figure 50. Slip-line field for stylus indentation angle of 35 degrees.

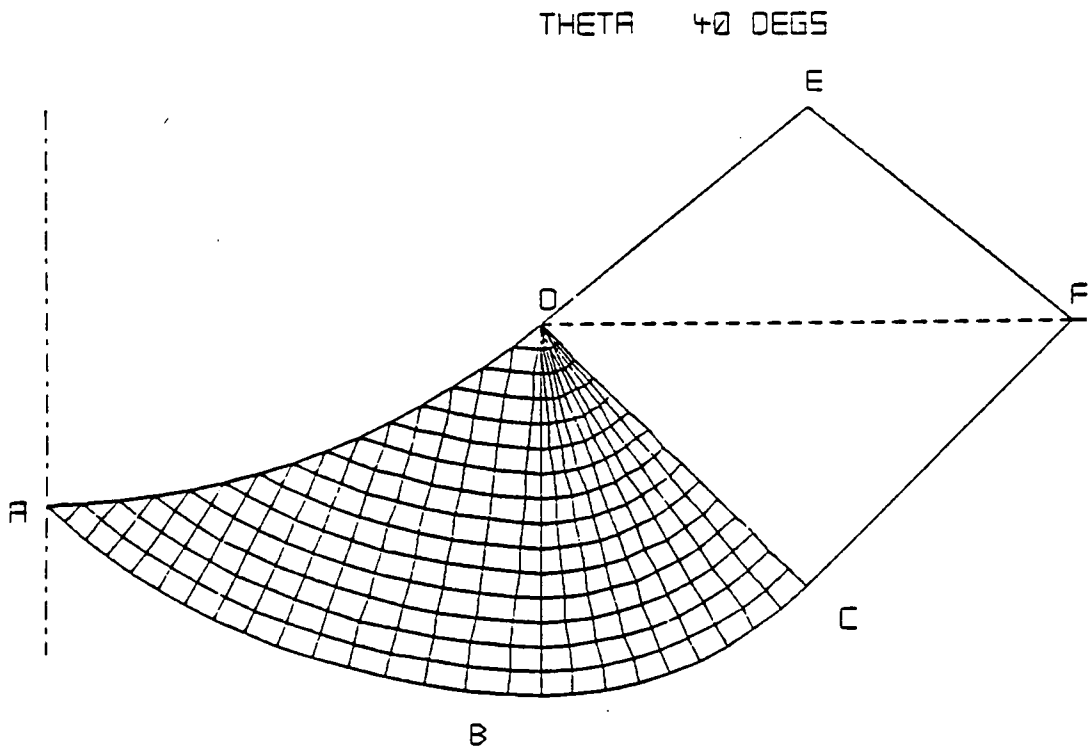

Figure 51. Slip-line field for stylus indentation angle of 40 degrees.

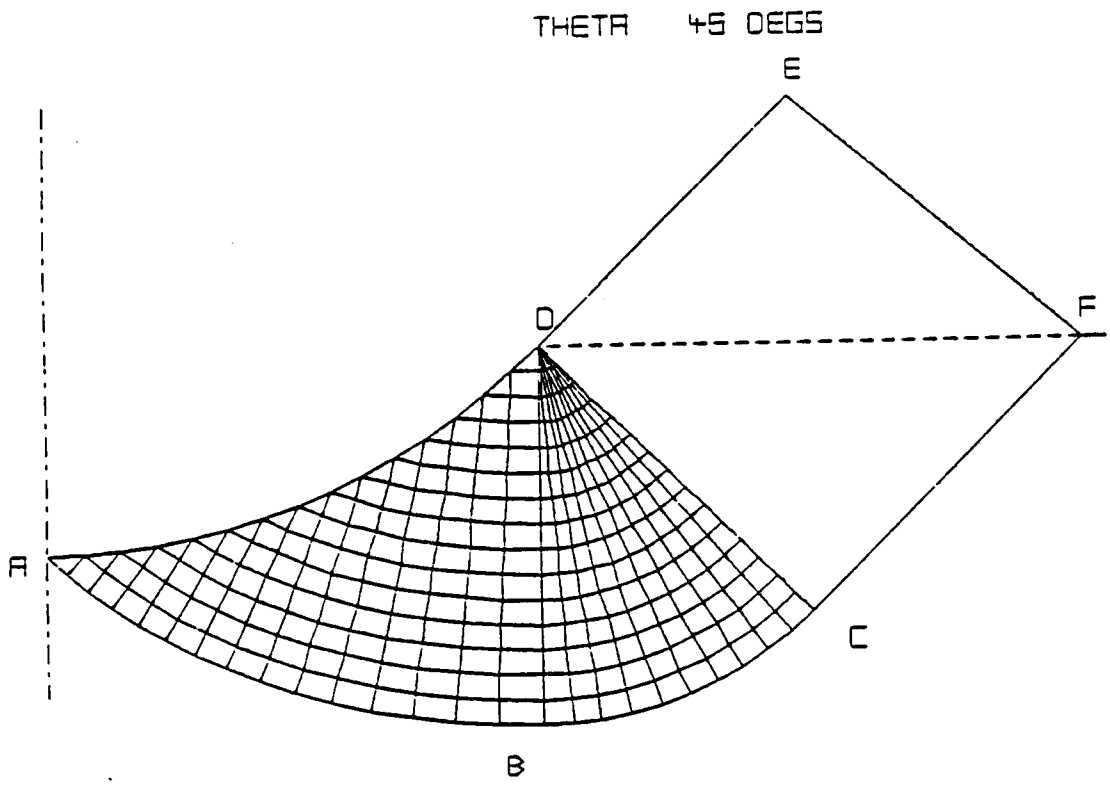

Figure 52. Slip-line field for stylus indentation angle of 45 degrees.

APPENDIX E. MEASUREMENT OF STYLUS TRACK DEPTH FROM MICROGRAPHS

The depth of the stylus track measured from the SEM photomicrographs using a Tektronix 4956 Graphics Tablet. The measurement was made by first assuming that the stylus track was a circular cavity plastically impressed into the surface of the polymer film. Then, by measuring the distance between two points on opposite sides of the track, the width may be may be calculated. Also, in doing so, it was required to account for the fact that the micrograph was taken with the stage of the microscope titled 20 degrees from the horizontal for better optical resolution. The measurement prosedure is illustrated in Figure 53. If the radius, R, of the stylus tip is known, the depth of the track may be estimated from the measured width by the following relation:

$$d = R - \sqrt{(R^2 - w^2/4)} \qquad (57)$$

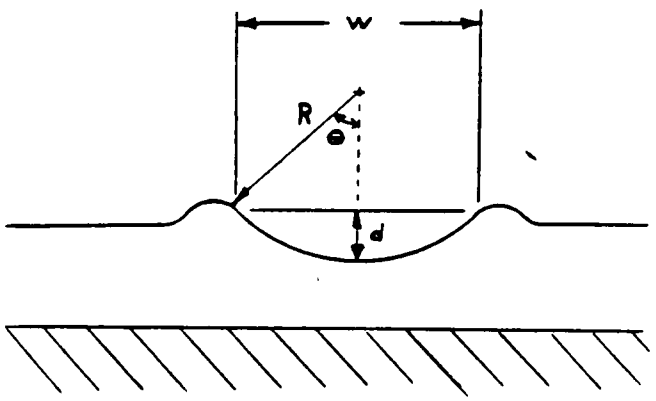

Figure 53. Estimation of the stylus track depth by measuring the width from a micrograph.

APPENDIX F. EXPERIMENTAL DATA FROM MICROGRAPHS

The following is a list of nomencature used in the table of data to follow.

SPEED — The stylus traversing speed expressed in mm/min

POLY — The type of polymer: (1) for polysulfone and (2) for polystrene

SUBR — The roughness of the substrate for that particular specimen in μm R_a

SUBAV — The average roughness for all substrates prepared in the same manner in μm R_a

SNOM — The nominal roughness for all substrates prepared in the same manner in μm R_a. This value was used for comparison between the different polymers.

FILMR — The measured film roughness obtained by the profile meter in μm R_a

SOL — The solution concentration used to prepare the polymer film in percent

THICK — The thickness of the polymer film measured by ellipsometry in μm

DEPTH — The mean depth of indentation of the stylus into the polymer film measured from micrographs in μm

DA — The average deviation of the stylus indentation depth from the mean depth in μm

SUBSK — The skewness of the substrate surface profile

FILMSK — The skewness of the film surface profile measured by the profile meter

AREA — The calculated area under the FRF curve in 1/μm

NA — The normalized area under the FRF curve (nondimensional).
Na = Area x [2 x sample interval (μm)]

SPEED	POLY	SUBR	SUBAV	SNOM	FILMR	SOL	THICK	DEPTH	RA	SUBSK	FILMSK	AREA	NA
91.4	1	0.0980	0.0897	0.1	0.1104	1.5	1.28	0.326	0.013	-1.258	-0.313	0.12830	0.7816
18.3	1	0.0941	0.0897	0.1	0.1124	1.5	1.28	0.393	0.028	-0.858	-0.451	0.18810	0.5737
3.6	1	0.0888	0.0897	0.1	0.0992	1.5	1.28	0.423	0.030	-1.183	-0.907	0.36370	0.8729
91.4	1	0.0803	0.0897	0.1	0.0889	3.0	2.80	0.473	0.020	-1.714	-0.912	0.17390	1.0590
18.3	1	0.0870	0.0897	0.1	0.1423	3.0	2.80	0.454	0.021	-1.824	-0.191	0.18850	0.5749
3.6	1	0.0899	0.0897	0.1	0.1055	3.0	2.80	0.426	0.031	-2.456	-0.772	0.20990	0.5038
91.4	1	0.0803	0.0897	0.1	0.0906	4.5	3.28	0.457	0.019	-1.714	-0.223	0.11210	0.6829
18.3	1	0.0870	0.0897	0.1	0.0830	4.5	3.28	0.441	0.013	-1.824	-0.724	0.13270	0.4047
3.6	1	0.0899	0.0897	0.1	0.0867	4.5	3.28	0.388	0.016	-2.456	-0.301	0.20500	0.4920
91.4	1	0.0980	0.0897	0.1	0.0966	6.0	4.67	0.415	0.019	-1.258	-0.239	0.08800	0.5361
18.3	1	0.0941	0.0897	0.1	0.0708	6.0	4.67	0.505	0.023	-0.858	-0.206	0.17610	0.5371
3.6	1	0.0888	0.0897	0.1	0.0791	6.0	4.67	0.505	0.019	-1.183	0.012	0.23520	0.5645
91.4	1	0.3211	0.3175	0.3	0.3129	1.5	1.28	0.454	0.053	-0.613	-0.501	0.12310	0.7499
18.3	1	0.3336	0.3175	0.3	0.2881	1.5	1.28	0.517	0.047	-0.964	-0.477	0.16240	0.4953
3.6	1	0.3198	0.3175	0.3	0.2440	1.5	1.28	0.436	0.089	-0.561	-0.337	0.24970	0.5993
91.4	1	0.3234	0.3175	0.3	0.2795	3.0	2.80	0.402	0.035	-0.518	-0.545	0.11970	0.7292
18.3	1	0.3149	0.3175	0.3	0.2368	3.0	2.80	0.437	0.026	-0.720	-0.747	0.12990	0.3962
3.6	1	0.2920	0.3175	0.3	0.2703	3.0	2.80	0.470	0.043	-0.619	-0.480	0.22540	0.5410
91.4	1	0.3234	0.3175	0.3	0.2426	4.5	3.28	0.400	0.016	-0.518	-0.374	0.08637	0.5262
18.3	1	0.3149	0.3175	0.3	0.2053	4.5	3.28	0.466	0.037	-0.720	-0.731	0.10190	0.3108
3.6	1	0.2920	0.3175	0.3	0.2163	4.5	3.28	0.486	0.028	-0.619	-0.257	0.12640	0.3034
91.4	1	0.3211	0.3175	0.3	0.2913	6.0	4.67	0.424	0.019	-0.613	-0.417	0.09315	0.5675
18.3	1	0.3336	0.3175	0.3	0.2194	6.0	4.67	0.272	0.015	-0.964	-0.161	0.11050	0.3370
3.6	1	0.3198	0.3175	0.3	0.2071	6.0	4.67	0.539	0.029	-0.561	-0.478	0.12850	0.3084
91.4	1	0.5756	0.5797	0.6	0.5659	1.5	1.28	0.358	0.040	-0.166	-0.049	0.11840	0.7213
18.3	1	0.5762	0.5797	0.6	0.5388	1.5	1.28	0.378	0.031	-0.128	0.141	0.18730	0.5713
3.6	1	0.5394	0.5797	0.6	0.5095	1.5	1.28	0.425	0.060	-0.114	-0.078	0.21200	0.5088
91.4	1	0.6078	0.5797	0.6	0.4872	3.0	2.80	0.363	0.041	-0.188	-0.145	0.14330	0.8730
18.3	1	0.5866	0.5797	0.6	0.4585	3.0	2.80	0.446	0.051	-0.151	0.080	0.21580	0.6582
3.6	1	0.5925	0.5797	0.6	0.4702	3.0	2.80	0.485	0.053	-0.218	0.037	0.28490	0.6838
91.4	1	0.6078	0.5797	0.6	0.5808	4.5	3.28	0.403	0.031	-0.188	-0.429	0.10840	0.6604
18.3	1	0.5866	0.5797	0.6	0.5013	4.5	3.28	0.442	0.034	-0.151	-0.159	0.21560	0.6576
3.6	1	0.5925	0.5797	0.6	0.4127	4.5	3.28	0.479	0.032	-0.218	-0.231	0.25030	0.6007
91.4	1	0.5756	0.5797	0.6	0.5310	6.0	4.67	0.386	0.020	-0.166	-0.195	0.08450	0.5148
18.3	1	0.5762	0.5797	0.6	0.4320	6.0	4.67	0.468	0.024	-0.128	-0.038	0.15380	0.4691
3.6	1	0.5394	0.5797	0.6	0.4435	6.0	4.67	0.549	0.026	-0.114	-0.186	0.24480	0.5875
91.4	1	0.7941	0.7641	0.8	0.7820	1.5	1.28	0.289	0.053	-0.057	-0.140	0.12720	0.7749
18.3	1	0.7496	0.7641	0.8	0.8267	1.5	1.28	0.406	0.047	-0.137	-0.372	0.22690	0.6920
3.6	1	0.7867	0.7641	0.8	0.6806	1.5	1.28	0.900	0.143	-0.156	-0.118	0.24540	0.5890
91.4	1	0.7838	0.7641	0.8	0.7954	3.0	2.80	0.391	0.061	-0.010	-0.114	0.10850	0.6610
18.3	1	0.7645	0.7641	0.8	0.9184	3.0	2.80	0.492	0.061	-0.335	-0.059	0.21750	0.6634
3.6	1	0.7059	0.7641	0.8	0.7087	3.0	2.80	0.471	0.048	0.022	-0.132	0.23980	0.5755
91.4	1	0.7838	0.7641	0.8	0.5549	4.5	3.28	0.463	0.045	-0.010	0.003	0.09222	0.5618
18.3	1	0.7645	0.7641	0.8	0.7071	4.5	3.28	0.540	0.050	-0.335	-0.177	0.21380	0.6521
3.6	1	0.7059	0.7641	0.8	0.5686	4.5	3.28	0.535	0.044	0.022	0.040	0.18240	0.4378
91.4	1	0.7941	0.7641	0.8	0.6039	6.0	4.67	0.734	0.052	-0.057	0.169	0.08237	0.5018
18.3	1	0.7496	0.7641	0.8	0.7081	6.0	4.67	0.770	0.057	0.137	-0.181	0.18290	0.5578
3.6	1	0.7867	0.7641	0.8	0.7100	6.0	4.67	0.817	0.051	-0.156	-0.036	0.17580	0.4219

91.4	2	0.0982	0.1030	0.1	0.1185	1.5	1.60	0.513	0.021	-0.714	-0.745	0.17010	1.0362
18.3	2	0.1116	0.1030	0.1	0.1003	1.5	1.60	0.593	0.039	-0.409	-0.900	0.19360	0.5905
3.6	2	0.1057	0.1030	0.1	0.1295	1.5	1.60	0.533	0.022	-0.493	-0.426	0.33090	0.7942
91.4	2	0.0978	0.1030	0.1	0.1126	3.0	3.29	0.196	0.019	-0.602	-0.779	0.14170	0.8632
18.3	2	0.1041	0.1030	0.1	0.0932	3.0	3.29	0.391	0.023	-0.675	-0.629	0.17930	0.5469
3.6	2	0.1005	0.1030	0.1	0.1028	3.0	3.29	0.372	0.033	-0.605	-0.238	0.20490	0.4918
91.4	2	0.0978	0.1030	0.1	0.1229	4.5	4.53	0.363	0.020	-0.602	-0.412	0.10990	0.6695
18.3	2	0.1041	0.1030	0.1	0.0851	4.5	4.53	0.387	0.017	-0.675	-0.309	0.16550	0.5048
3.6	2	0.1005	0.1030	0.1	0.1030	4.5	4.53	0.385	0.018	-0.605	-0.187	0.20370	0.4888
91.4	2	0.0982	0.1030	0.1	0.0984	6.0	5.19	0.519	0.036	-0.714	-0.823	0.10030	0.6110
18.3	2	0.1116	0.1030	0.1	0.0783	6.0	5.19	0.612	0.026	-0.409	-1.261	0.11940	0.3642
3.6	2	0.1057	0.1030	0.1	0.1062	6.0	5.19	0.670	0.025	-0.493	-0.226	0.17220	0.4133
91.4	2	0.3442	0.3220	0.3	0.3050	1.5	1.60	0.419	0.027	-0.663	-0.514	0.18510	1.1276
18.3	2	0.3304	0.3220	0.3	0.3086	1.5	1.60	0.426	0.041	-0.837	-0.438	0.27620	0.8424
3.6	2	0.3045	0.3220	0.3	0.3052	1.5	1.60	0.398	0.036	-0.943	-0.547	0.36580	0.8776
91.4	2	0.3356	0.3220	0.3	0.2789	3.0	3.29	0.550	0.051	-0.517	-0.657	0.12450	0.7585
18.3	2	0.3197	0.3220	0.3	0.2773	3.0	3.29	0.612	0.051	-0.951	-0.674	0.17150	0.5231
3.6	2	0.2973	0.3220	0.3	0.2594	3.0	3.29	0.715	0.061	-0.898	-0.926	0.16170	0.3881
91.4	2	0.3356	0.3220	0.3	0.2688	4.5	4.53	0.616	0.036	-0.517	-0.552	0.10900	0.6640
18.3	2	0.3197	0.3220	0.3	0.2666	4.5	4.53	0.690	0.038	-0.951	-0.588	0.13630	0.4157
3.6	2	0.2973	0.3220	0.3	0.2694	4.5	4.53	0.695	0.078	-0.898	-0.674	0.16210	0.3890
91.4	2	0.3442	0.3220	0.3	0.2442	6.0	5.19	0.427	0.022	-0.663	-0.907	0.09910	0.6037
18.3	2	0.3304	0.3220	0.3	0.2531	6.0	5.19	0.494	0.037	-0.837	-0.625	0.13510	0.4121
3.6	2	0.3045	0.3220	0.3	0.2674	6.0	5.19	0.438	0.015	-0.943	-0.406	0.18910	0.4538
91.4	2	0.5616	0.6059	0.6	0.6265	1.5	1.60	0.420	0.035	-0.239	-0.350	0.18530	1.1288
18.3	2	0.5990	0.6059	0.6	0.5029	1.5	1.60	0.462	0.028	-0.204	0.058	0.22080	0.6734
3.6	2	0.5429	0.6059	0.6	0.5418	1.5	1.60	0.471	0.048	-0.256	-0.221	0.33400	0.8016
91.4	2	0.6691	0.6059	0.6	0.5625	3.0	3.29	0.318	0.027	-0.328	-0.277	0.13180	0.8029
18.3	2	0.6421	0.6059	0.6	0.6005	3.0	3.29	0.350	0.026	-0.171	-0.287	0.20460	0.6240
3.6	2	0.6206	0.6059	0.6	0.5169	3.0	3.29	0.418	0.032	-0.076	-0.019	0.22710	0.5450
91.4	2	0.6691	0.6059	0.6	0.4972	4.5	4.53	0.346	0.016	-0.328	-0.092	0.09085	0.5535
18.3	2	0.6421	0.6059	0.6	0.5698	4.5	4.53	0.385	0.028	-0.171	-0.163	0.15160	0.4624
3.6	2	0.6206	0.6059	0.6	0.4749	4.5	4.53	0.448	0.033	-0.076	-0.150	0.15120	0.3629
91.4	2	0.5616	0.6059	0.6	0.5330	6.0	5.19	0.526	0.038	-0.239	-0.440	0.09285	0.5656
18.3	2	0.5990	0.6059	0.6	0.4320	6.0	5.19	0.525	0.026	-0.204	-0.071	0.16090	0.4907
3.6	2	0.5429	0.6059	0.6	0.5589	6.0	5.19	0.476	0.027	-0.256	-0.489	0.27040	0.6490
91.4	2	0.8352	0.7880	0.8	0.8380	1.5	1.60	0.443	0.052	-0.206	-0.214	0.18070	1.1008
18.3	2	0.8523	0.7880	0.8	0.6519	1.5	1.60	0.945	0.092	-0.243	0.046	0.29910	0.9123
3.6	2	0.7607	0.7880	0.8	0.7413	1.5	1.60	0.542	0.052	-0.050	0.092	0.27460	0.6590
91.4	2	0.8262	0.7880	0.8	0.6224	3.0	3.29	0.463	0.041	-0.196	-0.126	0.11990	0.7304
18.3	2	0.7118	0.7880	0.8	0.7103	3.0	3.29	0.517	0.052	-0.167	-0.028	0.23400	0.7137
3.6	2	0.7415	0.7880	0.8	0.7767	3.0	3.29	0.516	0.036	-0.113	-0.330	0.35580	0.8539
91.4	2	0.8262	0.7880	0.8	0.6669	4.5	4.53	0.504	0.040	-0.196	0.009	0.09851	0.9001
18.3	2	0.7118	0.7880	0.8	0.6209	4.5	4.53	0.551	0.037	-0.167	-0.339	0.18280	0.5575
3.6	2	0.7415	0.7880	0.8	0.6904	4.5	4.53	0.570	0.049	-0.113	-0.084	0.21530	0.5167
91.4	2	0.8352	0.7880	0.8	0.7741	6.0	5.19	0.554	0.055	-0.206	-0.072	0.10950	0.6671
18.3	2	0.8523	0.7880	0.8	0.5886	6.0	5.19	0.552	0.044	-0.243	-0.155	0.16310	0.4975
3.6	2	0.7607	0.7880	0.8	0.5897	6.0	5.19	0.675	0.067	-0.050	-0.189	0.18940	0.4546

The vita has been removed from the scanned document